HETEROGENEOUS PHOTOCATALYTIC WATER SPLITTING AS A SOURCE OF REDOX EQUIVALENTS FOR ORGANIC SYNTHESIS

DISSERTATION

ZUR ERLANGUNG DES DOKTORGRADES DER NATURWISSENSCHAFTEN

(DR. RER. NAT.)

AN DER FAKULTÄT FÜR CHEMIE UND PHARMAZIE

DER UNIVERSITÄT REGENSBURG

Vorgelegt Von

Antonín Králík

Aus Slaný, Tschechische Republik

Regensburg 2018

The experimental part of this work was carried out between December 2014 and July 2018 at the Institute of Organic Chemistry, University of Regensburg, under the supervision of Prof. Dr. Burkhard König.

Date of submission of the PhD Thesis:	3. 8. 2018
Date of the colloquium:	7. 9. 2018

Board of Examiners:

Prof. Dr. Julia Rehbein	(Chair)
Prof. Dr. Burkhard König	(1st Referee)
Prof. Dr. Arno Pfitzner	(2nd Referee)
Prof. Dr. Robert Wolf	(Examiner)

I, Antonín Králík, solemnly declare to have completed this work without any aid or help of any kind which is not mentioned in this Thesis.

_____

Antonín Králík

FOR DANÍ

“Mediocre!”

— Immortan Joe

Table of Contents

Chapter 1

Immobilisation of Water-Oxidising Amphiphilic Ruthenium Complexes on Unmodified Silica Gel

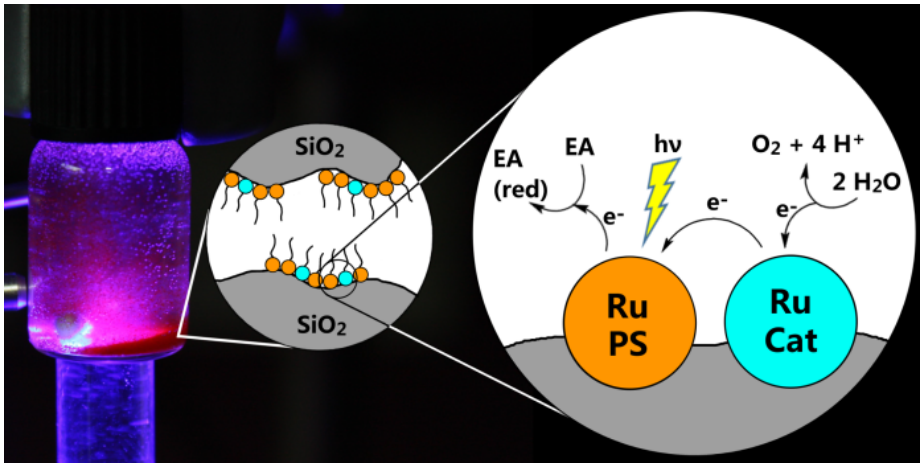

This chapter was published as:

Králík, A.; Hansen, M.; König, B., Immobilisation of water-oxidising amphiphilic ruthenium complexes on unmodified silica gel. *RSC Adv.* **2016**, *6* (7), 5739-5744. **DOI**: 10.1039/C5RA24088C
– Published by The Royal Society of Chemistry

AK developed the immobilisation method, studied properties of the immobilised catalytic systems, performed photocatalytic-water-oxidation experiments, and

wrote the corresponding part of the manuscript together with the Introduction. MH performed chemical-water-oxidation experiments and wrote the corresponding part of the manuscript. BK supervised the project and is the corresponding author.

1.1 Introduction

Global energy consumption is constantly increasing and renewable carbon-neutral alternatives to fossil fuels have to be found. Naturally, sunlight is the most promising renewable source of energy. It is available worldwide and its energy supply greatly exceeds the needs of our society.[1,2] However, the major challenge is to develop an efficient method for storage of the harvested energy, so it can be utilised also during night and transported. One of the possible forms of storage are chemical fuels, compounds with high energy density. From the industrial point of view, water could be a cheap and abundant source of oxygen, as well as electrons, which can be used to produce *e.g.* hydrogen or methanol by a reduction of CO_2. For research purposes, this process of water splitting can be divided into two parts that are studied separately, *i.e.* oxidative production of dioxygen and reductive production of dihydrogen.[3,4]

Water oxidation is especially challenging, requiring four-electron transfers accompanied by a formation of highly reactive oxygen species.[5] Related heterogeneous photocatalytic systems use photoelectrochemical cells,[6,7] photoactive semiconductors[8,9] or metal-oxide catalysts coupled with metal-complex photosensitisers,[10,11] while homogeneous systems usually consist of two main components – a photoredox-active photosensitiser (PS) and a water oxidation catalyst – together with a sacrificial electron acceptor, which is most often the peroxodisulfate anion.[4] These can be represented by two separate water-soluble metal complexes.[12] A proposed mechanism for this type of reaction can be seen in Fig. 1.1. This combination allows a rapid screening of different photosensitiser–catalyst couples. However, its activity is strongly dependent on concentration, since the required electron transfer between complexes is diffusion-controlled. To overcome this obstacle, several systems where the photosensitiser and the catalyst are covalently bound have been developed leading to a more efficient electron transfer.[13–16] On the other hand, each

combination of photosensitiser and catalyst requires a specific synthetic preparation, which makes screenings and complex variations notably difficult. We have recently developed self-assembled systems both for water oxidation and reduction based on amphiphilic metal complexes embedded in a phospholipid vesicular membrane, which increases the local concentration of photosensitiser and catalyst maintaining the activity even at low concentrations. The non-covalent interactions allow the facile variation of the system.[17,18]

In recent years, immobilisation of metal complexes on the surface of inert materials, mostly silica gel, is of particular interest as a way of turning existing homogeneous catalytic systems into heterogeneous ones.[19] This can be achieved covalently over Si–O bonds[20] or non-covalently via hydrogen bonds.[21,22] A different approach known as supported ionic liquid phase (SILP) uses catalytic metal complexes dissolved in a layer of ionic liquid immobilised on a solid supporting material.[23,24] During our study focused on an application of SILP in photocatalytic water oxidation, a strong affinity of amphiphilic metal complexes to an untreated silica gel was observed. This phenomenon where amphiphilic surfactants bearing long alkyl chains are attracted to the polar surface of bare silica was already described in studies focused on HPLC separation.[25–27] Gratifyingly, the immobilised complexes also maintain their catalytic activity. Therefore, we present a heterogeneous photocatalytic system for water oxidation based on amphiphilic ruthenium complexes as the photosensitiser (**1b**, Fig. 1.1) and the catalyst (**2b**) immobilised on a surface of silica gel. This setup overcomes several drawbacks. It can be prepared in one easy step, allows variations in complex types and ratios, and the heterogeneous nature may allow a facile recovery and recycling.

In a recently published study, a similar system utilising amphiphilic photosensitiser and cobalt catalyst non-covalently immobilised via hydrophobic interactions on a surface of silica gel modified with long alkyl chains in a presence of anionic or cationic surfactants was used for photocatalytic hydrogen evolution

from water.[28] However, our approach works with an unmodified silica gel and does not require additional additives.

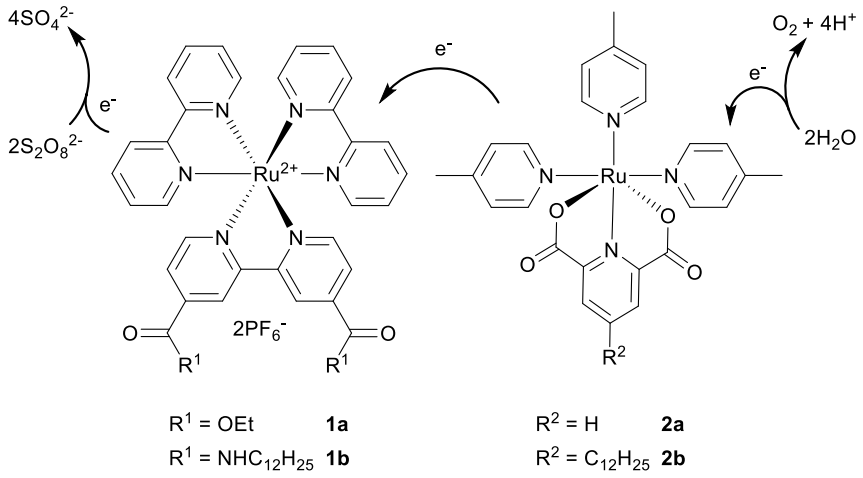

Figure 1.1. Structures of ruthenium photosensitiser (**1**) and catalyst (**2**), and a proposed mechanism for photocatalytic water oxidation.

1.2 Results and discussion

1.2.1 Immobilisation and stability

High affinity of the amphiphilic complexes **1b** and **2b** to silica gel can be already observed during the process of immobilisation. Both complexes are well soluble in chloroform forming a bright orange solution. After an addition of silica gel and a few minutes of stirring, significant decolourisation of the solution occurs, leaving the orange colour concentrated on the silica gel grains. The amount of adsorbed dye has been quantified using UV-Vis spectroscopy.

During this experiment, different amounts of silica gel have been added to a 0.1 mM solution of photosensitiser **1b** and after 5 minutes of stirring, the liquid phase has been analysed. Results are summarised in Table 1.1.

Table 1.1. Monitoring the amount of adsorption of photosensitiser **1b** onto silica gel.

Amount of SiO_2	c_{PS}[a]	% adsorbed[b]
25 mg	34.9 μM	65.1 %
50 mg	1.4 μM	98.6 %
100 mg	~ 0 μM	~ 100 %

[a]final concentration of PS solution (initial in all cases 0.1 mM); [b]amount of PS adsorbed onto silica gel

Using 50 mg of silica gel, corresponding to a loading of 10 μmol of photosensitiser per gram of silica gel, or more, results in almost quantitative adsorption leaving a colourless solution and providing orange-coloured solid particles.

Stability in aqueous solutions, in which the amphiphilic complexes are insoluble, was also investigated. Since a local lowering of pH can occur during the water oxidation reaction, neutral and acidic condition were chosen. Suspensions of silica gel with the immobilised complex **1b** (20 μmol g^{-1}) in aqueous buffers at pH 1, 4 and 7, respectively, were stirred for 48 hours. Table 1.2 shows the results confirming the high stability of the immobilised system in aqueous solutions. On the other hand, experiments conducted in acetonitrile and DMSO showed that in polar aprotic solvents, the complexes are washed off the silica gel surface.

Table 1.2. Monitoring the stability of immobilised photosensitiser **1b** in aqueous suspensions at different pH.

pH	c_{PS}[a]	% released[b]
7.0	0.94 μM	0.75 %
4.0	2.38 μM	1.9 %
1.0	4.15 μM	3.3 %

[a] concentration of PS in the solution after 48 hours; [b]amount of PS released into solution

A similar set of experiments in acetonitrile was conducted for water-soluble complexes **1a** and **2a**, which are insoluble in chloroform. No significant

absorption from acetonitrile solution and a strong leakage into water was observed.

1.2.2 Performance in photocatalytic water oxidation

The immobilised metal complexes maintain their photocatalytic water oxidation activity, which is comparable to experiments in homogeneous solution both in terms of turn-over numbers (TON) and reaction rate (Fig. 1.2). However, the fast photochemical degradation of the sensitiser molecule, limiting the photocatalysis to about 6 minutes, remains unchanged.[17] Experiments using silica gel with different amounts of immobilised complexes showed that the activity of the system, in terms of oxygen evolution, is independent on the loading in a tested range from 20 to 2 μmol of **1b** and 2 to 0.2 μmol of **2b** per gram of support (in all cases, the photosensitiser to catalyst ratio is 10 : 1) and also on the silica gel type.

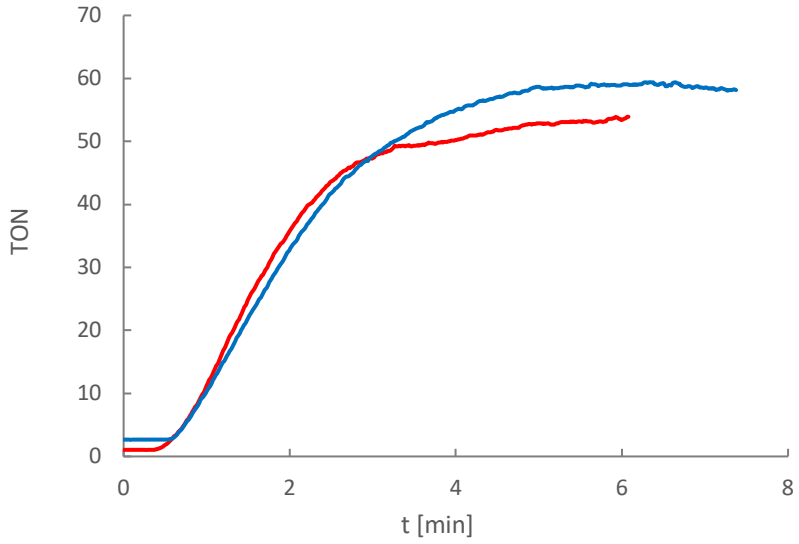

Figure 1.2. Comparison of oxygen evolution using a homogeneous system with water-soluble complexes **1a** and **2a** (red) and the heterogeneous system using silica-gel-bound complexes **1b** and **2b** (blue) monitored *in situ* by an oxygen probe.

Results are summarised in Table 1.3. Loadings below this range showed very low oxygen production due to an insufficient light penetration of the sample, because of large amount of solids.

Table 1.3. Turnover numbers for oxygen evolution using different types of silica gel with varying amounts of complexes **1b** and **2b**. Oxygen evolution was determined by a head-space gas chromatography.

Loading of **1b** [µmol/g]	Loading of **2b** [µmol/g]	Particle size [µm]	Amount of SiO_2 [mg]	TON[a]
20	2	63–200	30	48
10	1	63–200	60	34
5	0.5	63–200	120	53
2	0.2	63–200	300	42
20	2	4–63	30	41
10	1	4–63	60	30

[a] per catalyst

These observations also suggest that the silica gel surface is not evenly covered. In a case of an even coverage at the lowest functional loading, the calculated surface concentrations are 4×10^{-13} mol cm^{-2} for the photosensitiser and 4×10^{-14} mol cm^{-2} for the catalyst, respectively, implying a monolayer distribution with an average distance between the metal complexes around 20 nm. However, the required distance for an efficient electron transfer between a photosensitiser and a catalyst is much shorter.[29] This suggests that the complexes are forming specific hot-spots with increased local concentration, which helps to maintain the functionality even at lower loadings.

All experiments have been repeated three times with standard deviations under 5 % confirming the reproducibility of the results. The determined TON values based on the water oxidation catalyst lie between 30 and 50, which corresponds to previous homogeneous experiments utilising water-soluble complexes.[17] The fluctuations are caused by different experimental setups for each loading with varying ratios of solid to liquid phase.

To prove that the system's short lifetime is caused by a degradation of the photosensitiser, a silica-gel-bound catalytic system bearing 20 μmol of photosensitiser and 2 μmol of the water oxidation catalyst per gram that has been previously used in a water oxidation reaction was filtered off, washed, dried and used to immobilise a batch of fresh photosensitiser.
This system was then fully functional for water oxidation reaching TON of 40, which corresponds to 84% of the original value.

1.2.3 Performance in chemical water oxidation

The use of this immobilisation method for chemical water oxidation reaction with ruthenium complex **3** (Fig. 1.3) as the catalyst and cerium ammonium nitrate as the oxidising agent was investigated. Since the complex is poorly soluble in water, mixtures containing acetonitrile or trifluoroethanol had to be used for published homogeneous experiments.[30,31] The catalyst immobilised on silica gel is functional in solely aqueous solutions.

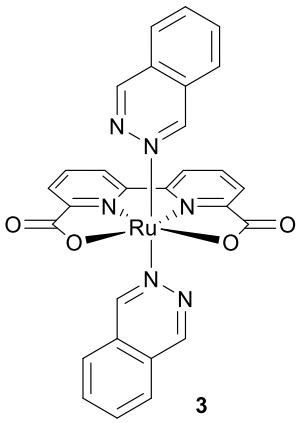

Figure 1.3. Structure of a ruthenium complex used for chemical water oxidation.

Complex **3** shows the same affinity to silica gel as previously described for photosensitiser **1b** – a complete decolourisation of its chloroform solution by an addition of the support was observed.

Table 1.4 shows that the activity of the system, in terms of oxygen production, is independent on the loading at a tested range from 2 to 0.1 μmol of catalyst per gram of support. All the experiments have been conducted three times with standard deviations mostly under 10 % (20 % for the loading of 0.1 μmol per gram), so they again show a good reproducibility. The obtained TON values are around 25 000, which is lower compared with the homogeneous experiment where values of TON reached 40 000 for our experiments and 55 000 as published.[31]

Table 1.4. Turnover numbers for oxygen evolution measurements using silica gel with different amounts of chemical water oxidation catalyst **3** measured by a head-space gas chromatography.

Loading of **3** [μmol/g]	Amount of SiO_2 [mg]	TON
homogeneous	–	41 000
2	2	29 000
1	4	24 000
0.5	8	26 000
0.2	20	17 000
0.1	40	25 000

1.3 Conclusions

A novel heterogeneous catalytic system for photocatalytic water oxidation is obtained by immobilising amphiphilic ruthenium complexes non-covalently on the surface of silica gel. The system is easy to prepare and the complexes maintain their catalytic activity, which is comparable to their water-soluble equivalents. However, the low stability of the photosensitiser under the reaction conditions still remains.

Likewise, the immobilisation of a catalyst for chemical water oxidation is possible, showing good activity. This simple immobilisation technique may facilitate the recovery and regeneration of the catalysts.

1.4 Experimental section

1.4.1 Preparation of silica-gel-based system for photocatalytic water oxidation

Stock solutions of photosensitiser **1b** (2 μL, 1 mM) and catalyst **2b** (200 μL, 1 mM), both in chloroform, were pipetted into a 10 mL round-bottom flask, diluted with chloroform to *ca.* 5 mL and silica gel (see Table 1.5 for amounts for different loadings) was added to the solution under stirring. This suspension was kept stirring for another 5 min, the solvent was then slowly evaporated under a mild vacuum (500 mbar at 40 ºC) and finally dried in high vacuum (<0.5 mbar, 1 hour).

Table 1.5. Amounts of silica gel needed for preparation of photocatalytic systems with different complex loadings.

Loading of PS [μmol/g]	Amount of SiO_2 [mg]
20	100
10	200
5	400
2	1000

1.4.2 Adsorption studies

Stock solution of photosensitiser **1b** (500 μL, 1 mM) in chloroform was diluted to 5 mL, transferred into a 10 mL round-bottom flask and silica gel (25, 50 or 100 mg, pore size 60 Å, particle size 63–200 μm) was added to the solution under stirring. After five minutes, the suspension was filtered and UV-Vis spectra of the filtrate were measured. Concentration of the PS complex was determined by a comparison with a 5 μM standard solution and its peak absorbance at 287 nm.

1.4.3 Stability studies

Silica gel (13 mg) bearing 20 μmol of photosensitiser **1b** per gram was added to 2 mL of aqueous buffer (pH 1.0, 4.0 or 7.0) in a small vial with a stirrer. The vial was closed, covered in an aluminium foil and the suspension was kept stirring for 48 hours. Then, it was filtered and UV-Vis spectra of the filtrate were measured. Concentration of the PS complex was determined by a comparison with a 5 μM standard solution and its peak absorbance at 287 nm.

The same process was used for stability measurements in DMSO and acetonitrile.

1.4.4 Photocatalytic water oxidation – homogeneous kinetic studies

Stock solutions of photosensitiser **1a** (260 μL, 1 mM) and catalyst **2a** (26 μL, 1 mM), both in chloroform, were pipetted into a small vial, evaporated on a shaker with a heating block and dried in high vacuum. Then, phosphate buffer (2.1 mL, 50 mM, pH 7.0) and sodium persulfate stock solution (5.25 μL, 1 M) were added (Table 1.6). The mixture was degassed by bubbling with nitrogen for *ca.* 10 minutes and it was transferred under a nitrogen atmosphere to a 2 mL vial equipped with a fluorescent spot for oxygen-probe measurements. The vial was filled to the top, so no air bubble was left inside to influence the results, closed, fastened under an upside down magnetic stirrer, its bottom was attached to a glass rod with a blue LED on the other side and the optical fiber of the oxygen detector was connected to the fluorescent spot. The reaction mixture was stirred and irradiated until the oxygen evolution ceased.

Table 1.6. Concentrations of particular components for both homogeneous and heterogeneous water oxidation in aqueous buffer.

Component	Concentration
Photosensitiser (**1**)	125 μM
Catalyst (**2**)	12.5 μM
$Na_2S_2O_8$	2.5 mM
Phosphate buffer	50 mM

1.4.5 Photocatalytic water oxidation – heterogeneous kinetic studies

The previously prepared silica-gel-based catalyst (13 mg) was weighed into a small vial. Then, phosphate buffer (2.1 mL, 50 mM, pH 7.0) and sodium persulfate stock solution (5.25 μL, 1 M) were added. The suspension was degassed by bubbling with nitrogen for *ca.* 10 minutes and it was transferred under nitrogen atmosphere to a 2 mL vial equipped with a fluorescent spot for oxygen-probe measurements, which was carried out in a same way as described in the previous paragraph.

1.4.6 Photocatalytic water oxidation – heterogeneous quantitative studies

The previously prepared silica-gel-based catalyst (different amounts for different loadings, see Table 1.3) was weighed into a small crimp-top vial. Then, phosphate buffer (4.5 mL, 50 mM, pH 7.0) and sodium persulfate stock solution (11.3 μL, 1 M) were added. The vial was sealed and the suspension was degassed by bubbling with argon for *ca.* 15 minutes. Then, it was irradiated for 20 minutes using an array of six blue LEDs and cooled by a tap water in an aluminium block. The samples were left for an hour to equilibrate back to laboratory temperature and the produced oxygen was quantified using head-space GC.

1.4.7 Reactivation

Collected suspensions containing silica gel with the highest loading of complexes used previously in water oxidation reaction were filtered, washed with distilled water until the filtrate was colourless and the solid residue was dried in high vacuum. Stock solution of photosensitiser **1b** (1 mL, 1 mM) in chloroform was pipetted into a round 10 mL flask, diluted with chloroform to *ca.* 5 mL and the reused silica gel (50 mg) was added to the solution under stirring. This suspension was kept stirring for another 5 min, the solvent was then slowly evaporated under mild vacuum (500 mbar at 40 °C) and finally dried in high vacuum (<0.5 mbar, 1 hour).

This treated silica gel (30 mg) was weighed into a small crimp-top vial and phosphate buffer (4.5 mL, 50 mM, pH 7.0) and sodium persulfate stock solution (11.3 μL, 1 M) were added. The vial was sealed; the suspension was degassed by bubbling with argon for *ca.* 15 minutes and then, an oxygen evolution reaction was carried out in the same way as described in the previous paragraph.

1.4.8 Preparation of silica-gel-based system for chemical water oxidation

Chloroform stock solution of catalyst **3** (10 μL, 1 mM) was pipetted into a 10 mL round-bottom flask, diluted with chloroform to *ca.* 5 mL and silica gel (see Table 1.7 for amounts for different loadings) was added to the solution under stirring. This suspension was kept stirring for another 5 min, the solvent was then slowly evaporated under mild vacuum (500 mbar at 40 °C) and finally dried in high vacuum (<0.5 mbar, 1 hour).

Table 1.7. Amounts of silica gel needed for preparation of catalytic systems for chemical water oxidation with different complex loadings.

Loading of catalyst [µmol/g]	Amount of SiO_2 [mg]
2.0	50
1.0	100
0.5	200
0.2	500
0.1	1000

1.4.9 Homogeneous chemical water oxidation

Degassed stock solution of catalyst **3** (4 µL, 1 mM) in trifluoroethanol was added via syringe into a small crimp-top vial previously purged with argon, then degassed stock solution of cerium ammonium nitrate in pH 1 triflic acid (2 mL, 500 mM) was added. The mixture was stirred for 1 hour and the produced oxygen was quantified using head-space GC.

1.4.10 Heterogeneous chemical water oxidation

The previously prepared silica-gel-based catalyst (different amounts for different loadings, see Table 1.4) was weighed into a 20 mL crimp-top vial filled with argon, which was sealed and purged with argon again for 5 minutes. Then, a degassed stock solution of cerium ammonium nitrate in pH 1 triflic acid (2 mL, 500 mM) was added. The mixture was stirred for 1 hour and the produced oxygen was quantified using head-space GC.

1.5 Supporting information

1.5.1 General methods and material

Fibox 3 fibre optic oxygen sensor (PreSens GmbH) was used for *in situ* monitoring of the oxygen evolution.

Head-space GC measurements were carried out on Inficon Micro GC 3000 with a 3 Å molecular sieve column, a thermal conductivity detector and argon as a carrier gas.

UV-VIS spectra were measured on Varian Cary 50 Bio UV-Visible.

For the visible light irradiation, OSRAM Oslon SSL 80 royal-blue LEDs were used.

Macherey-Nagel brand silica gels with 60 Å pore size and particle sizes of 63–200 or 40–63 μm were used for immobilisation.

Photosensitisers **1a**[31] and **1b**,[17] and catalysts **2a**,[33] **2b**[17] and **3**[34] were prepared according to literature procedures. Other commercially available chemicals were used without further purification.

1.5.2 Spectral data

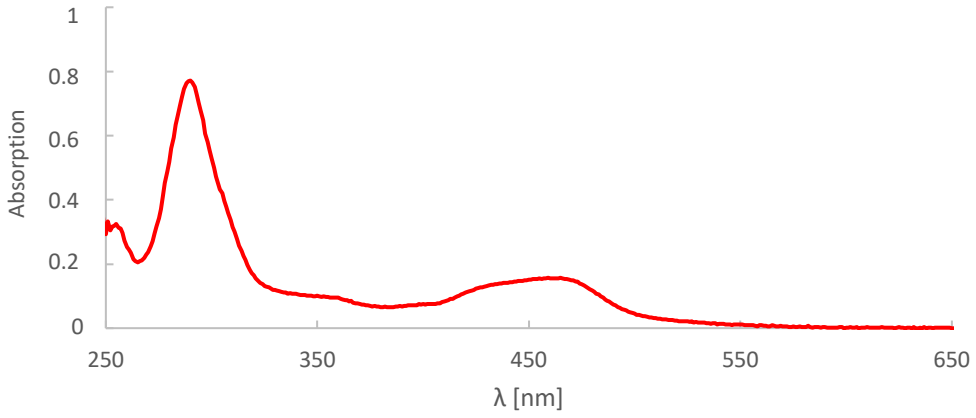

Figure S1.1. UV-VIS spectrum of 5 μM chloroform solution of photosensitiser **1b**.

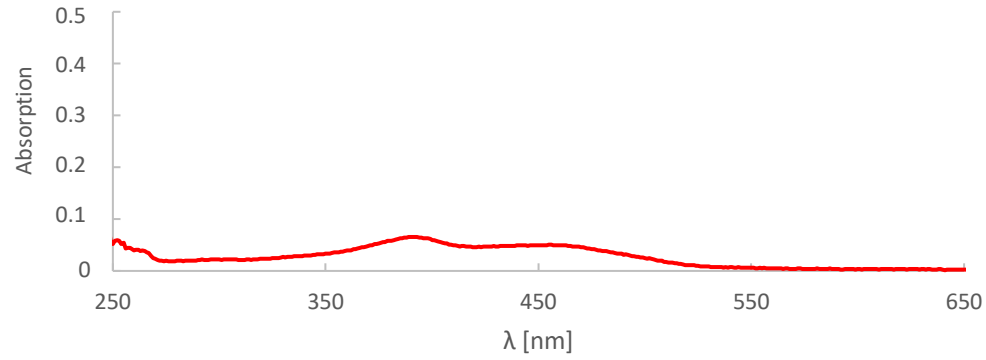

Figure S1.2. UV-VIS spectrum of 5 μM chloroform solution of catalyst **2b**.

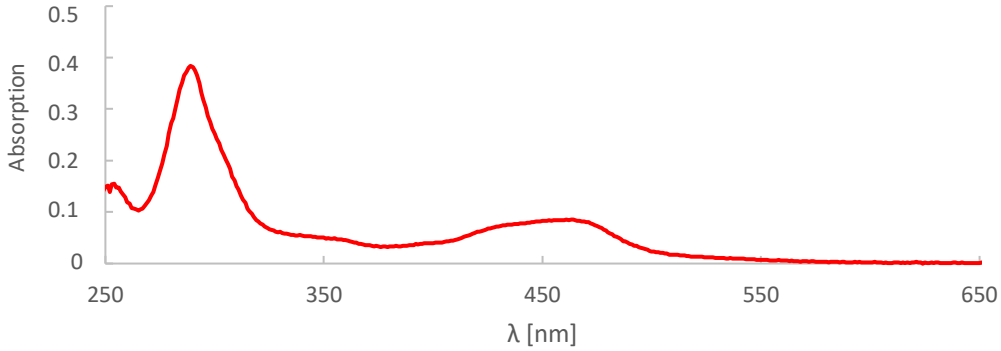

Figure S1.3. UV-VIS spectrum of chloroform solution containing photosensitiser **1b** (5 μM) and catalyst **2b** (0.5 μM).

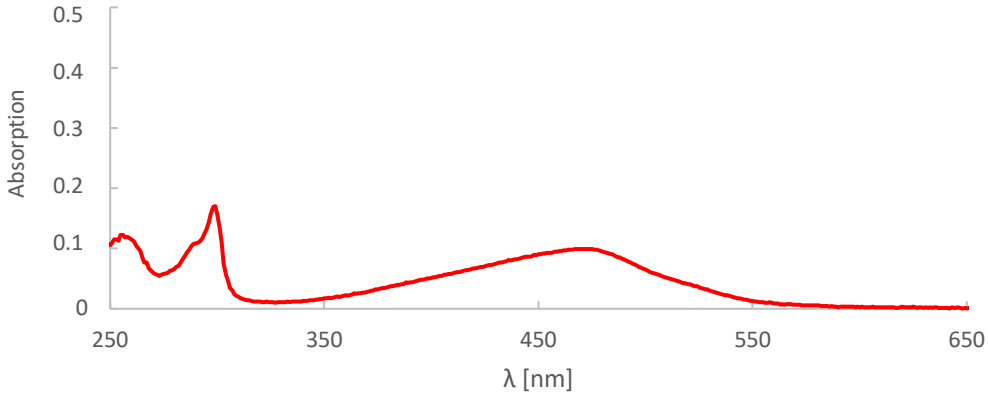

Figure S1.4. UV-VIS spectrum of 5 μM chloroform solution of catalyst **3**.

1.5.3 Heterogeneous photocatalytic water oxidation

Table S1.1. Summarised experimental data

Entry	Loading of **1b** [μmol/g]	Loading of **2b** [μmol/g]	PS:Cat ratio	Amount of SiO_2 [mg]	Amount of **1b** [μmol]	Amount of **2b** [μmol]	Evolved oxygen [μmol]	TON
1	20	2	10:1	30[a]	0.6	0.06	2.8	48
2	10	1	10:1	60[a]	0.6	0.06	2.1	34
3	5	0.5	10:1	120[a]	0.6	0.06	3.2	53
4	2	0.2	10:1	300[a]	0.6	0.06	2.6	42
5	20	2	10:1	30[b]	0.6	0.06	2.5	41
6	10	1	10:1	60[b]	0.6	0.06	1.8	30

[a]particle size 63–200 μm; [b]particle size 40–63 μm

Table S1.2. Reactivation

Entry	Loading of **1b** [μmol/g]	Loading of **2b** [μmol/g]	PS:Cat ratio	Amount of SiO_2 [mg]	Amount of **1b** [μmol]	Amount of **2b** [μmol]	Evolved oxygen [μmol]	TON
1	20	2	10:1	30	0.6	0.06	2.8	48
2	20[a]	2[b]	10[a]:1[b]	30[c]	0.6[a]	0.06[b]	2.4	40

[a] fresh batch of photosensitiser; [b] leftover catalyst from previous water oxidation reaction; [c] silica gel recovered from Entry 1

1.5.4 Heterogeneous chemical water oxidation

Table S1.3. Summarised experimental data

Entry	Loading of **3** [μmol/g]	Amount of SiO_2 [mg]	Amount of **1b** [nmol]	Evolved oxygen [μmol]	TON
1[a]	-	-	4	0.16	41 000
2	2	2	4	0.11	29 000
3	1	4	4	0.09	24 000
4	0.5	8	4	0.10	26 000
5	0.2	20	4	0.07	17 000
6	0.1	40	4	0.10	25 000

[a] homogeneous experiment

1.6 References

1. Barber, J.; Tran, P. D., From natural to artificial photosynthesis. *J. R. Soc. Interface* **2013**, *10* (81).
2. Lewis, N. S.; Nocera, D. G., Powering the planet: Chemical challenges in solar energy utilization. *Proc. Natl. Acad. Sci.* **2006**, *103* (43), 15729-15735.
3. Cook, T. R.; Dogutan, D. K.; Reece, S. Y.; Surendranath, Y.; Teets, T. S.; Nocera, D. G., Solar Energy Supply and Storage for the Legacy and Nonlegacy Worlds. *Chem. Rev.* **2010**, *110* (11), 6474-6502.
4. Frischmann, P. D.; Mahata, K.; Würthner, F., Powering the future of molecular artificial photosynthesis with light-harvesting metallosupramolecular dye assemblies. *Chem. Soc. Rev.* **2013**, *42* (4), 1847-1870.
5. Meyer, T. J., The art of splitting water. *Nature* **2008**, *451*, 778.
6. Khaselev, O.; Turner, J. A., A Monolithic Photovoltaic-Photoelectrochemical Device for Hydrogen Production via Water Splitting. *Science* **1998**, *280* (5362), 425-427.
7. Zhong, D. K.; Sun, J.; Inumaru, H.; Gamelin, D. R., Solar Water Oxidation by Composite Catalyst/α-Fe2O3 Photoanodes. *J. Am. Chem. Soc.* **2009**, *131* (17), 6086-6087.
8. Khan, S. U. M.; Al-Shahry, M.; Ingler, W. B., Efficient Photochemical Water Splitting by a Chemically Modified n-TiO2. *Science* **2002**, *297* (5590), 2243-2245.
9. Zou, Z.; Ye, J.; Sayama, K.; Arakawa, H., Direct splitting of water under visible light irradiation with an oxide semiconductor photocatalyst. *Nature* **2001**, *414*, 625.
10. Kalyanasundaram, K.; Grätzel, M., Cyclic Cleavage of Water into H2 and O2 by Visible Light with Coupled Redox Catalysts. *Angew. Chem. Int. Ed.* **1979**, *18* (9), 701-702.

11. Youngblood, W. J.; Lee, S.-H. A.; Kobayashi, Y.; Hernandez-Pagan, E. A.; Hoertz, P. G.; Moore, T. A.; Moore, A. L.; Gust, D.; Mallouk, T. E., Photoassisted Overall Water Splitting in a Visible Light-Absorbing Dye-Sensitized Photoelectrochemical Cell. *J. Am. Chem. Soc.* **2009**, *131* (3), 926-927.
12. Wasylenko, D. J.; Palmer, R. D.; Berlinguette, C. P., Homogeneous water oxidation catalysts containing a single metal site. *Chem. Commun.* **2013**, *49* (3), 218-227.
13. Li, F.; Jiang, Y.; Zhang, B.; Huang, F.; Gao, Y.; Sun, L., Towards A Solar Fuel Device: Light-Driven Water Oxidation Catalyzed by a Supramolecular Assembly. *Angew. Chem. Int. Ed.* **2012**, *51* (10), 2417-2420.
14. Kaveevivitchai, N.; Chitta, R.; Zong, R.; El Ojaimi, M.; Thummel, R. P., A Molecular Light-Driven Water Oxidation Catalyst. *J. Am. Chem. Soc.* **2012**, *134* (26), 10721-10724.
15. Norris, M. R.; Concepcion, J. J.; Harrison, D. P.; Binstead, R. A.; Ashford, D. L.; Fang, Z.; Templeton, J. L.; Meyer, T. J., Redox Mediator Effect on Water Oxidation in a Ruthenium-Based Chromophore–Catalyst Assembly. *J. Am. Chem. Soc.* **2013**, *135* (6), 2080-2083.
16. Ashford, D. L.; Stewart, D. J.; Glasson, C. R.; Binstead, R. A.; Harrison, D. P.; Norris, M. R.; Concepcion, J. J.; Fang, Z.; Templeton, J. L.; Meyer, T. J., An Amide-Linked Chromophore–Catalyst Assembly for Water Oxidation. *Inorg. Chem.* **2012**, *51* (12), 6428-6430.
17. Hansen, M.; Li, F.; Sun, L.; König, B., Photocatalytic water oxidation at soft interfaces. *Chem. Sci.* **2014**, *5* (7), 2683-2687.
18. Troppmann, S.; König, B., Functionalized Membranes for Photocatalytic Hydrogen Production. *Chem.-Eur. J.* **2014**, *20* (45), 14570-14574.
19. A. Kirschning, *Immobilized Catalysts*, Springer, Germany, 2004.
20. Jana, A.; Mondal, J.; Borah, P.; Mondal, S.; Bhaumik, A.; Zhao, Y., Ruthenium bipyridyl tethered porous organosilica: a versatile, durable and

reusable heterogeneous photocatalyst. *Chem. Commun.* **2015**, *51* (53), 10746-10749.

21. Bianchini, C.; Burnaby, D. G.; Evans, J.; Frediani, P.; Meli, A.; Oberhauser, W.; Psaro, R.; Sordelli, L.; Vizza, F., Preparation, Characterization, and Performance of Tripodal Polyphosphine Rhodium Catalysts Immobilized on Silica via Hydrogen Bonding. *J. Am. Chem. Soc.* **1999**, *121* (25), 5961-5971.
22. Bianchini, C.; Barbaro, P.; Dal Santo, V.; Gobetto, R.; Meli, A.; Oberhauser, W.; Psaro, R.; Vizza, F., Immobilization of Optically Active Rhodium-Diphosphine Complexes on Porous Silica via Hydrogen Bonding. *Adv. Synth. Catal.* **2001**, *343* (1), 41-45.
23. Mehnert, C. P.; Cook, R. A.; Dispenziere, N. C.; Afeworki, M., Supported Ionic Liquid Catalysis − A New Concept for Homogeneous Hydroformylation Catalysis. *J. Am. Chem. Soc.* **2002**, *124* (44), 12932-12933.
24. Riisagera, A.; Fehrmanna, R.; Haumannb, M.; Wasserscheidb, P., Supported ionic liquids: versatile reaction and separation media. *Top. Catal.* **2006**, *40* (1), 91-102.
25. Knox, J. H.; Laird, G. R., Soap chromatography—a new high-performance liquid chromatographic technique for separation of ionizable materials: Dyestuff intermediates. *J. Chromatogr. A* **1976**, *122*, 17-34.
26. Ghaemi, Y.; Wall, R. A., Hydrophobic chromatography with dynamically coated stationary phases: III. Non-ionic surfactant effects. *J. Chromatogr. A* **1980**, *198* (4), 397-405.
27. Juskowiak, B., Binaphthyl-based amphiphile as a reagent for dynamically modified silica and fluorescence detection in high-performance liquid chromatography. *J. Chromatogr. A* **1994**, *668* (2), 313-321.
28. Bachmann, C.; Probst, B.; Oberholzer, M.; Fox, T.; Alberto, R., Photocatalytic proton reduction with ruthenium and cobalt complexes immobilized on fumed reversed-phase silica. *Chem. Sci.* **2016**, *7* (1), 436-445.
29. B. König, *Chemical Photocatalysis*, De Gruyter, Berlin, 2013.

30. Duan, L.; Bozoglian, F.; Mandal, S.; Stewart, B.; Privalov, T.; Llobet, A.; Sun, L., A molecular ruthenium catalyst with water-oxidation activity comparable to that of photosystem II. *Nat. Chem.* **2012**, *4*, 418.
31. Duan, L.; Araujo, C. M.; Ahlquist, M. S. G.; Sun, L., Highly efficient and robust molecular ruthenium catalysts for water oxidation. *Proc. Natl. Acad. Sci.* **2012**, *109* (39), 15584-15588.
32. Xia, H.; Zhu, Y.; Lu, D.; Li, M.; Zhang, C.; Yang, B.; Ma, Y., Ruthenium(II) Complexes with the Mixed Ligands 2,2′-Bipyridine and 4,4′-Dialkyl Ester-2,2′-bipyridine as Pure Red Dopants for a Single-Layer Electrophosphorescent Device. *J. Phys. Chem. B* **2006**, *110* (37), 18718-18723.
33. Duan, L.; Xu, Y.; Gorlov, M.; Tong, L.; Andersson, S.; Sun, L., Chemical and Photochemical Water Oxidation Catalyzed by Mononuclear Ruthenium Complexes with a Negatively Charged Tridentate Ligand. *Chem.-Eur. J.* **2010**, *16* (15), 4659-4668.
34. Wang, L.; Duan, L.; Wang, Y.; Ahlquist, M. S. G.; Sun, L., Highly efficient and robust molecular water oxidation catalysts based on ruthenium complexes. *Chem. Commun.* **2014**, *50* (85), 12947-12950.

Chapter 2

Heterogeneous Photocatalytic Water Splitting as a Source of Redox Equivalents for Organic Synthesis

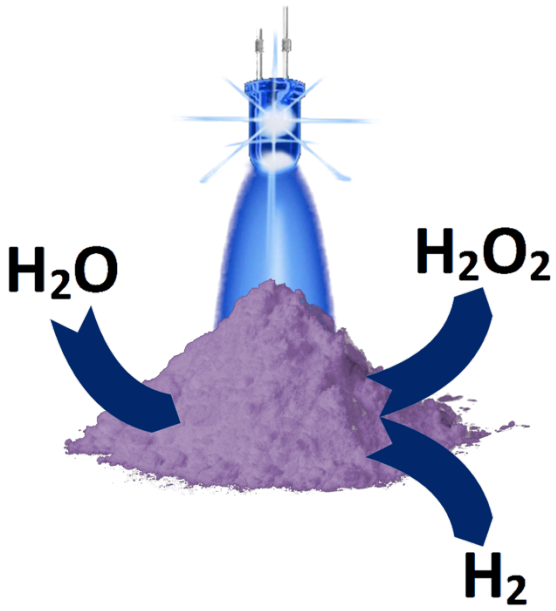

2.1 Feasibility of Heterogeneous Photocatalytic Water Splitting with Visible Light and Evaluation of Photocatalytic Properties of Titanium Disilicide

2.1.1 Introduction

The global energy consumption is constantly increasing—it is assumed to double by the year 2050 due to the population and industrial growth in developing countries. Also, approximately 85 % of the produced energy comes from fossil fuels, which are limited in amount and their burning is a major source of pollution.[1] These facts make the contemporary situation unsustainable and alternative, carbon-neutral sources have to be found.

Naturally, sunlight is the most promising alternative energy source. It is globally available and its energy supply greatly exceeds the needs of our society.[2] Therefore, this field has been extensively studied and the major challenge is to develop an efficient method for storage of the harvested energy, so it can be utilised also during the night and transported to locations lacking the needed infrastructure.[3]

One of the possible forms of storage are chemical fuels, compounds with high energy density produced in a process of "artificial photosynthesis". In nature, light is used to split water according to the following equation:

$$H_2O \rightarrow \frac{1}{2} O_2 + 2 H^+ + 2 e^- \qquad (2.1.1)$$

The resulting protons and electrons are subsequently utilised to form carbohydrates from CO_2 or to produce reducing agents, such as NADH.[4] From the industrial point of view, water could be a cheap and abundant source of oxygen as well as electrons, which can be used to produce fuels, *e.g.* hydrogen from water or methanol by the reduction of CO_2. This process—called water

splitting—and related photocatalytic systems were extensively studied in the past years.[3]

In their pioneering work, Fujishima and Honda demonstrated that TiO_2 and other semiconductors can be used to split water into oxygen and hydrogen upon irradiation.[5,6] In principle, a photon of an appropriate wavelength (which is determined by the band-gap energy of the semiconductor) is absorbed causing a charge separation generating an oxidative hole in the valence band and reductive free electron in the conduction band of the semiconductor (see Scheme 2.1.1).[7] Generated electrons and holes can then drive half-reactions (Equation 2.1.3 and 2.1.4) of the overall water splitting shown in Equation 2.1.2.

$$H_2O \rightarrow \tfrac{1}{2}\, O_2 + H_2 \qquad (2.1.2)$$

$$H_2O + 2\, h^+ \rightarrow \tfrac{1}{2}\, O_2 + 2\, H^+ \qquad (2.1.3)$$

$$2\, H^+ + 2\, e^- \rightarrow H_2 \qquad (2.1.4)$$

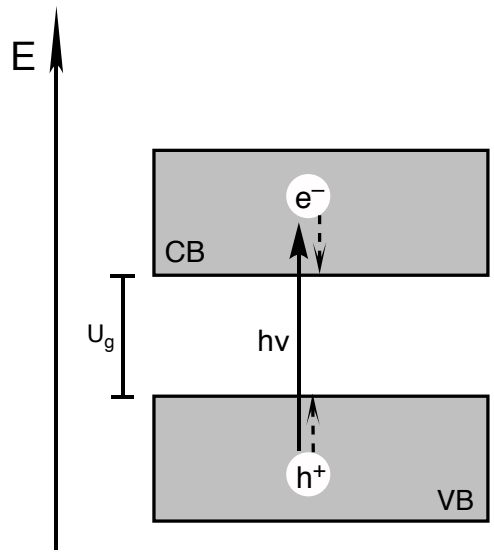

Scheme 2.1.1. Generation of charge-separated state in semiconductors. Solid arrow represents formation of free electron and hole upon absorption of photon, dashed arrows represent intraband thermalisation processes. Adapted from Ref. 8. *VB – valence band; CB – conduction band; U_g – band-gap energy*

The standard cell potential of reaction in Equation 2.1.2 is 1.229 V. Equations 2.1.3 and 2.1.4 show that splitting one molecule of water requires transfer of two electrons (two charge-separation processes), and therefore absorption of two photons. This means that each proton has to provide in average 1.229 eV of Gibbs free energy. Considering theoretical energy losses in a system represented in Scheme 2.1.1, Bolton *et al.* determined that band gap of at least 1.60 eV is required. This corresponds to light with wavelength of 775 nm and shorter. When considering a real semiconductor system, where energy losses will be even bigger, the threshold band gap needs to be 2.0 eV and higher, corresponding to a wavelength of 610 nm and shorter.[9] This proves that photocatalytic water splitting with a single-band-gap semiconductor system under visible light is theoretically possible. However, the practical application of such systems has several limitations, which will be discussed in following paragraphs.

The band-gap energy is not the only crucial factor for a successful water splitting. Band potentials are just as important. Valence band needs to be sufficiently positive for oxygen generation and conduction band needs to be sufficiently negative for hydrogen generation. For example, while TiO_2 is capable of water splitting in aqueous media,[5] oxygen generation in acetonitrile is practically impossible because of an insufficient oxidation potential caused by a solvent-related potential shift.[7,10] This has to be kept in mind when designing a semiconductor-based photocatalytic system.

Another practical problem is too broad band gap, especially in metal-oxide and metal-sulphide semiconductors. For example, TiO_2 has a band gap of 3.0 eV (corresponding to wavelength of 415 nm),[11] $SrTiO_3$ 3.2 eV (390 nm),[9] and ZnS even 3.6 eV (345 nm).[11] Although these materials are cheap and abundant, their application is limited to UV light, and therefore they are not appropriate for an efficient conversion of solar energy. To increase their absorbance in visible region, they can be doped with non-metals[12] or metal ions,[13,14] which generates accessible energy levels in semiconductor's forbidden band. However,

photocatalytic activity of doped semiconductors proved to be significantly lower compared with their non-doped counterparts.[15]

Another possible method is dye sensitisation. A redox-active dye absorbing visible light is adsorbed on the semiconductors surface. If its energy levels have a suitable position towards valence and conduction bands of the semiconductor, it can act as an electron donor (Scheme 2.1.2, left) or electron acceptor (Scheme 2.1.2, right). In case of acting as electron donor, which is much more common, the excited dye injects an electron into the semiconductor's conduction band. As a result, a follow-up redox reaction can occur where the oxidation half-reaction is carried out by the oxidised dye and reduction takes place on the surface of the semiconductor. If the dye acts as an electron acceptor, after its excitation it captures an electron from the valence band and can perform a reduction of given substrate, while the hole in the valence band acts as an oxidant.[7]

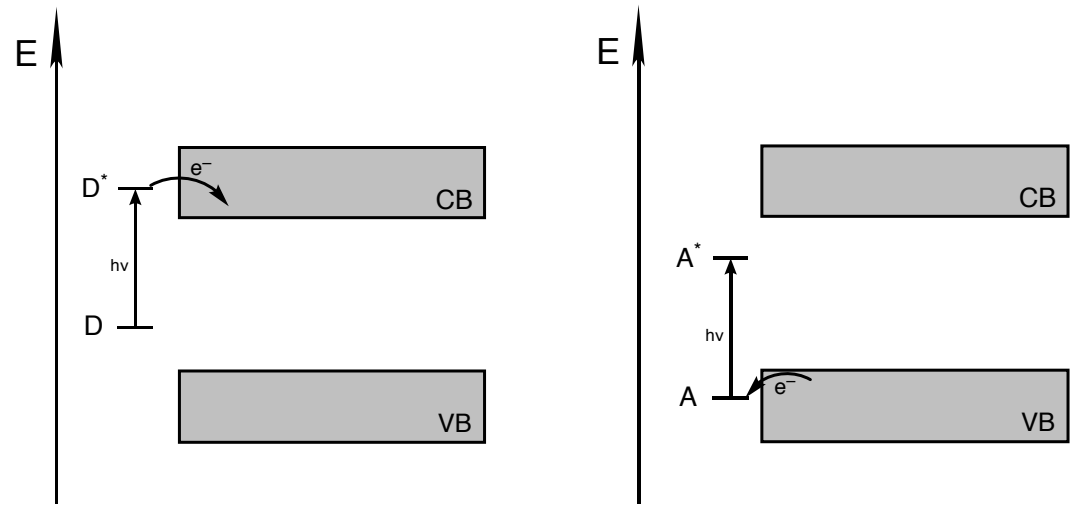

Scheme 2.1.2. Principle of dye sensitisation of semiconductors. Left – more common case where dye acts as an electron donor (D). Right – case where dye acts as an electron acceptor (A). Adapted from Ref. 7.
VB – valence band; CB – conduction band

Successful sensitisation for photocatalytic water reduction, *i.e.* generation of hydrogen in the presence of a sacrificial electron donor (triethanolamine

or hydroquinone), was achieved using *e.g.* xanthane dyes,[16] metalloporphyrins,[17] or ruthenium complexes[18]. Oxidation of water to oxygen with this method has two main limiting factors: possible insufficient oxidation potential of the photosensitising dye[17] and low stability of photosensitisers under strongly oxidative conditions.[19]

Another complication that has to be avoided is photocorrosion. Upon irradiation, the semiconductor can undergo destructive oxidative or reductive transformations. To find out if a given material is prone to decomposition, potentials of theoretical destructive reactions can be compared with potentials of band edges. If the reaction's potential lies within the forbidden band, it can take place upon irradiation. For example, TiO_2 can theoretically undergo reductive transformation depicted in Equation 2.1.5 or oxidative transformation depicted in Equation 2.1.6.[7]

$$TiO_2 + 4\ H^+ + 4\ e^- \rightarrow Ti + 2\ H_2O \qquad (2.1.5)$$

$$TiO_2 + 4\ Cl^- + 4\ h^+ \rightarrow TiCl_4 + O_2 \qquad (2.1.6)$$

Out of these two, only Reaction 2.1.6 lies within the forbidden band. Therefore, TiO_2 is stable against reductive degradation, but it can be oxidatively decomposed. However, competing oxidation of water (Equation 2.1.3) to oxygen has lower oxidation potential, thus this reaction takes place predominantly and acts as a photoprotection. Thus, TiO_2 is very stable in aqueous environments.[7] On the other hand, CdS—which has band-gap energy of 2.4 eV (520 nm),[11] and could be therefore potentially used as a visible-light photocatalyst—is prone to intensive photocorrosion in aqueous environments. It can undergo reactions depicted in Equations 2.1.7 and 2.1.8, which both lie within the forbidden band. Cadmium sulphide is especially liable to oxidative decomposition. A way to protect CdS photoanodes against photocorrosion is an addition of sulphide anions, which are more easily oxidised (Equation 2.1.9).[7]

$$CdS + 2\ e^- \rightarrow Cd + S^{2-} \quad (2.1.7)$$

$$CdS + 2\ h^+ \rightarrow Cd^{2+} + S \quad (2.1.8)$$

$$2\ S^{2-} + 2\ h^+ \rightarrow S_2^{2-} \quad (2.1.9)$$

Despite the abovementioned limitations, a wide variety of semiconductor systems claiming activity in additive-free water splitting under visible light was described in literature in recent years—materials based on mixed metal oxides (for overview see Dissertation of Melanie Hacker[20]), but also novel organic semiconductors, such as graphene oxide[21] or carbon nitride[22].

Considering the high complexity of abovementioned materials, it was surprising when the group of Demuth reported a photocatalytic water splitting to oxygen and hydrogen under visible-light irradiation using simple, unmodified titanium disilicide ($TiSi_2$), which is a cheap and commercially available material.[23] Goal of the project described in this part of Chapter 2 was to reproduce their results, evaluate photocatalytic activity of $TiSi_2$, and potentially apply this material in redox organic synthesis.

2.1.2 Results and discussion

2.1.2.1 Features of $TiSi_2$ described in literature

Measurements showed that $TiSi_2$ has a band gap ranging from 3.4 eV (360 nm) to 1.5 eV (800 nm), which is ideal for utilisation of the whole visible spectrum. Demuth's group stated that Fermi levels of the material are sufficient for hydrogen and oxygen generation via water splitting, but do not provide exact band-edge potentials under given conditions. They observed hydrogen evolution from aqueous suspensions at elevated temperature (55 °C) under UV (350±60 nm) and green (540±60 nm) irradiation with comparable kinetics and divided this

process into two phases. During Phase A, hydrogen is produced chemically through hydrolysis of $TiSi_2$ following Equation 2.1.10.

$$TiSi_2 + 6\ H_2O \rightarrow TiO_2 + 2\ SiO_2 + 6\ H_2 \qquad (2.1.10)$$

When heated in dark, the surface of the material passivates by forming a layer of titanium and silicon oxides and hydrogen evolution stops after ca 150 h. However, when light is applied during this phase, hydrogen evolution continues beyond the point of 150 h and proceeds photocatalytically in a linear fashion for hundreds of hours (Phase B). Since once passivated the material doesn't show photocatalytic activity, the group proposed a mechanism where catalytic centres are formed on the semiconductor's surface via photocorrosion during Phase A. Oxygen formed as the other product of water splitting is photoadsorbed on the material during the process and can be released by heating the suspension in dark to 100 °C. Photocatalytic nature of this process was supported by three arguments: 1) Hydrogen production in a continuous run exceeded 12 times the stoichiometric amount of hydrogen that would be theoretically produced by a full hydrolysis of the material; 2) Amount of released hydrogen and oxygen was in 2:1 ratio; 3) Formation of $^{18}O_2$ was observed in ^{18}O-enriched water.[23]

2.1.2.2 Behaviour of $TiSi_2$ in aqueous suspensions

Different light sources

For our studies, we have purchased two batches of $TiSi_2$ (hereafter referred to as *Batch 1* and *Batch 2*). Although both were from the same manufacturer with the same product number and the same declared particle size (~200 mesh), they manifested a significantly different behaviour in aqueous suspensions upon irradiation. When the amount of hydrogen generated under different lighting

conditions after 24 hours using fresh $TiSi_2$—and therefore within Phase A—was compared, it was observed that reaction in dark and under blue light (455 nm) generated approximately the same amount of H_2. This is in direct contradiction with Demuth's report, who claims a significantly (ca 20-fold) higher H_2 outcome under irradiation. More interestingly, behaviour of *Batch 1* seemed to be wavelength-dependent—blue light did not make a difference, but green (535 nm) and especially UV (375 nm) light were supressing hydrogen evolution (see Figure 2.1.1). On the other hand, *Batch 2* not only had a higher overall activity, but the presence of light—no matter of which wavelength—had no significant effect on the reaction outcome (see Figure 2.1.2).

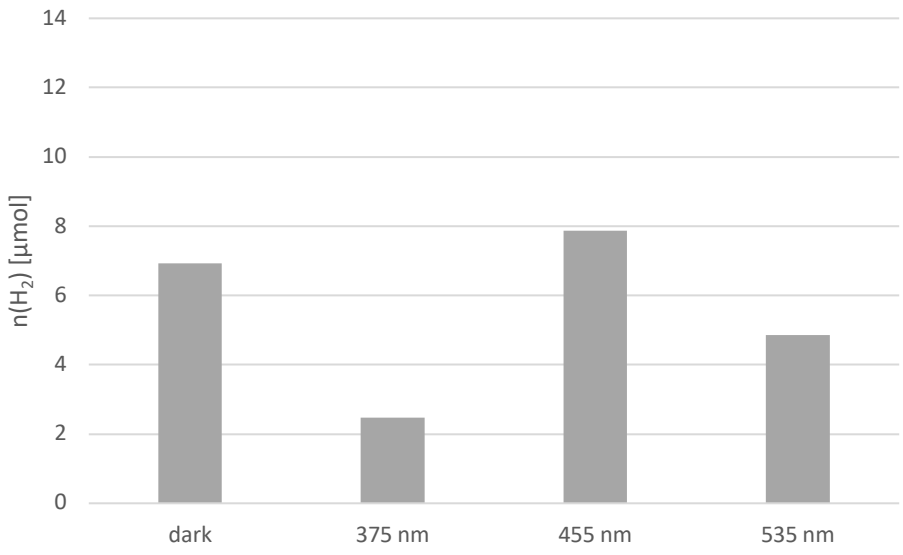

Figure 2.1.1. Amount of hydrogen evolved from $TiSi_2$ *Batch 1* after 24 hours under different lighting conditions (*crimp-top vial, 65 °C, 54 mg $TiSi_2$, 4.5 mL H_2O*).

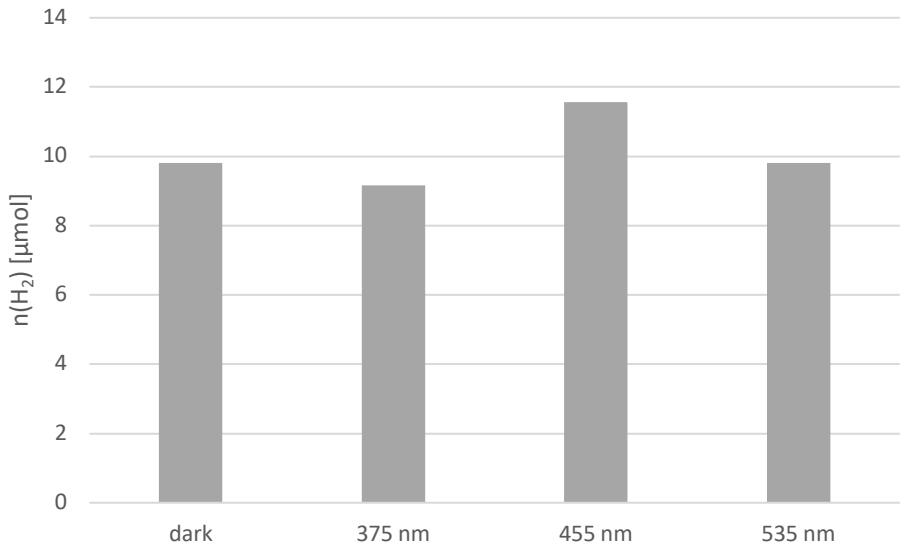

Figure 2.1.2. Amount of hydrogen evolved from $TiSi_2$ *Batch 2* after 24 hours under different lighting conditions (*crimp-top vial, 65 ℃, 54 mg $TiSi_2$, 4.5 mL H_2O*).

In addition, kinetic measurements monitoring the amount of evolved hydrogen in time showed a significantly different behaviour between the two batches. Hydrogen production using *Batch 1* ceased after ca 90 hours, which is significantly earlier than literature-reported 150 h. Irradiation again showed different outcomes in terms of overall hydrogen production, but most importantly, H_2 evolution in irradiated reactions slowed down and stopped with the same rate as the dark reaction and no transition into Phase B took place (see Figure 2.1.3). *Batch 2* behaved as theoretically expected—dark reaction stopped after ca 150 hours, while reactions under blue and green irradiation continued beyond this point in a linear fashion. However, within the first 120 hours, both light and dark reactions generated comparable amounts of hydrogen (see Figure 2.1.4).

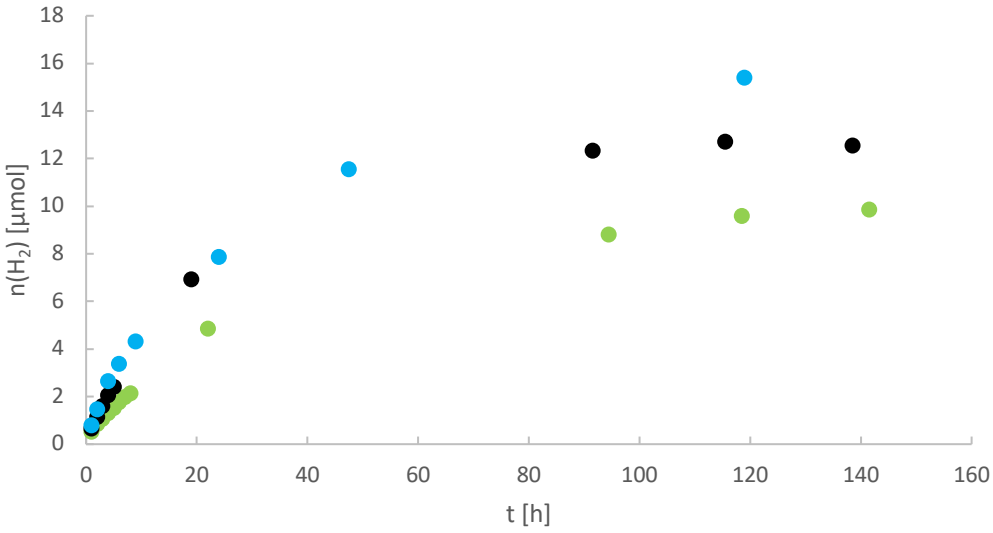

Figure 2.1.3. Development of hydrogen evolution in time using $TiSi_2$ *Batch 1* under different lighting conditions (*crimp-top vial, 65 °C, 54 mg* $TiSi_2$*, 4.5 mL* H_2O*). black* – dark, *blue* – 455 nm, *green* – 535 nm

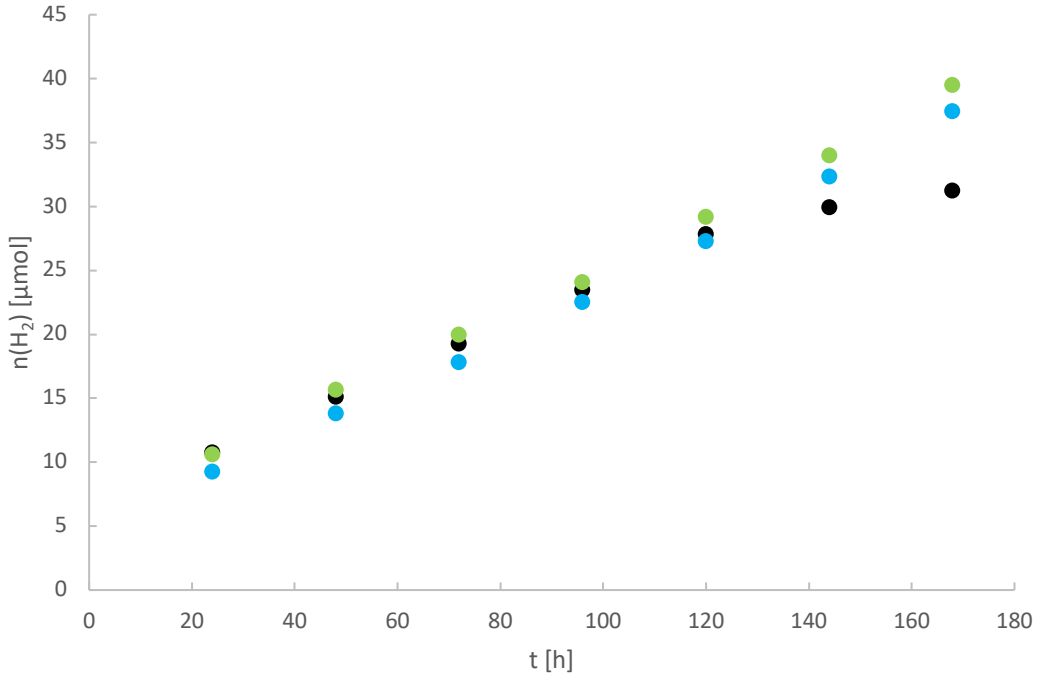

Figure 2.1.4. Development of hydrogen evolution in time using $TiSi_2$ *Batch 2* under different lighting conditions (*crimp-top vial, 65 °C, 54 mg* $TiSi_2$*, 4.5 mL* H_2O*). black* – dark, *blue* – 455 nm, *green* – 535 nm

Better results with *Batch 1* were achieved using a light source with broad emission. When irradiated with a halogen light bulb (emission spectrum

in Figure 2.1.5), hydrogen evolution was not only higher than in the case of the dark reaction, but also it did not stop and continued in relatively linear fashion for over 500 hours (see Figure 2.1.6). For this purpose, the reaction was performed in a cylindrical photoreactor tempered with inner heating circuit and irradiated from the outside using either circular green-LED array or three lamps equipped with halogen bulbs. Comparative irradiation with green LEDs showed suppressed hydrogen evolution and the reaction stopped after ca 100 hours.

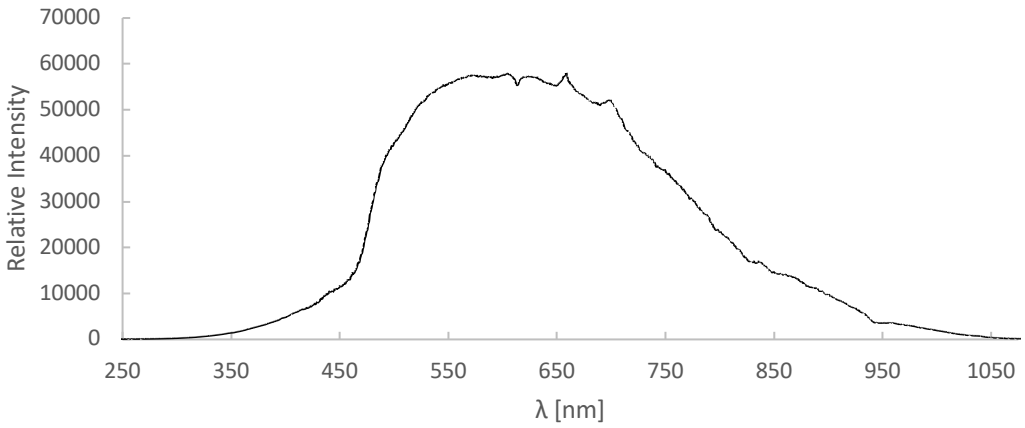

Figure 2.1.5. Emission spectrum of halogen light bulb.

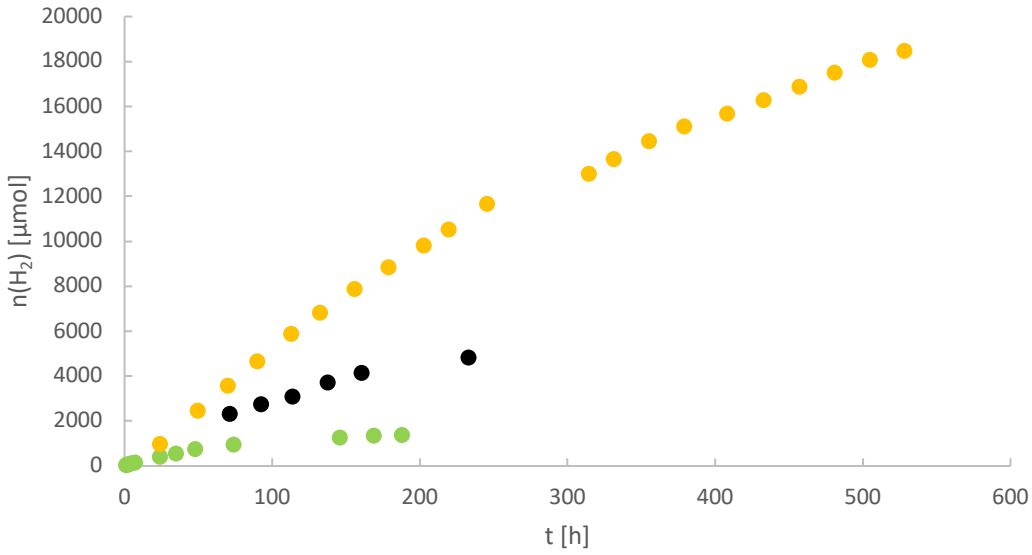

Figure 2.1.6. Development of hydrogen evolution in time under different lighting conditions using $TiSi_2$ *Batch 1* (*reactor, 65 ℃, 1440 mg* $TiSi_2$*, 120 mL* H_2O). *black* – dark; *green* – 535 nm; *orange* – halogen

Irradiation of *Batch 2* in the photoreactor with cool-white LED lamps (another broad-emission light source, spectrum depicted in Figure 2.1.7) also showed a linear generation of hydrogen within at least 500 hours and the amount of evolved H_2 was comparable to *Batch 1* under halogen-bulb irradiation.

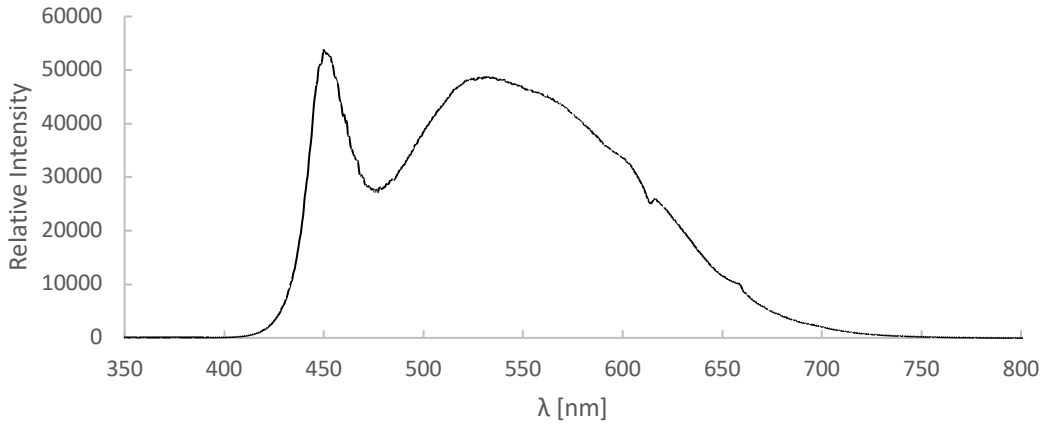

Figure 2.1.7. Emission spectrum of 6500 K cool-white LED.

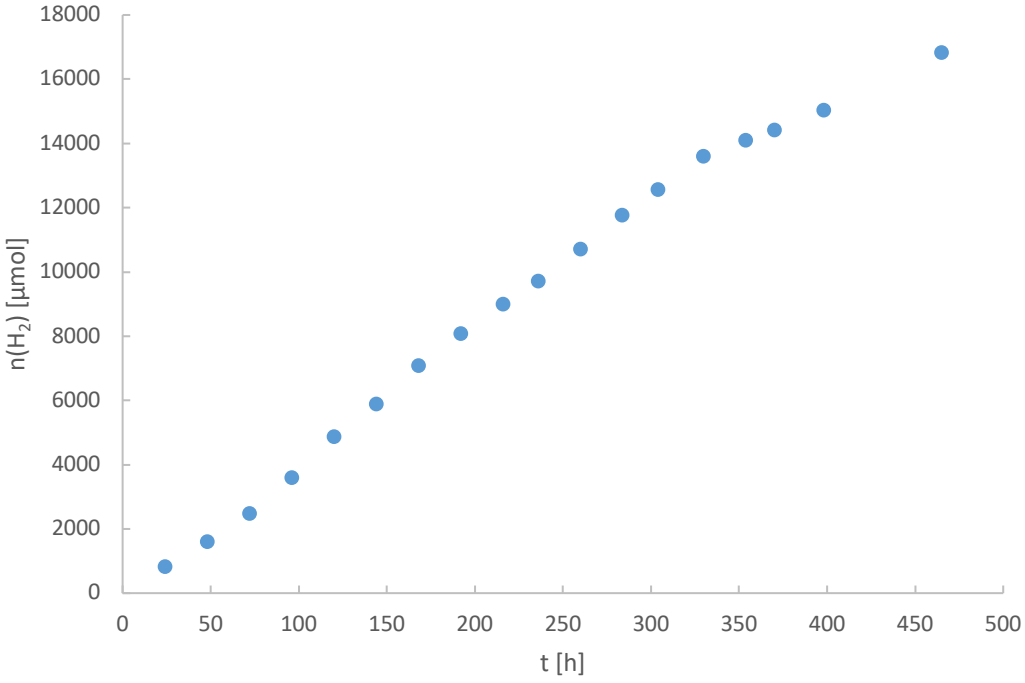

Figure 2.1.8. Development of hydrogen evolution in time under 6500 K cool-white LED lamp using $TiSi_2$ *Batch 2* (*reactor, 65 ℃, 1440 mg* $TiSi_2$*, 120 mL* H_2O).

Rate of hydrogen evolution depicted in Figures 2.1.6 and 2.1.8 was ca 600 μmol per 1 g of $TiSi_2$ per 24 hours. This seems to be a limiting value, since it was achieved independently using two different batches and two different irradiation sources. However, this value means that reaching and exceeding the amount of hydrogen equivalent to a stoichiometric hydrolysis of $TiSi_2$ (Equation 2.1.10) to prove that photocatalytic water splitting takes place would take at least 96 days. Therefore, Demuth's claim of reaching 12 equivalents of generated H_2 seems implausible.

Pre-irradiation of the photocatalyst

Linear evolution of hydrogen shown in Figures 2.1.6 and 2.1.8 suggested that Phase B—where only photocatalytic water splitting takes place—was reached. To test this assumption, a sample of a suspension of $TiSi_2$ *Batch 2* irradiated previously for 370 hours with cool-white LED lamps was collected. The sample was divided into two parts—one was left in its original suspension, the other was centrifuged, the solid phase was removed, washed several times with distilled water, dried, and resuspended in fresh distilled water. The obtained suspensions were then further divided into two parts—one was irradiated for 24 hours at 65 °C with green LED (535 nm), the other was stirred in dark for 24 hours at 65 °C. Theoretically, only traces of hydrogen should have been detected in samples left in dark, while irradiated samples should have kept producing H_2 at their original rate. However, results of this experiment in Figure 2.1.9 show that both irradiated and non-irradiated samples produced a comparable amount of hydrogen suggesting that even after 370 hours of visible-light irradiation, $TiSi_2$ is still prone to hydrolysis, even though its surface should be already passivated bearing developed photocatalytic centres.

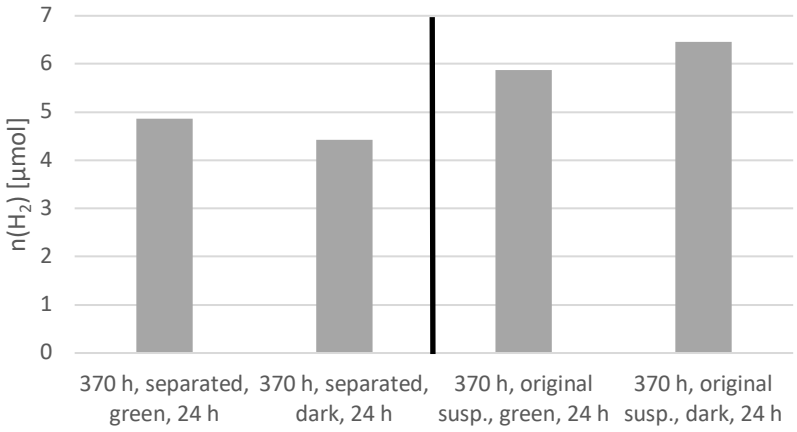

Figure 2.1.9. Amount of hydrogen generated in 24 hours using a pre-treated $TiSi_2$ *Batch* 2 under green-light irradiation and in dark (*crimp-top vial, 65 °C, 54 mg* $TiSi_2$*, 4.5 mL* H_2O*).* *separated* – catalyst that was separated, washed, and dried prior to the experiment; *original susp.* – catalyst left in the original suspension

Reactivation of passivated $TiSi_2$

The observation described in the previous section suggests that light has a different role in $TiSi_2$-mediated generation of hydrogen than expected. Rather than causing a photocatalytic water splitting, it prevents the material's surface from passivation—either via photocorrosion or through a simple localised thermal effect—and keeps it hydrolytically active. To examine the possibility of thermal reactivation of once passivated $TiSi_2$, *Batch 2* was heated in dark for 160 hours till no further generation of hydrogen was observed. The material was separated by centrifugation, washed with fresh distilled water, dried at 70 °C overnight, and divided into four samples. First sample was left without further treatment, second one was heated to 200 °C under nitrogen atmosphere for 1 hour, third one was heated to 200 °C in vacuum for 1 hour, and fourth one was boiled in distilled water for 1 hour. All samples were then resuspended in fresh distilled water, heated to 65 °C for 24 hours in dark, and the amount of generated hydrogen was compared with fresh *Batch 2* $TiSi_2$. Results in Figure 2.1.10 show that by boiling in water, it is possible to disrupt passivation layer on the surface of inactivated $TiSi_2$, which then becomes prone to further hydrolysis.

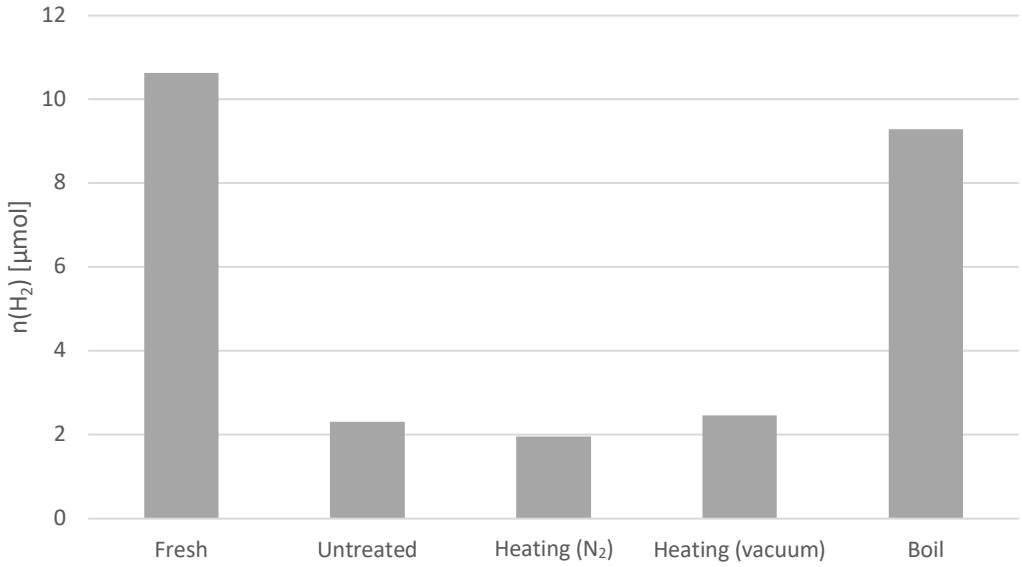

Figure 2.1.10. Comparison of activity (amount of generated hydrogen after 24 hours of irradiation) of passivated $TiSi_2$ *Batch 2* after different reactivation treatments with an untreated sample and a fresh material (*crimp-top vial, 65 ℃, 54 mg* $TiSi_2$*, dark*).

Energy-dispersive X-ray spectroscopic analysis (EDX) of fresh, passivated, and reactivated *Batch 2* $TiSi_2$ showed that while the fresh sample contains only minor amount of oxygen, its content in both passivated and reactivated samples is significantly increased. This suggests that while boiling in water, the passivated layer is only disrupted, rather than completely removed from the surface. These disruptions caused by photocorrosion, which keep the material active under irradiation, could have been falsely mistaken by Demuth's group for catalytic centres.

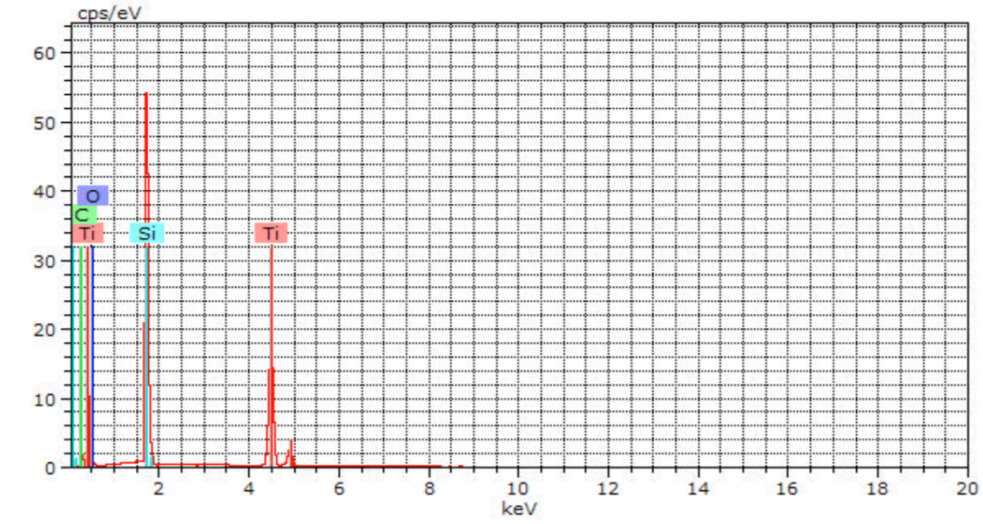

Spc0 Datum:01.06.2005 21:28:53 HV:20.0kV ImpD.:12.11kcps

El	OZ	Serie	unn. C [Gew.%]	norm. C [Gew.%]	Atom. C [At.%]	Fehler [%]
Ti	22	K-Serie	47.09	47.44	31.19	1.3
C	6	K-Serie	4.11	4.14	10.86	0.7
O	8	K-Serie	4.32	4.36	8.57	7.1
Si	14	K-Serie	43.73	44.06	49.38	1.9
		Summe:	99.25	100.00	100.00	

Figure 2.1.11. EDX analysis of fresh *Batch 2* $TiSi_2$.

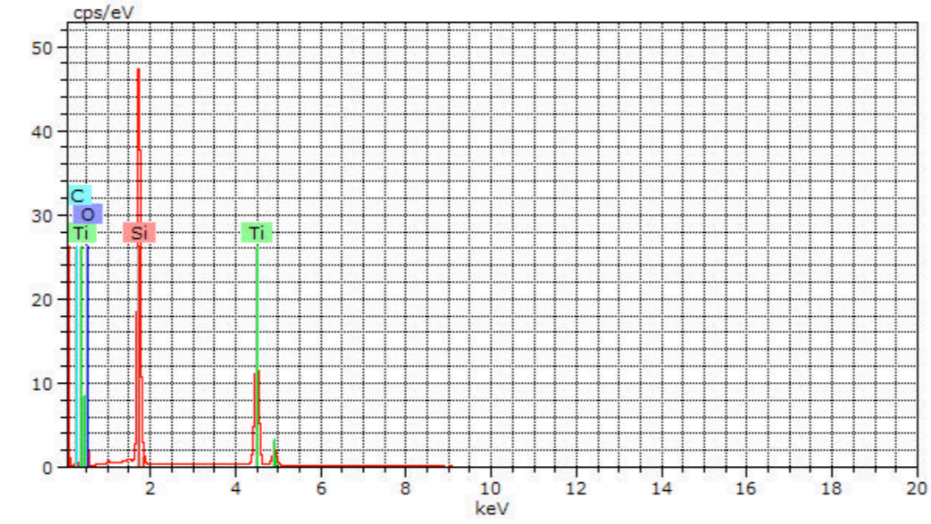

Spc0 Datum:01.06.2005 21:43:17 HV:20.0kV ImpD.:11.14kcps

El	OZ	Serie	unn. C [Gew.%]	norm. C [Gew.%]	Atom. C [At.%]	Fehler [%]
Si	14	K-Serie	39.98	35.56	31.56	1.7
Ti	22	K-Serie	36.17	32.18	16.75	1.0
O	8	K-Serie	33.12	29.46	45.90	21.0
C	6	K-Serie	3.14	2.79	5.80	0.5
		Summe:	112.41	100.00	100.00	

Figure 2.1.12. EDX analysis of passivated *Batch 2* $TiSi_2$.

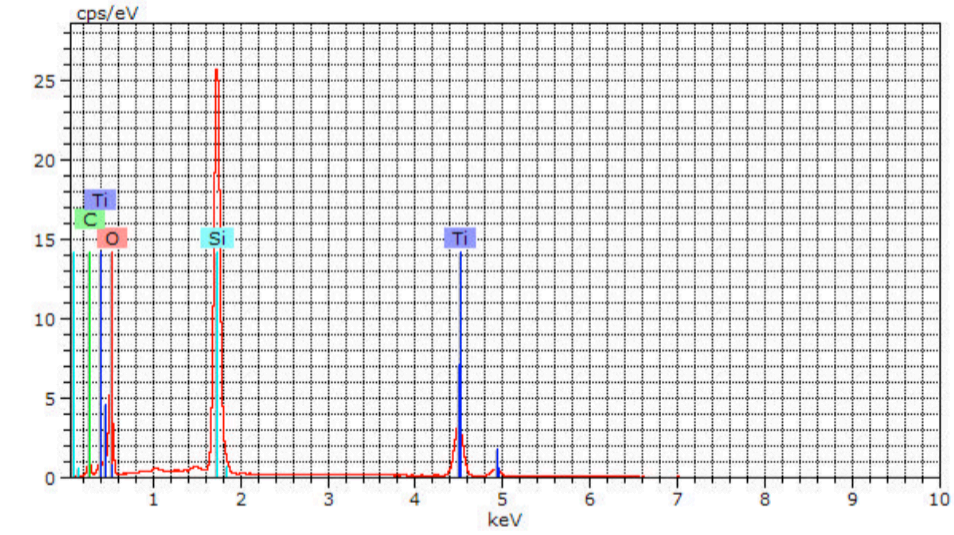

El	OZ	Serie	unn. C [Gew.%]	norm. C [Gew.%]	Atom. C [At.%]	Fehler [%]
O	8	K-Serie	22.47	19.15	31.74	10.5
C	6	K-Serie	2.98	2.54	5.60	0.5
Ti	22	K-Serie	33.94	28.93	16.02	1.2
Si	14	K-Serie	57.94	49.38	46.63	2.4
		Summe:	117.32	100.00	100.00	

Figure 2.1.13. EDX analysis of reactivated *Batch 2* $TiSi_2$.

2.1.3 Conclusions

The behaviour of titanium disilicide in aqueous suspensions in the dark and under irradiation presented and discussed in this subchapter suggests that claims about efficient visible-light-photocatalytic water splitting to oxygen and hydrogen using this material as a catalyst published by the group of Demuth[23] might be incorrect.

It was possible to reproduce results where hydrogen evolution ceases after 150 hours of heating in the dark, but continues in a linear fashion for hundreds of hours under visible-light irradiation. However, amounts of hydrogen generated within the first 150 hours were almost the same in both dark and light reactions. This contradicts published observation that light reactions produce ca 20-times higher amounts of hydrogen than dark reactions. Also, the highest achieved rate of hydrogen evolution was 600 μmol per gram per day, which is too slow and makes exceeding stoichiometric amounts of produced hydrogen—

presented as a main proof of catalytic activity of $TiSi_2$—highly unlikely in practical terms.

Further experiments showed that when irradiated, the material can undergo hydrolysis even after spending 370 hours in aqueous suspension at elevated temperature and amounts of hydrolytically produced hydrogen are comparable to amounts generated under further irradiation. In dark, the material is passivated and hydrolytically inactive already after 150 hours. However, it can be reactivated by boiling in distilled water.

Observations summarised above suggest that light has a different role in this reaction than assumed. It does not cause water splitting via semiconductor-mediated photocatalysis, but it prevents build-up of uniform, passivating oxide layers on the surface of $TiSi_2$ and keeps the material hydrolytically active. Therefore, we propose that all observed hydrogen is generated chemically via $TiSi_2$ hydrolysis shown in Equation 2.1.10 and the material cannot be efficiently used as a photocatalyst for water splitting.

However, our experiments do not explain the formation of oxygen in 1:2 ratio to hydrogen also observed by Demuth's group.

2.1.4 Experimental section

2.1.4.1 General methods and materials

Head-space CG measurements were performed on INFICON 3000 Micro GC equipped with MS-5A column and thermal conductivity detector using argon as a carrier gas.

Light-source emission spectra were obtained with Avantes AvaSpec-3648 spectrometer.

Elemental analysis was performed on digital scanning electron microscope Zeiss DSM 940 A equipped with EDX detector. The samples were mounted on carbon

tape and studied with the following operating parameters: working distance 9–35 mm, 10–20 kV, enlargement 100–1000x.

Samples were irradiated using lamps equipped with OSRAM Halogen Superstar light bulbs (400 W, 8750 lm) or Yuiip Cool-White LED light bulbs (6500 K, 10 W, 1100 lm).

$TiSi_2$ was purchased from Alfa Aesar (99.5 % (metal basis), ~200 mesh powder).

2.1.4.2 General procedure for hydrogen generation in a vial

$TiSi_2$ (54 mg) was suspended in 4.5 mL of distilled water in a crimp-top vial equipped with a stirrer. Vial was sealed with a septum and the content was flushed with nitrogen several times. The vial was placed in an aluminium block tempered to 65 °C and irradiated from the bottom with LEDs of selected wavelength under stirring. In a case of a dark reaction, the whole block was covered in aluminium foil. In selected time intervals, the vial was taken out and a hydrogen content was measured by a head-space GC. After each measurement, vial was opened, sealed with a new septum, flushed with nitrogen, and put back in the aluminium block.

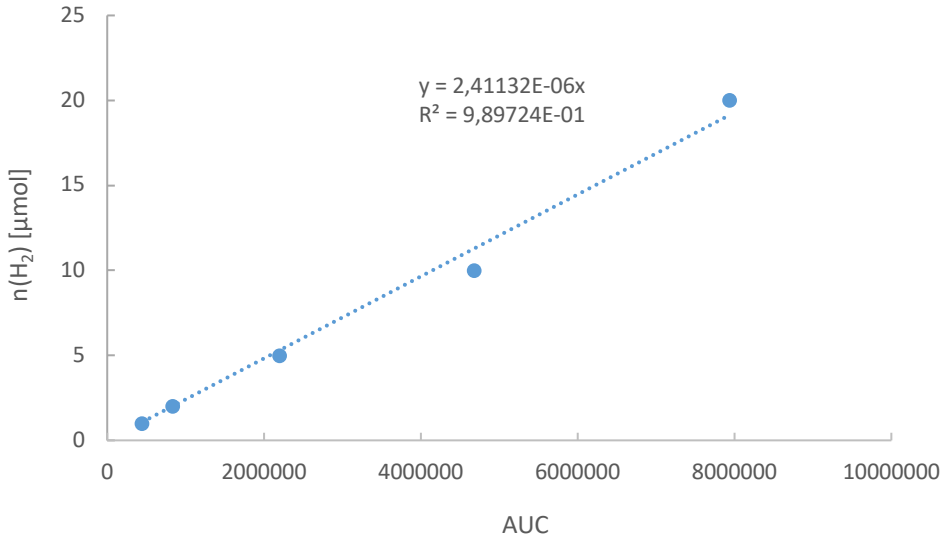

Figure 2.1.14. Calibration curve for head-space GC for crimp-top vials containing 4.5 mL of water.

2.1.4.3 General procedure for hydrogen generation in a photoreactor

$TiSi_2$ (1440 mg) was suspended in 120 mL of water in a photoreactor. One of the openings was closed with a glass stopper, the other one with a rubber septum, and the content was flushed with nitrogen several times. Reactor's cooling/heating circuit was connected to a thermostat set to 65 °C and it was irradiated from the outside (circular LED setup or lamps) under stirring. In a case of a dark reaction, the whole reactor was covered in aluminium foil. In selected intervals, the reactor was disconnected and hydrogen content was measured by head-space GC through the rubber septum. After each measurement, the gas phase was released, new septum was applied, content was flushed with nitrogen several times, reactor was connected back, and the system was further irradiated.

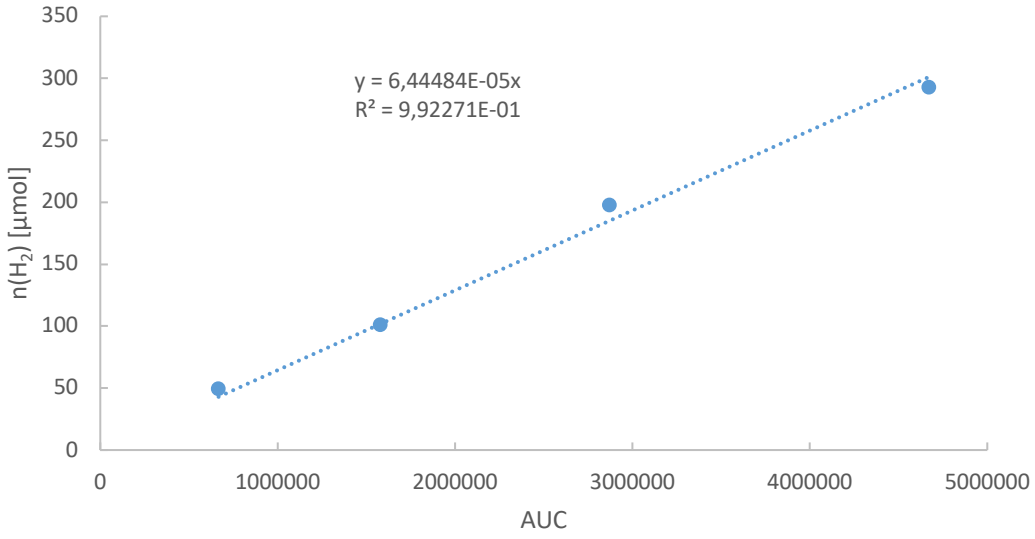

Figure 2.1.15. Calibration curve for head-space GC for photoreactor containing 120 mL of water.

2.1.4.4 Analysis of pre-irradiated $TiSi_2$

$TiSi_2$ (1440 mg) was suspended in 120 mL of water in a photoreactor. One of the openings was closed with a glass stopper, the other one with a rubber septum, and the content was flushed with nitrogen several times. Reactor's cooling/heating circuit was connected to a thermostat set to 65 °C and it was irradiated from the outside with two lamps equipped with cool-white LED light bulbs under stirring. Every 24 hours, the reactor was disconnected and hydrogen content was measured by a head-space GC through the rubber septum. After each measurement, the gas phase was released, new septum was applied, the content was flushed with nitrogen several times, the reactor was connected back, and the system was further irradiated. After 370 hours, 30 mL of reaction suspension was extracted and divided into two equal parts.

First part was transferred directly into small crimp-top vials (two-times 4.5 mL of suspension) equipped with magnetic stirring bars, the vials were sealed with septa and the head space was flushed with nitrogen. Vials were placed into aluminium heating blocks tempered to 65 °C and stirred for 24 hours. One of them was irradiated with a green LED (535 nm), the other one was covered in aluminium foil. After 24 hours, the amount of generated hydrogen was analysed using a head-space GC.

Second part was centrifuged for 15 minutes. Afterwards, the supernatant liquid was replaced with distilled water, suspension was thoroughly shaken and centrifuged again for 15 minutes. This step was repeated two more times. The solid residue was then removed and dried at 70 °C overnight. Two-times 54 mg of the dried catalyst was weighed into small crimp-top vials containing a magnetic stirrer, 4.5 mL of distilled water was added, vials were sealed with septa, and the head space was flushed with nitrogen. Vials were placed into aluminium heating blocks tempered to 65 °C and stirred for 24 hours. One of them was irradiated with a green LED (535 nm), the other one was

covered in aluminium foil. After 24 hours, the amount of generated hydrogen was analysed using a head-space GC.

2.1.4.5 Recovery of passivated $TiSi_2$

Hydrogen evolution reaction was run in a photoreactor in dark as described in Section 2.1.4.3 until no hydrogen generation was detected between two measurements. Suspension was then removed from the reactor and centrifuged for 15 minutes to separate the solid phase. Afterwards, the supernatant liquid was replaced with distilled water, suspension was thoroughly shaken and centrifuged again for 15 minutes. This step was repeated two more times. The solid residue was then removed and dried at 70 °C overnight.

2.1.4.6 $TiSi_2$ reactivation by heating under nitrogen

Recovered $TiSi_2$ (100 mg) was sealed in a crimp-top vial, content was flushed with nitrogen several times, and heated to 200 °C with a heat gun for 1 hour. After cooling down, the material was used for hydrogen-evolution reaction in the dark as described in Section 2.1.4.2.

2.1.4.7 $TiSi_2$ reactivation by heating under vacuum

Recovered $TiSi_2$ (100 mg) was sealed in a crimp-top vial, connected to a membrane pump (6 mbar) via syringe, and heated to 200 °C with a heat gun for 1 hour. After cooling down, the material was used for hydrogen-evolution reaction in the dark as described in Section 2.1.4.2.

2.1.4.8 $TiSi_2$ reactivation by boiling in water

Recovered $TiSi_2$ (200 mg) was suspended in distilled water (15 mL) in 50 mL round-bottom flask and refluxed for one hour. After cooling down, the catalyst was separated by centrifugation, washed with distilled water two times and dried at 70 °C overnight. Afterwards, the material was used for hydrogen-evolution reaction in dark as described in Section 2.1.4.2.

2.1.5 Contributions

EDX measurements were performed by Melanie Iwanow (Fraunhofer IGB, Straubing, Germany).

2.1.6 References

1. Barber, J.; Tran, P. D., From natural to artificial photosynthesis. *J. R. Soc. Interface* **2013**, *10* (81).
2. Lewis, N. S.; Nocera, D. G., Powering the planet: Chemical challenges in solar energy utilization. *P. Natl. Acad. Sci.* **2006**, *103* (43), 15729-15735.
3. Cook, T. R.; Dogutan, D. K.; Reece, S. Y.; Surendranath, Y.; Teets, T. S.; Nocera, D. G., Solar Energy Supply and Storage for the Legacy and Nonlegacy Worlds. *Chem. Rev.* **2010**, *110* (11), 6474-6502.
4. Hambourger, M.; Moore, G. F.; Kramer, D. M.; Gust, D.; Moore, A. L.; Moore, T. A., Biology and technology for photochemical fuel production. *Chem. Soc. Rev.* **2009**, *38* (1), 25-35.
5. Fujishima, A.; Honda, K., Electrochemical Photolysis of Water at a Semiconductor Electrode. *Nature* **1972**, *238*, 37.
6. Fujishima, A.; Honda, K., Electrochemical Evidence for the Mechanism of the Primary Stage of Photosynthesis. *B. Chem. Soc. Jpn.* **1971**, *44* (4), 1148-1150.

7. Gurevich, Y. Y.; Pleskov, Y. V., Chapter 4 Photoelectrochemistry of Semiconductors. In *Semiconductors and Semimetals*, Willardson, R. K.; Beer, A. C., Eds. Elsevier: 1983; Vol. 19, pp 255-328.
8. Archer, M. D.; Bolton, J. R., Requirements for ideal performance of photochemical and photovoltaic solar energy converters. *J. Phys. Chem.-US* **1990**, *94* (21), 8028-8036.
9. Bolton, J. R.; Strickler, S. J.; Connolly, J. S., Limiting and realizable efficiencies of solar photolysis of water. *Nature* **1985**, *316*, 495.
10. Cherevatskaya, M.; Neumann, M.; Füldner, S.; Harlander, C.; Kümmel, S.; Dankesreiter, S.; Pfitzner, A.; Zeitler, K.; König, B., Visible-Light-Promoted Stereoselective Alkylation by Combining Heterogeneous Photocatalysis with Organocatalysis. *Angew. Chem. Int. Ed.* **2012**, *51* (17), 4062-4066.
11. Kisch, H., Semiconductor Photocatalysis for Organic Synthesis. In *Advances in Photochemistry*, 2001.
12. Asahi, R.; Morikawa, T.; Ohwaki, T.; Aoki, K.; Taga, Y., Visible-Light Photocatalysis in Nitrogen-Doped Titanium Oxides. *Science* **2001**, *293* (5528), 269-271.
13. Herrmann, J.-M.; Disdier, J.; Pichat, P., Effect of chromium doping on the electrical and catalytic properties of powder titania under UV and visible illumination. *Chem. Phys. Lett.* **1984**, *108* (6), 618-622.
14. Serpone, N.; Lawless, D.; Disdier, J.; Herrmann, J.-M., Spectroscopic, Photoconductivity, and Photocatalytic Studies of TiO2 Colloids: Naked and with the Lattice Doped with Cr3+, Fe3+, and V5+ Cations. *Langmuir* **1994**, *10* (3), 643-652.
15. Kato, H.; Kudo, A., Visible-Light-Response and Photocatalytic Activities of TiO2 and SrTiO3 Photocatalysts Codoped with Antimony and Chromium. *J. Phys. Chem. B* **2002**, *106* (19), 5029-5034.

16. Shimidzu, T.; Iyoda, T.; Koide, Y., An advanced visible-light-induced water reduction with dye-sensitized semiconductor powder catalyst. *J. Am. Chem. Soc.* **1985**, *107* (1), 35-41.
17. Breddels, P. A.; Blasse, G., Spectral sensitization of SrTiO3 electrodes with magnesium tetraphenylporphene. *Chem. Phys. Lett.* **1981**, *79* (2), 209-213.
18. Dabestani, R.; Bard, A. J.; Campion, A.; Fox, M. A.; Mallouk, T. E.; Webber, S. E.; White, J. M., Sensitization of titanium dioxide and strontium titanate electrodes by ruthenium(II) tris(2,2'-bipyridine-4,4'-dicarboxylic acid) and zinc tetrakis(4-carboxyphenyl)porphyrin: an evaluation of sensitization efficiency for component photoelectrodes in a multipanel device. *J. Phys. Chem.-US* **1988**, *92* (7), 1872-1878.
19. Wang, L.; Duan, L.; Tong, L.; Sun, L., Visible light-driven water oxidation catalyzed by mononuclear ruthenium complexes. *J. Catal.* **2013**, *306*, 129-132.
20. Hacker, M. Reversed vesicular membranes and photobiocatalytic reduction systems. University of Regensburg, Regensburg, Germany, 2017.
21. Hou, W.-C.; Wang, Y.-S., Photocatalytic Generation of H2O2 by Graphene Oxide in Organic Electron Donor-Free Condition under Sunlight. *ACS Sustain. Chem. Eng.* **2017**, *5* (4), 2994-3001.
22. Guo, F.; Shi, W.; Zhu, C.; Li, H.; Kang, Z., CoO and g-C3N4 complement each other for highly efficient overall water splitting under visible light. *Appl. Catal. B-Environ.* **2018**, *226*, 412-420.
23. Ritterskamp, P.; Kuklya, A.; Wüstkamp, M.-A.; Kerpen, K.; Weidenthaler, C.; Demuth, M., A Titanium Disilicide Derived Semiconducting Catalyst for Water Splitting under Solar Radiation—Reversible Storage of Oxygen and Hydrogen. *Angew. Chem. Int. Ed.* **2007**, *46* (41), 7770-7774.

2.2 Evaluation of Gold-Doped Titanium Dioxide as a Heterogeneous Photocatalyst for Additive-Free Water Splitting

2.2.1 Introduction

One possible method of employing water as a source of redox equivalents for organic synthesis is an indirect approach, where electrons obtained by water oxidation are used to generate a highly energetic, redox-active compound, which subsequently undergoes a desired reaction. Ideal candidate for this task is hydrogen peroxide. It's usually being used as an oxidant—while producing only water as a by-product, so it can be considered a "green" reagent—but it can also act as a reductant or undergo redox-neutral reactions, such as additions and substitutions.[1,2]

Heterogeneous, photocatalytic generation of hydrogen peroxide from water can be simply achieved by UV irradiation of unmodified titanium dioxide in oxygenated aqueous suspensions through water oxidation and subsequent oxygen reduction, or via recombination of hydroxyl radicals. However, this process has a very low efficiency and a steady-state concentration of H_2O_2 is only around 1 μM.[3] One reason is a quick recombination of photogenerated electron–hole pair before it can reach the semiconductor's surface from the bulk wasting invested energy as heat.[4,5] The other, more important reason is a photocatalytic decomposition of hydrogen peroxide, which occurs under both UV (via direct reduction, Equation 2.2.1) and visible-light (via generation of surface complexes, Equations 2.2.2–2.2.5) irradiation.[6]

$$H_2O_2 + e^- \rightarrow {}^{\bullet}OH + OH^- \quad (2.2.1)$$

$$(Ti^{IV}—OH)_{surf} + H_2O_2 \rightarrow (Ti^{IV}—OOH)_{surf} + H_2O \quad (2.2.2)$$

$$(Ti^{IV}—OOH)_{surf} + h\nu \rightarrow (Ti^{IV}—OOH)^*_{surf} \quad (2.2.3)$$

$$(Ti^{IV}—OOH)^{*}_{surf} \rightarrow (Ti^{IV}—{}^{+\bullet}OOH)_{surf} + e^{-} \quad (2.2.4)$$

$$(Ti^{IV}—{}^{+\bullet}OOH)_{surf} + OH^{-} \rightarrow (Ti^{IV}—OH)_{surf} + ½\ H_2O_2 + ½\ O_2 \quad (2.2.5)$$

One possible way to increase the efficiency of H_2O_2 generation is a modification of the semiconductor's surface, such as fluorination, which prevents the formation of surface peroxides (Equation 2.2.2).[7] Another way is a direct modification of the material's electronic properties. The group of Hiroaki Tada reported a use of TiO_2 doped with gold nanoparticles (AuNP) for an efficient generation of hydrogen peroxide under both UV[8] and visible-light[9] irradiation. These materials—also called plasmonic photocatalysts for exhibiting a localised surface plasmon resonance (LSPR) effect—were previously used for a wide variety of visible-light-catalysed, redox organic transformations.[10] In principle, AuNP absorbs a photon in a visible range and the excited electron is injected into the conduction band of the adjacent semiconductor, thus forming a reduction site on the semiconductor's surface and an oxidation site on the gold surface.[11] For H_2O_2 generation, Tada introduced two systems with different proposed mechanisms of action.

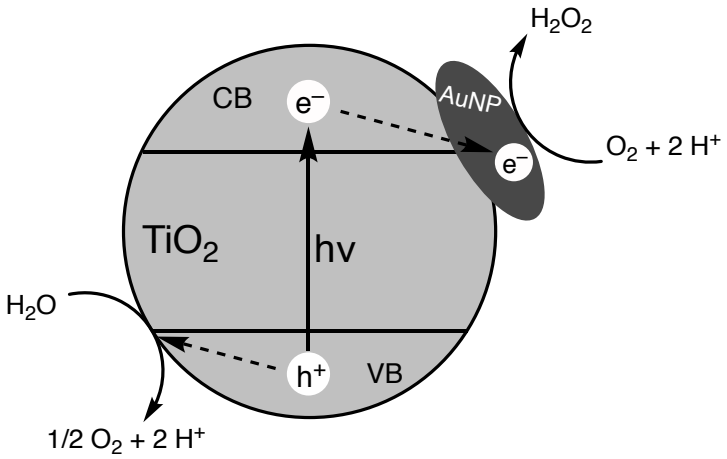

Scheme 2.2.1. Proposed mechanism for H_2O_2 generation via water oxidation and oxygen reduction using TiO_2 doped with uniform AuNPs upon UV irradiation. Adapted from Ref. 8.
VB – valence band; CB – conduction band

Titanium dioxide doped with uniform AuNPs shows activity upon UV irradiation (λ > 300 nm, Scheme 2.2.1). TiO_2 absorbs a photon, which leads to a charge separation. A hole in the valence band (VB) moves to the surface where it oxidises water to oxygen. The electron in the conduction band (CB) moves to the AuNP via interfacial electron transfer (IET) where it is trapped due to a formation of a Schottky barrier[12] on the interface between Au and TiO_2. This stabilises the charge separation and provides a spatial separation of oxidation and reduction sites, suppressing the unwanted degradation of hydrogen peroxide.[8, 13]

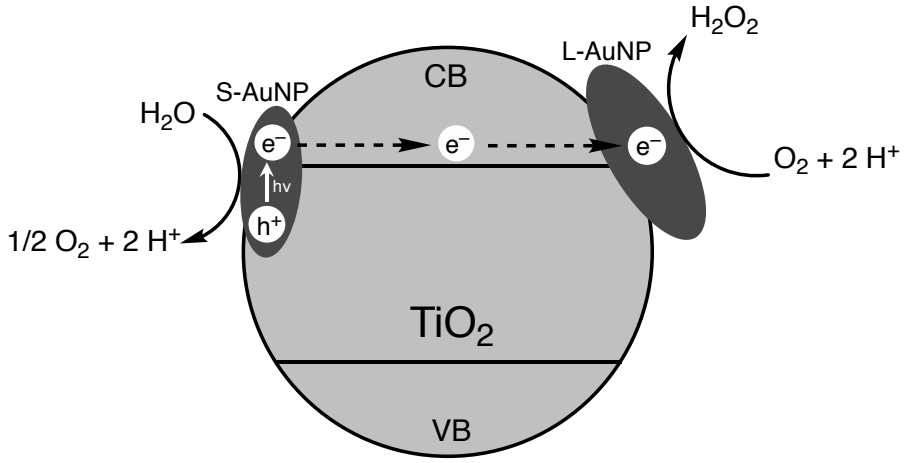

Scheme 2.2.2. Proposed mechanism for H_2O_2 generation via water oxidation and oxygen reduction using TiO_2 doped with bimodal AuNPs upon visible-light irradiation. Adapted from Ref. 9.
VB – valence band; CB – conduction band; S-AuNP – smaller AuNP; L-AuNP – larger AuNP

A system containing bimodal AuNPs (10.6 and 2.3 nm) is active also under visible light (λ > 430 nm, Scheme 2.2.2). The function of the system is based on the different behaviour of AuNPs of different size. Smaller NP absorb photons via LSPR and injects an electron into conduction band of the supporting semiconductor, through which the electron is transferred into larger NP and trapped. Oxidation of water then takes place on the surface of smaller NPs and reduction of oxygen on the surface of larger NPs.[9]

Under inert atmosphere, AuNP-doped titanium dioxide is also capable of photocatalytic water reduction, *i.e.* reduction of protons to dihydrogen, using both UV and visible light.[14,15] This reaction is important not only from an application perspective as a source of so-called "solar fuels"—an alternative to fossil fuels[16]—but hydrogen also qualifies as an energetic compound applicable in reductive organic syntheses[17] as discussed in the first paragraph.

However, in all abovementioned studies, reaction mixtures for H_2O_2 and H_2 generation contained sacrificial electron donors, such as ethanol or formic acid. These compounds have a lower oxidation potential than water, and therefore ease this process and increase its efficiency. Thus, these experiments cannot be characterised as water-oxidation or overall-water-splitting processes, since water does not act as a source of redox equivalents. When working with TiO_2 doped with bimodal AuNPs, Tada's group did observe H_2O_2 generation using pure water as a reaction medium, but the steady-state concentration was only around 35 μM, a significantly lower value than 1 mM achieved in aqueous media containing 4 % of HCOOH.[9] The first one to describe a use AuNP-doped TiO_2 for an efficient H_2O_2 generation using water oxidation as a source of electrons was the Hollmann's group in 2018 when they successfully utilised photocatalytically produced hydrogen peroxide for biocatalytic C–H oxygenation using a halogen bulb as a light source.[18] However, they did not provide a sufficient insight into the H_2O_2 generation itself, such as achieved steady-state concentrations.

We have obtained a sample of AuNP-doped TiO_2 from the Hollmann group and the aim of the project described in this chapter was to evaluate photocatalytic properties of the material, study conditions influencing H_2O_2 and H_2 generation, examine the synthesis of the catalyst and its reproducibility, and find applications for this system in organic synthesis.

2.2.2 Results and Discussion

2.2.2.1 Screening of light sources

First of all, AuNP-doped TiO_2 (further on abbreviated as Au–TiO_2) was analysed via solid-state UV-Vis spectroscopy, which revealed that the presence of gold nanoparticles is responsible for a broad absorption band in a visible region with a maximum around 550 nm (Figure 2.2.1). Pure titanium dioxide has a strong absorption band below 400 nm, which can be also seen in Figure 2.2.1, but doesn't absorb light in a visible region.[19] In a macroscopic appearance, pure TiO_2 has a white colour, while Au–TiO_2 is grey or slightly purple.

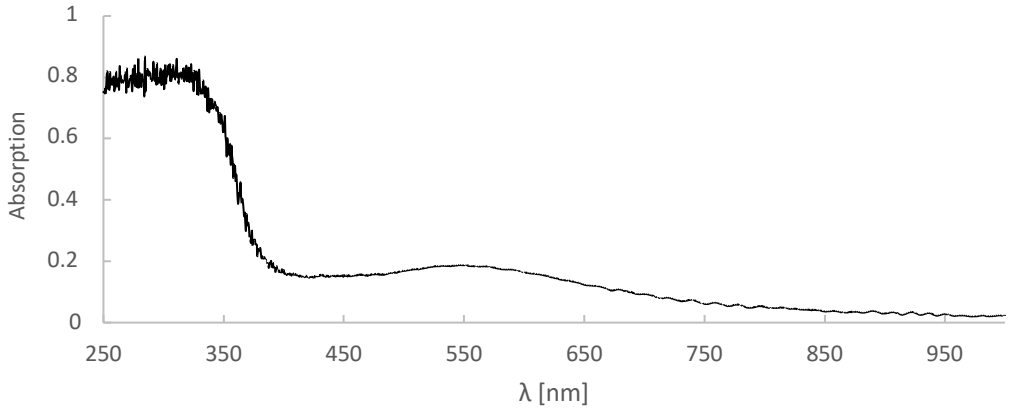

Figure 2.2.1. Solid-state UV-Vis spectrum of titanium dioxide (anatase) doped with gold nanoparticles.

Since a halogen bulb used in Ref. 18 is a highly inefficient light source (emission spectrum in Figure 2.2.2), LEDs were tested as an alternative irradiation method. Screening contained LEDs with narrow emission bands—UV (375 nm), blue (455 nm), and green (535 nm)—and a white LED as a broad-emission source (emission spectrum in Figure 2.2.3) to cover the whole absorption band of the material. The screening was performed in distilled water and in water containing 5 vol% of methanol. The concentration of photocatalytically-generated H_2O_2 in aqueous suspension after 1 hour of irradiation under oxygen atmosphere was

chosen as a marker for the activity assessment. To quantitatively analyse H_2O_2 concentrations, an enzymatic assay was used. Dye-precursor DA-64 (**1**) is oxidatively cleaved by horseradish peroxidase (HRP) in a presence of hydrogen peroxide forming bright-green dye **2**, which has an absorption maximum at 725 nm (Scheme 2.2.3). Concentration of hydrogen peroxide can be determined by a spectroscopic analysis of the assay solution, because absorbance at 725 nm is linearly dependent on the H_2O_2 concentration.[20]

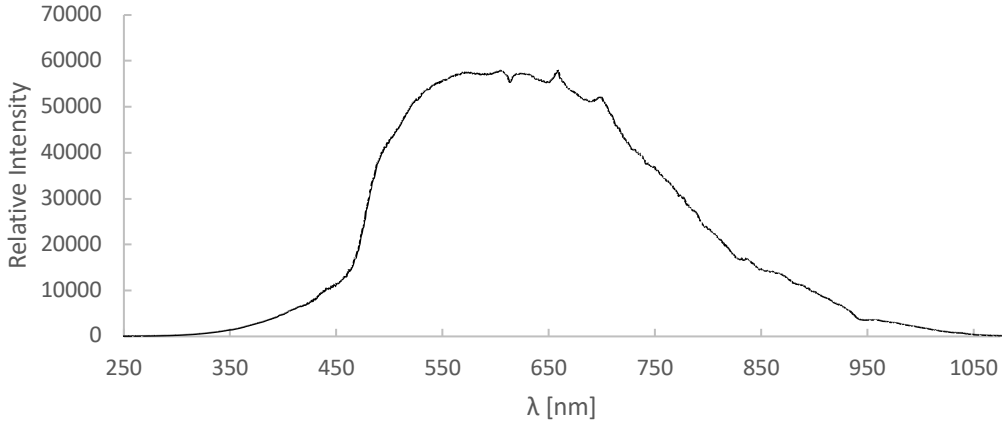

Figure 2.2.2. Emission spectrum of halogen light bulb.

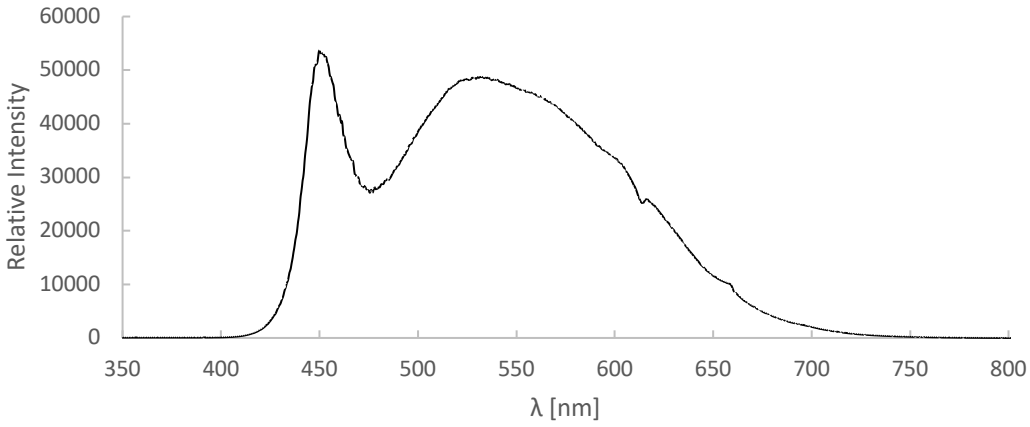

Figure 2.2.3. Emission spectrum of 6000 K cool-white LED.

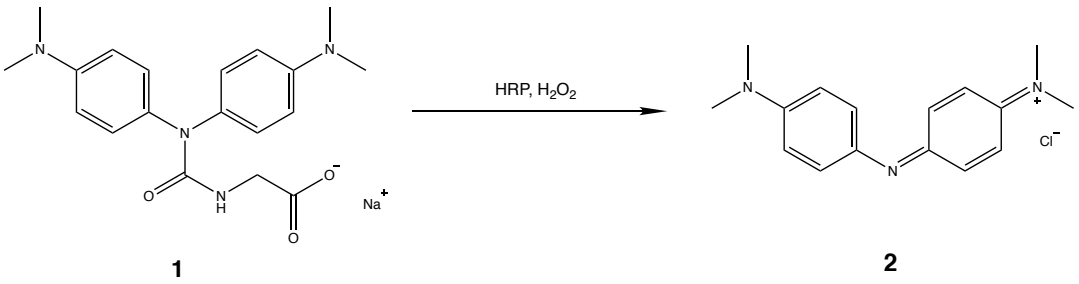

Scheme 2.2.3. Oxidative enzymatic transformation of colourless DA-64 (**1**) to green dye **2**.

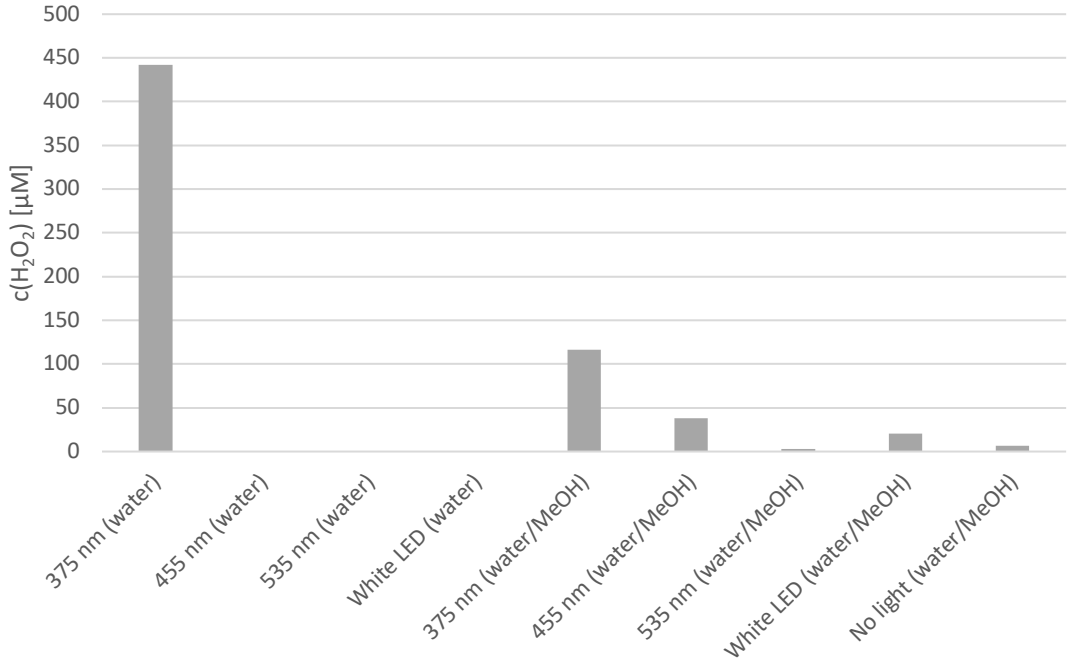

Figure 2.2.4. Concentration of H_2O_2 in Au–TiO_2 suspensions after 1 h of irradiation under oxygen atmosphere (*crimp-top vial, 25 ℃, 5 mg Au–TiO_2, 1 mL of solvent)*.

Results of the screening can be seen in Figure 2.2.4. In pure water, hydrogen peroxide was generated only under UV irradiation. This is in direct contrast with Hollmann's claim that the material is capable of visible-light-mediated water oxidation.[18] His positive results can be explained by the use of a halogen bulb as a light source, since it also has a weak UV-A emission (see Figure 2.2.2) responsible for the material's activity. Based on these results, we can conclude that in a presence of water as the sole source of electrons, Au–TiO_2 is active only under UV irradiation in an absorption region of titanium dioxide, and thus generation of H_2O_2 follows the mechanism shown in Figure 2.2.1. However,

irradiation at 375 nm can be still considered as mild conditions, UV-A LEDs are efficient and relatively cheap, and our experiment successfully proved that Au–TiO_2 can utilise water as a source of redox equivalents. Therefore, properties of the material were further evaluated under these conditions.

Results in Figure 2.2.4 also showed that when MeOH is present as a sacrificial electron donor, Au–TiO_2 is active also under blue irradiation (and white due to its blue emission band, but with lower overall efficiency). This suggests plasmonic activity depicted in Scheme 2.2.2, even though the preparation method used for this specific material does not claim to produce bimodal AuNPs.[15] Possibly, the size-distribution of formed nanoparticles is so broad that both S-AuNPs and L-AuNPs are present.

2.2.2.2 Self-preparation of Au–TiO_2

A batch of Au–TiO_2 was prepared using a deposition–precipitation method following a literature procedure.[15] This method is relatively easy and does not require any specialised equipment, such as furnaces for calcination. Neutralised solution of $AuCl_3$ is heated and stirred in an aqueous suspension of TiO_2. After cooling down, the solid residue is separated via centrifugation and properly dried. Drying seems to be a crucial step, because the activity of a material dried over one and two night differs significantly (Figure 2.2.5).

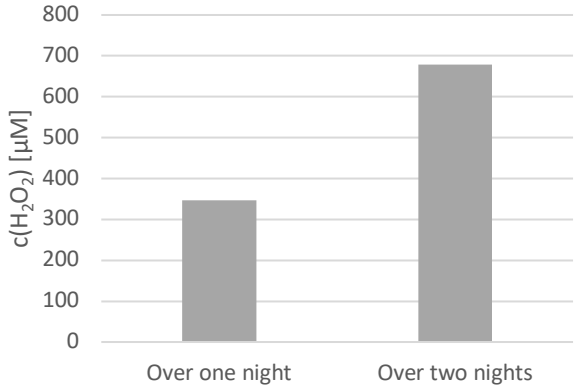

Figure 2.2.5. Concentration of H_2O_2 after 4 minutes of irradiation with 375 nm light in distilled water under oxygen atmosphere using prepared Au–TiO_2 dried over either one or two nights (*crimp-top vial, 25 °C, 5 mg Au–TiO_2, 1 mL of H_2O).*

Reproducibility of this method of preparation seems to be also good. When compared with a material provided by the Hollmann group, the self-prepared catalyst showed a comparable activity (Figure 2.2.6) and kinetic profile of H_2O_2 generation (Figures 2.2.7 and 2.2.8). When pure TiO_2 was used as a control sample, no measurable amounts of hydrogen peroxide were detected.

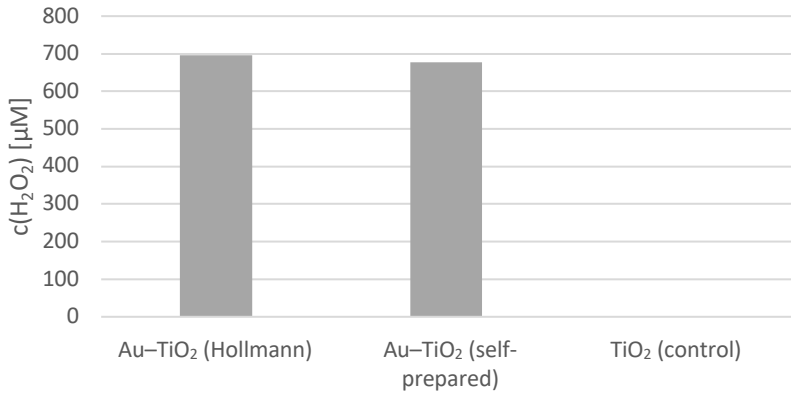

Figure 2.2.6. Concentration of H_2O_2 after 4 minutes of irradiation with 375 nm light in water under oxygen atmosphere using catalyst provided by Hollmann group as a benchmark (left), self-prepared catalyst (middle), and pure TiO_2 as a negative control (right) (*crimp-top vial, 25 ℃, 5 mg Au–TiO_2, 1 mL of H_2O).*

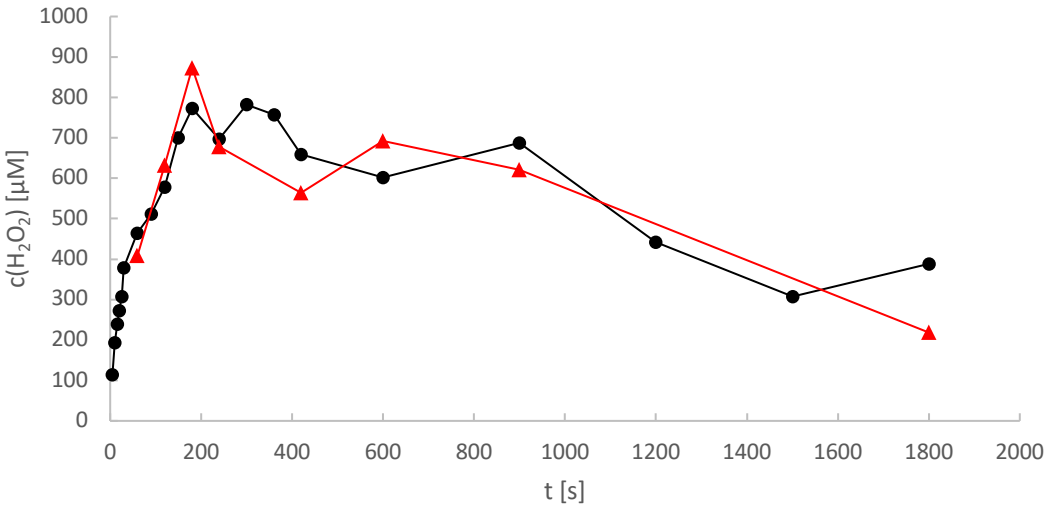

Figure 2.2.7. Kinetic profile of H_2O_2 generation in water under oxygen atmosphere upon 375 nm irradiation. Time-scale from 0 to 30 min (*crimp-top vial, 25 ℃, 5 mg Au–TiO_2, 1 mL of H_2O).* *black* – catalyst from Hollmann group; *red* – self-prepared catalyst

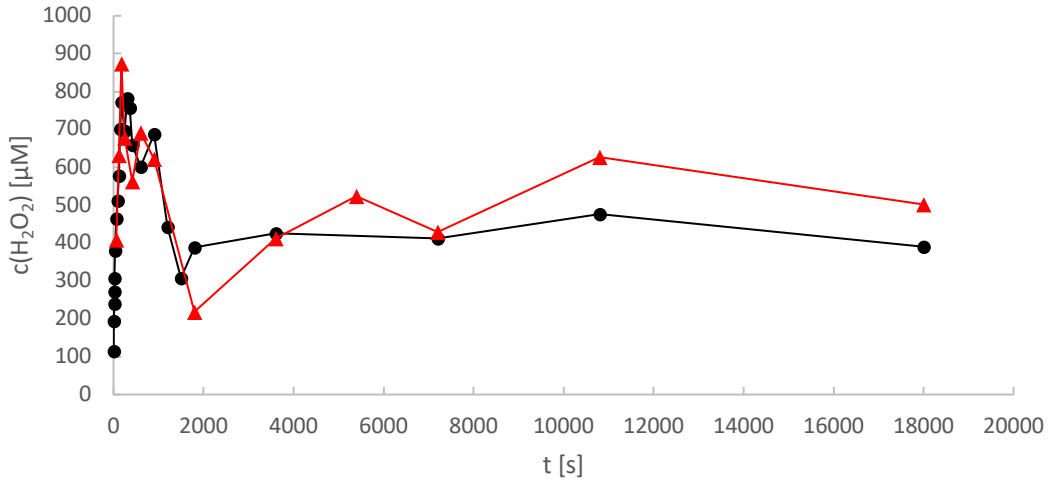

Figure 2.2.8. Kinetic profile of H_2O_2 generation in water under oxygen atmosphere upon 375 nm irradiation. Time-scale from 0 to 5 hours (*crimp-top vial, 25 °C, 5 mg Au–TiO₂, 1 mL of H₂O). black* – catalyst from Hollmann group; *red* – self-prepared catalyst

After 30 minutes of irradiation, the system reaches a steady-state concentration of ca 500 µM of photogenerated H_2O_2. However, the kinetic profile shows a peak and two subsequent plateaus. Since the measured concentration always shows an equilibrium between hydrogen peroxide being produced and decomposed, this hints to a loss of activity of the catalyst in time. This conclusion is also supported by an observed colour change. Upon irradiation, the originally grey suspension turns purple. The colouration then slowly disappears and after 24 hours of 375 nm irradiation under oxygen atmosphere the suspension is left completely white and the material is not catalytically active anymore, suggesting a degradation or loss of gold nanoparticles. This behaviour seems to require the presence of both light and oxygen. When irradiated under inert atmosphere, the suspension turns purple, but no further bleaching is observed and the material keeps its catalytic activity even after several days of irradiation. Also, dry, unused Au–TiO_2 slowly turns purple when exposed to air and light, but stays grey when kept in dark.

2.2.2.3 Conditions influencing activity of H_2O_2 generation

The peak of H_2O_2 concentration after 4 minutes of irradiation was chosen to be a standard reaction time for evaluation of catalyst activity. All following experiments were performed with a single batch of self-prepared material using a suspension of 5 mg of Au–TiO_2 in 1 mL of solvent (unless stated otherwise).

Polymorph of TiO_2

Although the two most common polymorphs of titanium dioxide—anatase and rutile—are often described to have uneven photocatalytic activities,[21,22] results shown in Section 1.2.2 show that with this type of Au–TiO_2 and under these conditions, activities of the two polymorphs are comparable, because Hollmann's catalyst was rutile based, while our first batch of catalyst was based on P25 TiO_2, which is a standardised formulation consisting of 75–85 % anatase, 15 % rutile, and small amount of amorphous phase.[23] This observation was confirmed by a preparation of our own rutile-based catalyst, which also showed a comparable activity.

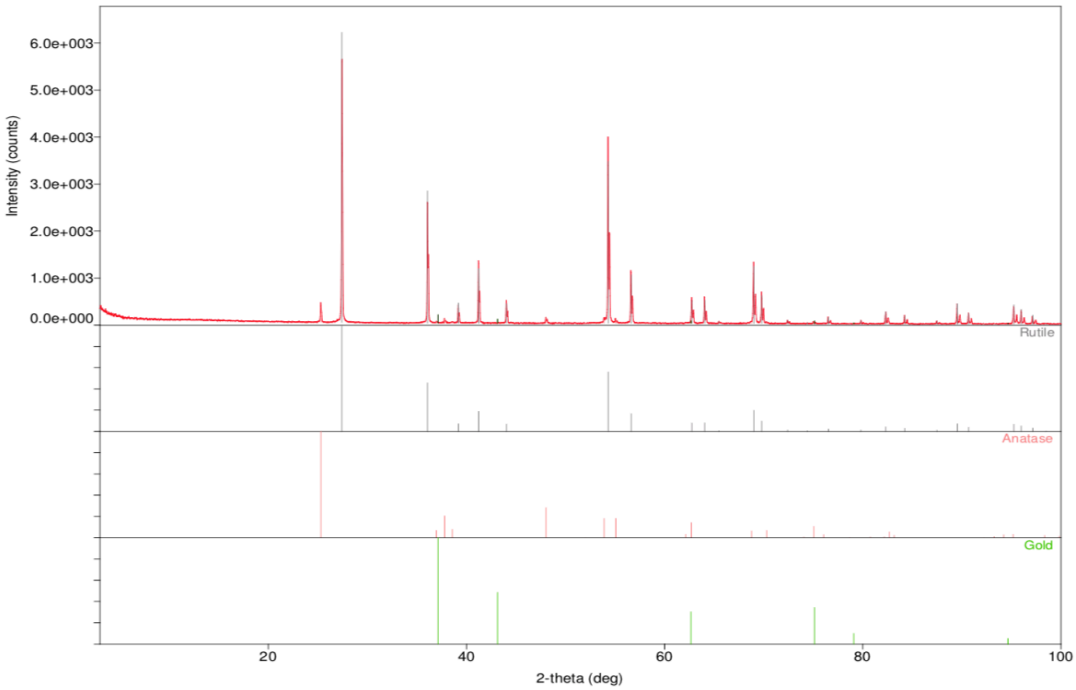

Figure 2.2.9. Powder XRD spectrum of rutile-based Au–TiO_2 (top) with calculated theoretical signals of rutile, anatase, and gold.

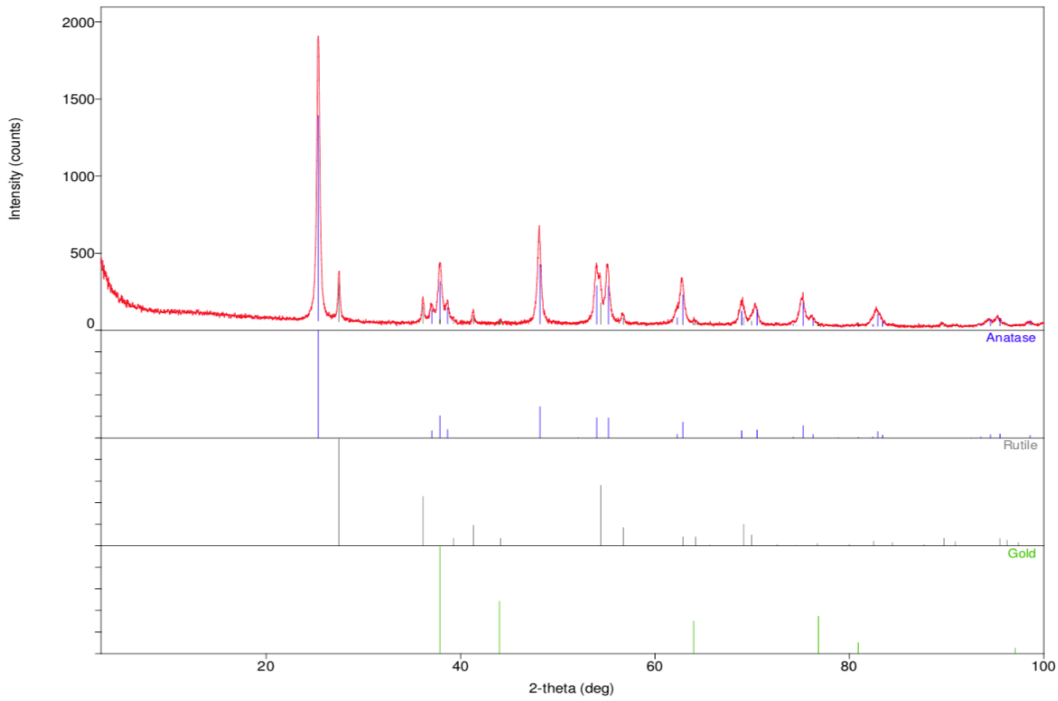

Figure 2.2.10. Powder XRD spectrum of P25-based Au–TiO_2 (top) with calculated theoretical signals of anatase, rutile, and gold.

Excitation wavelength

To identify borderline wavelength under which the catalyst still keeps its activity, light-source screening was repeated using narrow-emission-band LEDs with maxima at 375 nm, 385 nm, 400 nm, and 455 nm. As results in Figure 2.2.11 show, activity of Au–TiO_2 drops at 400 nm and no measurable activity is observed under blue-light irradiation.

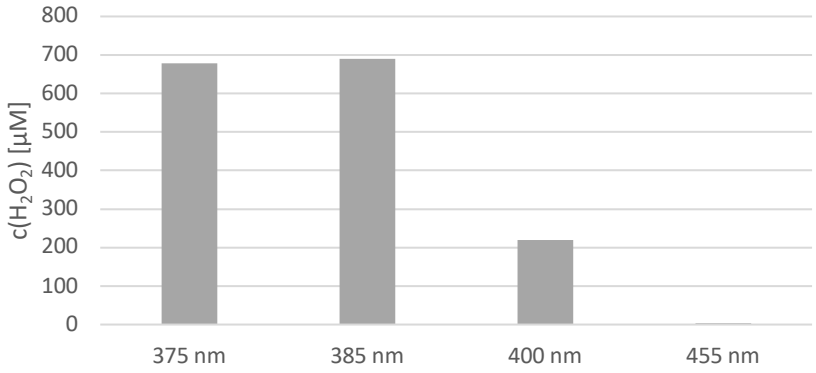

Figure 2.2.11. Concentration of H_2O_2 after 4 minutes of irradiation in distilled water under oxygen atmosphere using LED light of different wavelengths (*crimp-top vial, 25 °C, 5 mg Au–TiO_2, 1 mL of H_2O).*

Atmosphere

The crucial role of oxygen in H_2O_2 generation was confirmed by results shown in Figure 2.2.12. Since the catalyst activity is higher under pure oxygen atmosphere, all other reactions are carried out under oxygen instead of air.

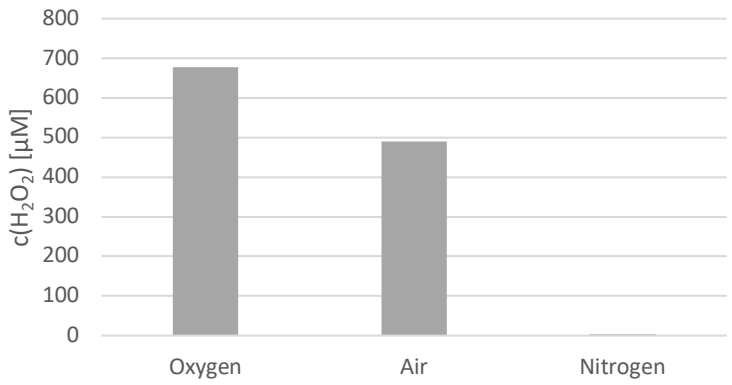

Figure 2.2.12. Concentration of H_2O_2 after 4 minutes of irradiation with 375 nm light in distilled water under different atmospheres (*crimp-top vial, 25 °C, 5 mg Au–TiO_2, 1 mL of H_2O).*

Amount of Au–TiO_2 in reaction mixture

To find the ideal amount of Au–TiO_2 in a reaction mixture, activity of suspensions containing different amounts of catalyst was evaluated. Figure 2.2.13 shows that a peak of activity is at 5 mg per mL of solvent. At higher concentrations, the amount of generated hydrogen peroxide quickly drops. This observation suggests that a maximum of incoming light is absorbed already at 5 mg/mL, and therefore further addition of catalyst doesn't contribute to H_2O_2 generation, only to its degradation. This was confirmed by a photometer measurement. Light intensity at 375 nm above an empty vial was 11.8 mW/cm^2, whereas above a stirred suspension containing 5 mg in 1 mL of water, the measured light intensity was only 280 μW/cm^2. Therefore, over 97 % of the incoming light was absorbed (or possibly reflected) by the catalyst.

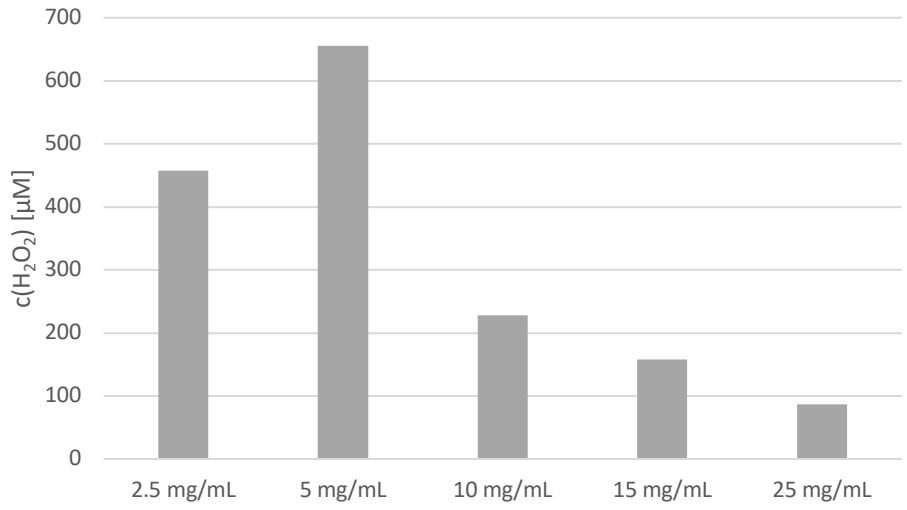

Figure 2.2.13. Concentration of H_2O_2 after 4 minutes of irradiation with 375 nm light in distilled water under oxygen atmosphere using suspensions containing different amounts of catalyst (*crimp-top vial, 25 ℃, 1 mL of H_2O).*

Solvent

In order to utilise this source of hydrogen peroxide in organic synthesis, a shift from aqueous to organic solutions has to be made. Ideally, water should be present only in a reactant amount. Therefore, systems consisting of mixtures of organic solvents with water and their activity have been tested.

Each graph contains a column showing activity in distilled water as a direct benchmark.

Acetonitrile

As Figure 2.2.14 shows, acetonitrile is strongly affecting the catalyst activity. Already in a presence of 5 vol% of MeCN, the activity drops to below 10 %. With acetonitrile concentrations of 25 vol% and higher, no presence of H_2O_2 can be detected.

Possible explanation is a shift of band potentials due to a change of solvent, where holes in valence band are no longer able to oxidise water. In pure acetonitrile, potentials of valence and conduction bands of TiO_2 are lower by 1.25 V compared with water at pH 7.[24] Single-electron oxidation of water

($H_2O \rightarrow HO^{\bullet} + H^+ + e^-$), which might be the first step of water oxidation on the catalyst surface, has a potential of 2.15 V vs. SCE,[25] and therefore is only slightly exoergic (valence-band hole potential in water is 2.25 V vs. SCE[24]). The presence of even a small amount of acetonitrile could lower the potential enough to thermodynamically disfavour this process.

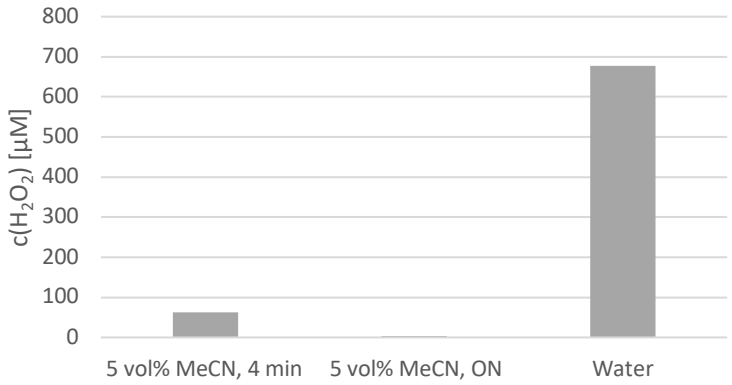

Figure 2.2.14. Concentration of H_2O_2 after irradiation with 375 nm light under oxygen in a mixture of water and acetonitrile (*crimp-top vial, 25 °C, 5 mg Au–TiO_2, 1 mL of solvent). ON* – irradiation over night

Tetrahydrofuran

Presence of THF in the reaction mixture increases the formation of hydrogen peroxide (Figure 2.2.15). However, the fact that H_2O_2 generation in pure (but not dry) THF is still significantly higher than in water suggests that THF acts as a source of electrons in this case. Oxidation of THF, which is thermodynamically favoured over oxidation of water due to its lower oxidation potential (1.75 V vs. SCE[25]), was previously observed when its aqueous mixture was irradiated in a presence of ZnS[25] and tetrahydrofuran was even successfully used as a sacrificial electron donor for photocatalytic organic transformations.[26] However, the presence of water apparently has a synergistic effect. That can be explained by a formation of hydroxyl radicals, which promote the formation of easily further oxidisable THF radicals.[25]

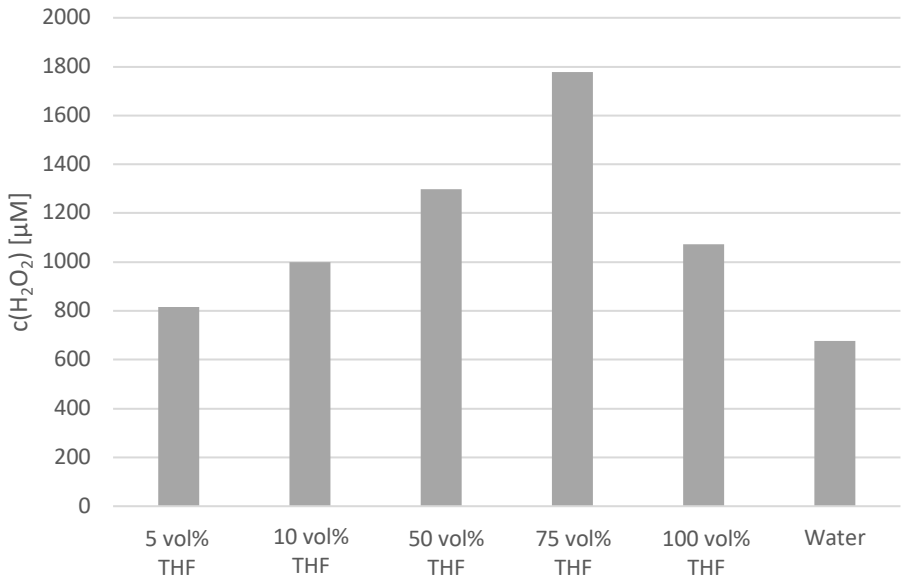

Figure 2.2.15. Concentration of H_2O_2 after 4 minutes of irradiation with 375 nm light under oxygen in mixtures of water and THF (*crimp-top vial, 25 ℃, 5 mg Au–TiO_2, 1 mL of solvent).*

Acetone

Presence of acetone in the reaction mixture also significantly increases H_2O_2 generation (Figure 2.2.16). However, the pattern is different than in the case of THF. Activity remains constant with high amounts of water in the mixture and drops at low water concentrations. In pure (but not dry) acetone, the activity is lower than in pure water. This suggests that in this case, water still acts as a source of electrons. Synergistic effect of the presence of acetone might be explained the same way as antagonistic effect of acetonitrile, *i.e.* change in band potentials of the semiconductor. Unfortunately, to the best of our knowledge, no literature data describing electronic properties of TiO_2 or any other semiconductor in acetone are available.

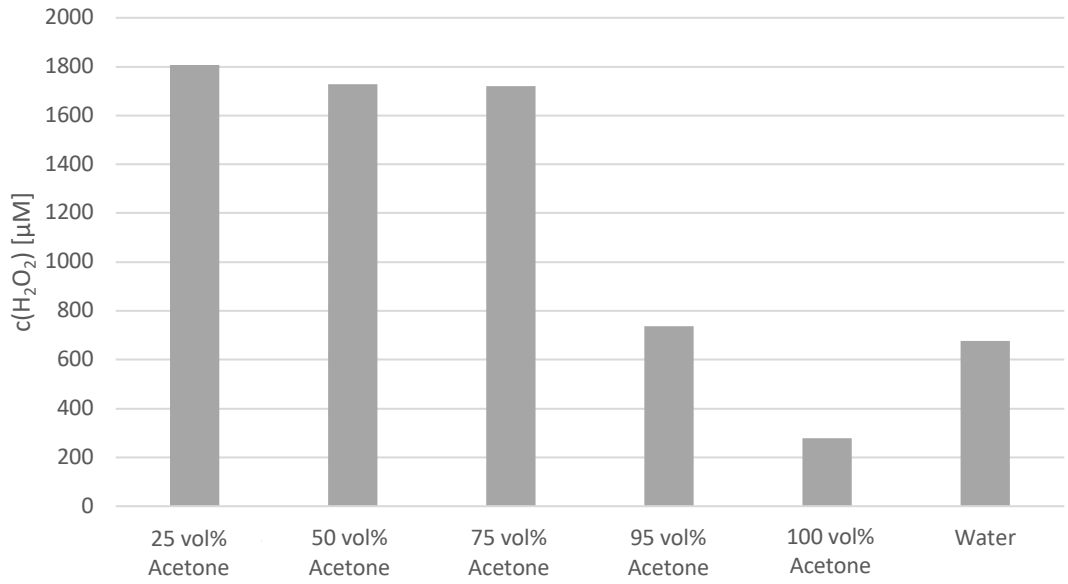

Figure 2.2.16. Concentration of H_2O_2 after 4 minutes of irradiation with 375 nm light under oxygen in mixtures of water and acetone (*crimp-top vial, 25 °C, 5 mg Au–TiO_2, 1 mL of solvent).*

Toluene

Toluene has been chosen to test the possibility of using a system with two liquid phases. This is important for synthetic applications requiring non-polar conditions, because the reaction mixture can be dissolved in the organic phase while the aqueous phase acts only as a source of hydrogen peroxide.

As results in Figure 2.2.17 show, mobility and dispersion of the catalyst is important. With a high volume of aqueous phase, H_2O_2 production is comparable to pure water. But when the amount of water is too low to allow a good mobility of the suspended catalyst, activity significantly drops. "Wet catalyst" stands for a setup where Au–TiO_2 was soaked with only a drop of water and stayed completely immobile on the bottom of a reaction vial, even while stirring.

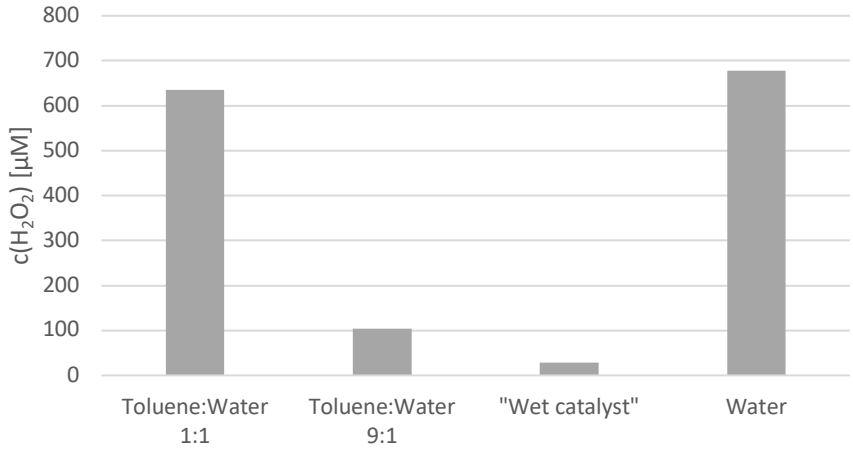

Figure 2.2.17. Concentration of H_2O_2 after 4 minutes of irradiation with 375 nm light under oxygen in two-phase mixtures of water and toluene (*crimp-top vial, 25 °C, 5 mg Au–TiO_2, 1 mL of solvent)*.

Methanol

Methanol was tested as an alternative source of electrons. Its advantage is that hydrogen peroxide is generated even under visible-light irradiation. Activity upon 455 nm irradiation is relatively low, but still within possibly utilisable values (Figure 2.2.18). A use of an irradiation source emitting 400 nm leads to a significant increase in activity.

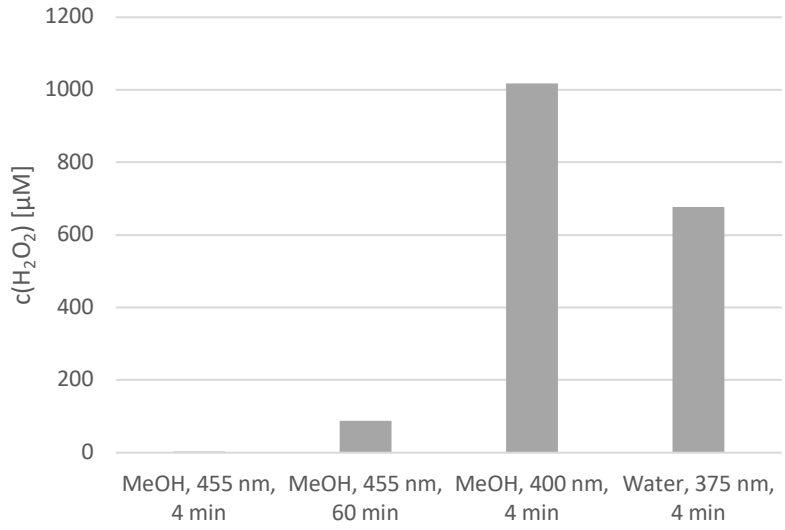

Figure 2.2.18. Concentration of H_2O_2 after irradiation with different light sources under oxygen in pure methanol (*crimp-top vial, 25 °C, 5 mg Au–TiO_2, 1 mL of solvent)*.

2.2.2.4 Conditions influencing activity of H_2 generation

As previously mentioned, Au–TiO_2 is also capable of photocatalytic hydrogen generation via proton reduction when irradiated under inert atmosphere.[15] Results presented in this section show that we were able to confirm this observation successfully utilising THF and water as sources of electrons. Activity of the system under different conditions was assessed as an overall amount of hydrogen—quantified by head-space GC—generated under irradiation for a specific amount of time (usually 3 hours). All following experiments were performed with a single batch of self-prepared catalyst using a suspension of 5 mg of Au–TiO_2 in 1 mL of solvent.

Solvent

Activity of the catalytic system in different solvents was examined using distilled water, THF, acetone, toluene, and their respective aqueous mixtures. As Figure 2.2.19 shows, obtain results correlate with solvent effects observed for H_2O_2 generation.

By far the highest amount of hydrogen was generated in the presence of THF. Heterogeneous, photocatalytic hydrogen evolution via oxidation of THF was previously observed by the group of Kisch when a suspension of ZnS in aqueous tetrahydrofuran was irradiated with UV light.[25] A synergistic effect of water can be observed in Figure 2.2.20 where the activity of hydrogen evolution is compared between dry THF, untreated commercial THF (containing 0.029 % of water according to manufacturer), and THF containing 50 vol% of water.

Bottom part of Figure 2.2.19 contains data with exclusion of THF to increase resolution. In distilled water, 8.5 μmol of hydrogen was produced after 3 hours of irradiation, which again proves that Au–TiO_2 is capable of water oxidation under UV-A irradiation. When acetone is present in a mixture with water, a synergistic effect increasing the activity almost 3-fold is observable, while activity in pure (but not dry) acetone is lower compared with pure water. Finally,

toluene–water system with two liquid phases showed activity comparable to pure water.

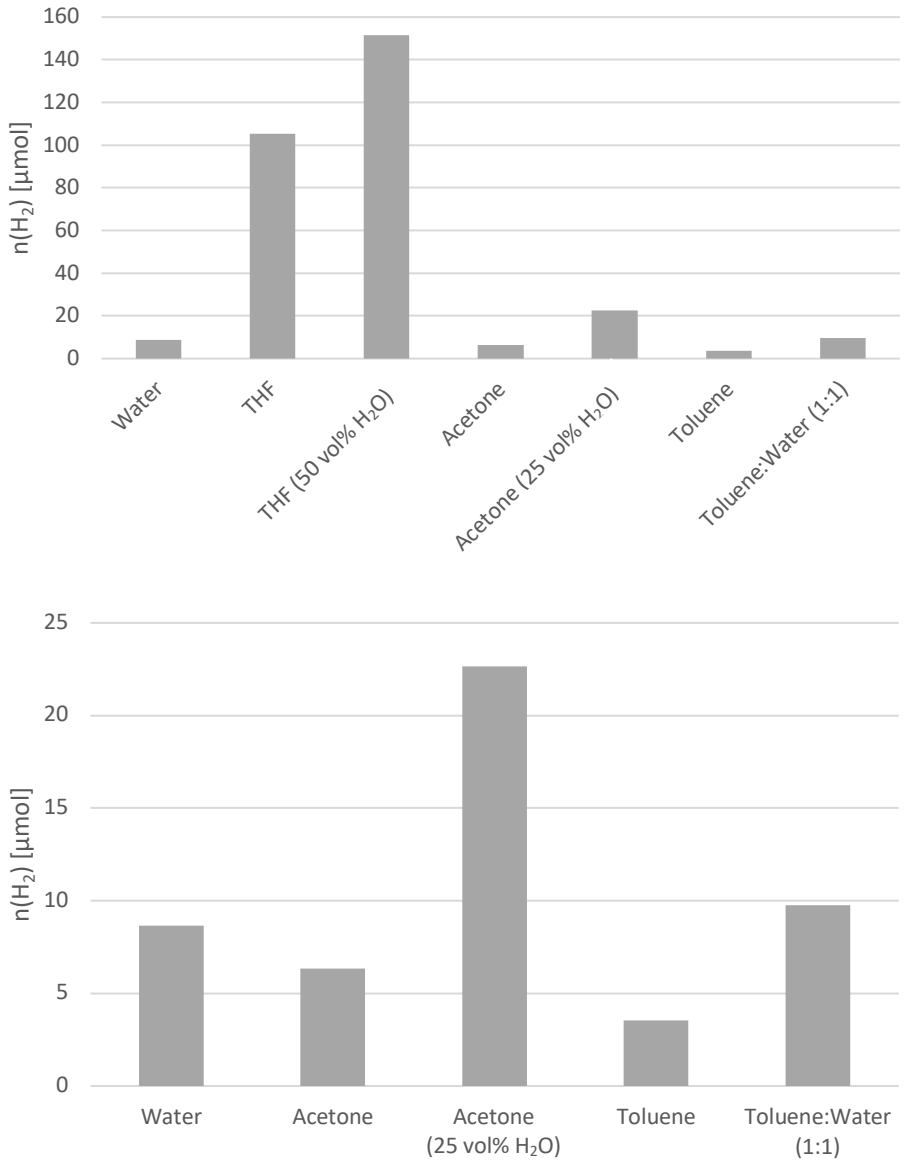

Figure 2.2.19. Amount of hydrogen generated after 3 hours of irradiation with 375 nm light under nitrogen in different solvent mixtures (*crimp-top vial, 25 ℃, 5 mg Au–TiO_2, 1 mL of solvent). Bottom* – the same set of data with an exclusion of THF

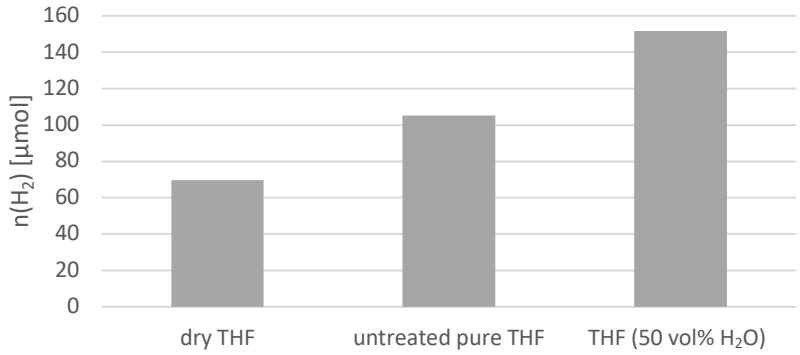

Figure 2.2.20. Amount of hydrogen generated after 3 hours of irradiation with 375 nm light under nitrogen in THF with different amount of water content (*crimp-top vial, 25 ℃, 5 mg Au–TiO_2, 1 mL of solvent)*.

Wavelength

Comparison of hydrogen evolution in samples of Au–TiO_2 suspension in THF irradiated with different wavelength showed that UV-A light is required for an efficient THF oxidation and proton reduction. Under blue irradiation (455 nm), no measurable amounts of H_2 were detected even after 24 hours. This suggests that the plasmonic effect (Scheme 2.2.2) does not generate enough oxidative power to oxidise THF and that charge-separation provided by semiconductor excitation (Scheme 2.2.1) is required. Also, a control sample stirred in dark for 3 hours showed no hydrogen evolution. Results can be seen in Figure 2.2.21.

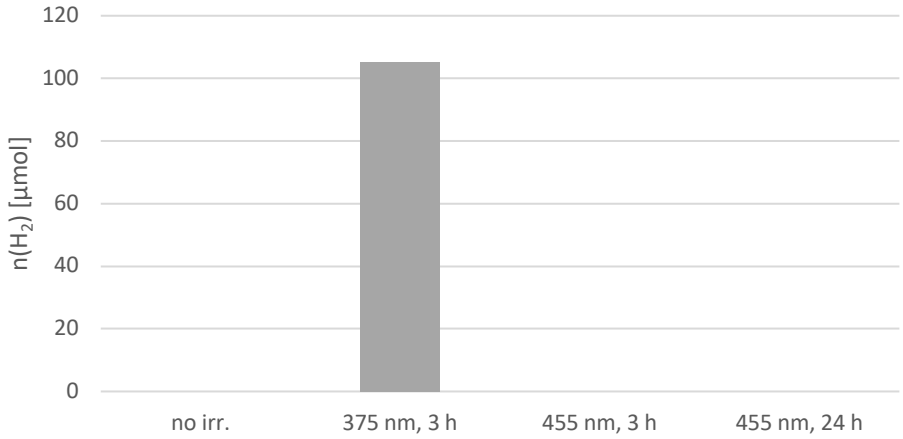

Figure 2.2.21. Amount of hydrogen generated after irradiation with either UV (375 nm) or blue (455 nm) light under nitrogen in pure THF (*crimp-top vial, 25 ℃, 5 mg Au–TiO_2, 1 mL of solvent)*.

Catalyst material

Comparison between pure P25 TiO_2 and Au–TiO_2 proved a crucial role of AuNPs for efficient catalytic activity. While titanium dioxide itself is able to photocatalytically produce hydrogen in both THF and water, addition of gold nanoparticles—which stabilise charge-separation via entrapment of electrons (Scheme 2.2.1)—increased activity almost 20-fold in water and over 100-fold in THF. Results can be seen in Figure 2.2.22.

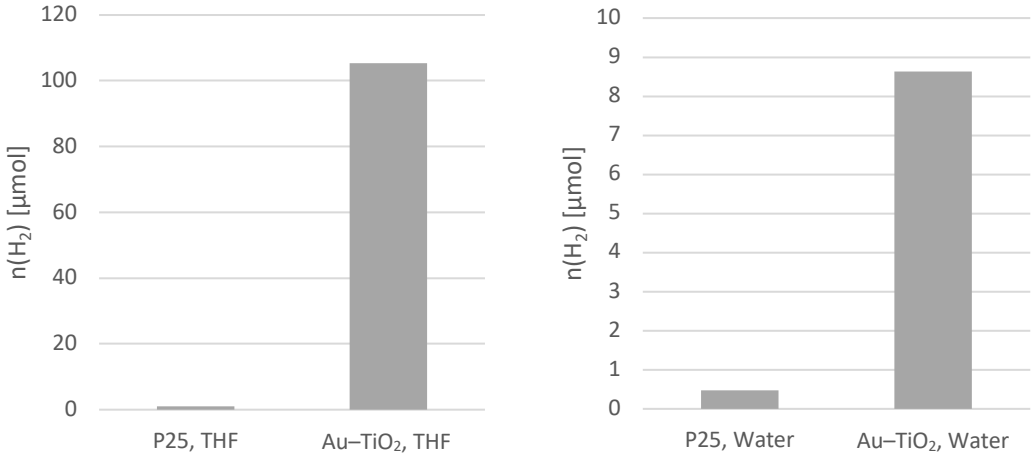

Figure 2.2.22. Amount of hydrogen generated after 3 hours of irradiation with 375 nm light under nitrogen in THF (left graph) and water (right graph) using either pure P25 TiO_2 (left columns) or Au–TiO_2 (right columns) (*crimp-top vial, 25 °C, 5 mg catalyst, 1 mL of solvent)*.

Atmosphere

The importance of an inert atmosphere for efficient photocatalytic hydrogen generation was demonstrated by head-space GC measurement of aqueous suspension of Au–TiO_2 irradiated under oxygen atmosphere, which showed no detectable traces of hydrogen in the gas phase. This observation shows that two-electron reduction of oxygen ($O_2 + 2\ H^+ + 2\ e^- \rightarrow H_2O_2$) is favoured over the reduction of protons, specifically due to a positive redox potential of this step (0.695 V vs. NHE at pH 0)[27].

2.2.2.5 Hydrogen generation – Identification of by-products

Abovementioned results prove that when Au–TiO_2 is irradiated with 375 nm light in aqueous suspension under inert atmosphere, hydrogen is produced via proton reduction using oxidation of water acts as a source of electrons. However, identification of products of water oxidation proved to be somewhat challenging. Theoretical products are either hydrogen peroxide (generated by two-electron oxidation of water or via recombination of hydroxyl radicals) or oxygen (generated by four-electron oxidation of water). These products can undergo further transformations. Oxygen can be reduced to H_2O_2 on gold nanoparticles and hydrogen peroxide can be either reduced following Equation 2.2.1 (generating $^{\bullet}OH$ and OH^-) or oxidised following Equations 2.2.2–2.2.5 (generating oxygen). Therefore, after irradiation, we should be able to observe either an increase of pH, or oxygen in the gas phase, or hydrogen peroxide in the liquid phase, or any combination of those three effects.

Suspensions of Au–TiO_2 (5 mg/mL) in pure water and in acetone containing 25 vol% of water were irradiated for 24 hours with 375 light under inert atmosphere. In this case, argon was used instead of nitrogen, because nitrogen could interfere during head-space-GC measurements. Afterwards, samples were analysed by head-space GC to identify oxygen, by HRP assay to identify hydrogen peroxide, and by pH meter. However, the pH of samples after irradiation was never higher than 8, no measurable concentration of H_2O_2 was detected in any sample, and no significant amounts of generated oxygen were observed. To exclude possible adsorption of oxygen on the semiconductor's surface, sealed samples were heated to 95 ºC overnight, but even after that there was only a minor increase of oxygen concentrations in the head space compared with blank samples.

A possible explanation of this strange behaviour can be found in a paper published by Harbour *et al.*,[28] who also observed a significant oxygen-mass disbalance when irradiating a suspension of TiO_2 in a presence of H_2O_2 and O_2.

They claim that upon irradiation, oxygen is photoadsorbed and hydrogen peroxide is chemisorbed onto the surface and even into the bulk of TiO_2 causing internal hydroxylation of the material and formation of peroxo-species, which are relatively stable in electron-donor-free systems. This is supported by previous studies of Boonstra and Mutsaers, who described the same processes and stated that desorption of oxygen from TiO_2 requires vacuum and temperatures above 50 °C and decomposition of hydrogen peroxide needs up to 150 °C.[29,30]

2.2.2.6 Application of Au–TiO_2 in organic synthesis

Since it was proven that TiO_2 doped with gold nanoparticles is capable of photocatalytic generation of hydrogen or hydrogen peroxide using water oxidation as a source of electrons, their possible utilisation in organic synthesis was examined. This section shows that Au–TiO_2 can be used for oxidation, reduction, and C–H-bond activation.

Oxidation of benzyl alcohol to benzaldehyde in a presence of Br_2

In a presence of a catalytic amount of bromine, hydrogen peroxide can indirectly oxidise alcohols to the corresponding carbonyl compounds and esters under mild conditions.[31] Alcohols are oxidised by bromine in a radical-chain process (Equations 2.2.6–2.2.7) while the resulting HBr is reoxidised by H_2O_2 (Equation 2.2.8). Formation of alkyl bromide via reaction of an alcohol with HBr is prevented by using a two-phase mixture of water and organic solvent to spatially separate the two processes. In some cases, hydrogen peroxide has to be added in a controlled fashion to avoid overoxidation. Therefore, our method of *in situ* generation of H_2O_2 can be ideal for this application.

$$R–CH_2OH + Br^{\bullet} \rightarrow R–{}^{\bullet}CHOH + HBr \qquad (2.2.6)$$

$$R–{}^{\bullet}CHOH + Br_2 \rightarrow R–CHO + Br^{\bullet} + HBr \qquad (2.2.7)$$

$$2\ HBr + H_2O_2 \rightarrow Br_2 + 2\ H_2O \qquad (2.2.8)$$

Oxidation of benzyl alcohol to benzaldehyde in a two-phase mixture of DCM and water in a presence of 7.5 mol% of bromine as shown in Scheme 2.2.4 was chosen as a test reaction. For results see Table 2.2.1.

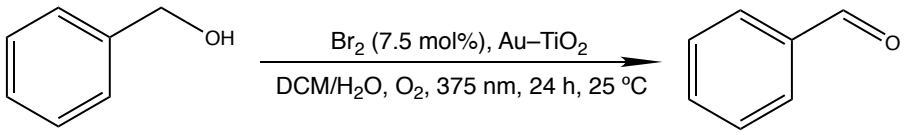

Scheme 2.2.4. Oxidation of benzyl alcohol by photocatalytically generated hydrogen peroxide in a presence of bromine.

Table 2.2.1. Results of oxidation of benzyl alcohol by photocatalytically generated hydrogen peroxide in a presence of bromine together with control experiments.

Entry	Br_2 [mol%]	$Au–TiO_2$ [mg/mL]	Atm.	λ [nm]	Conv.[a] [%]
1	7.5	5	O_2	375	38
2	—	5	O_2	375	4
3	7.5	—	O_2	375	7
4	7.5	5	N_2	375	2
5	7.5	5	O_2	—	5

[a]overall GC yields determined by an internal standard were quantitative. Conversion after 24 h of irradiation

A conversion of 38 % was achieved after 24 hours of irradiation and control experiments (Entries 2–5) show that all components of the reaction—bromine, $Au–TiO_2$, oxygen, and irradiation—are necessary for a successful oxidation of benzyl alcohol, and therefore $Au–TiO_2$ can be used to drive an oxidative organic reaction. Although a study previously published by Shiraishi *et al.* claims that titanium dioxide can directly oxidise benzyl alcohol to benzaldehyde under

UV (λ > 280 nm) irradiation,[32] results of our control experiments (especially Entry 2) prove that this is not the case under our milder conditions.

However, our 38 % conversion after 24 hours is inferior to literature results where 92 % conversion was achieved after just 4 hours (albeit with an excess of H_2O_2 and at elevated temperature), suggesting that the steady-state concentration of H_2O_2 is too low, which causes the reaction to slow down. This could be usually overcome by a longer reaction time, but a short lifetime of Au–TiO_2 under oxygen atmosphere poses a problem. Photocatalyst recovered after 24 hours of irradiation was completely bleached and no measurable H_2O_2 formation was detected when suspended in fresh distilled water and irradiated. On the other hand, this slow generation of hydrogen peroxide proved to be favourable for a biocatalytic, H_2O_2-dependent reaction catalysed by VHPO-class of enzymes, which is discussed in the next chapter.

Reduction of α-methylstyrene to cumene

The ability to utilise hydrogen produced from photocatalytic water splitting with Au–TiO_2 in organic synthesis was demonstrated on a simple Pd/C-catalysed reduction of α-methylstyrene as shown in Scheme 2.2.5 using water or aqueous acetone as a solvent. Obtained results are summarised in Table 2.2.2.

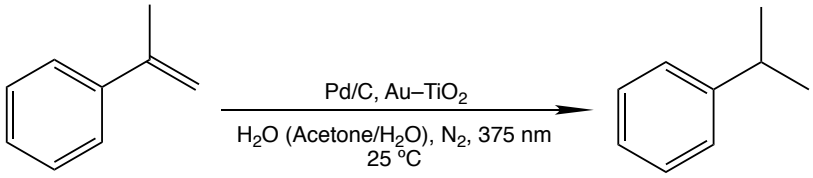

Scheme 2.2.5. Reduction of α-methylstyrene by photocatalytically generated hydrogen in a presence of Pd/C.

Table 2.2.2. Results of reduction of α-methylstyrene by photocatalytically generated hydrogen in a presence of Pd/C.

Entry	Solvent	Au–TiO_2 [mg/mL]	Pd/C [mol%]	λ [nm]	Time [h]	Conv.[a] [%]
1	H_2O	5	5	375	24	3
2	Acetone (25 vol% H_2O)	5	5	375	24	11
3	H_2O	5	5	375	72	3
4	Acetone (25 vol% H_2O)	5	5	375	72	38
5	H_2O	5	5	375	144	3
6	Acetone (25 vol% H_2O)	5	5	375	144	57
7	H_2O	–	5	375	24	–
8	Acetone (25 vol% H_2O)	–	5	375	24	–
9	H_2O	5	–	375	24	trace
10	Acetone (25 vol% H_2O)	5	–	375	24	0.5
11	H_2O	5	5	–	24	–
12	Acetone (25 vol% H_2O)	5	5	–	24	–
13	H_2O	5[b]	5[b]	375	24	2
14	Acetone (25 vol% H_2O)	5[b]	5[b]	375	24	14
15	H_2O	5	10	375	72	1.5
16	Acetone (25 vol% H_2O)	5	10	375	72	9
17	H_2O	10	5	375	72	1.5
18	Acetone (25 vol% H_2O)	10	5	375	72	15
19	H_2O	5[c]	5	375	72	4
20	Acetone (25 vol% H_2O)	5[c]	5	375	72	74

[a]overall GC yields determined by an internal standard were quantitative; [b]recycled solid phase from Entries 3 and 4, respectively; [c]double catalyst-suspension loading

Entries 1–6 show that while hydrogenation of styrene occurs in both tested solvents, aqueous acetone is clearly the superior medium for this purpose. After 24 hours of irradiation, acetone provides a conversion of 11 %, which is further increasing in a relatively linear fashion over the course of at least six day, while water reaches only 3 % conversion, which does not increase with longer

irradiation. This cannot be a simple issue of substrate solubility, because two-phase mixture of water and toluene showed also only a 3 % conversion. We can again conclude that in a presence of acetone, the catalyst has a higher overall activity.

Entries 7–12 contain control experiments. No product of hydrogenation was observed in an absence of Au–TiO_2 or in dark and when Pd/C is not present, only trace amounts of cumene can be detected.

Entries 2, 4, and 6 confirm that under inert atmosphere, Au–TiO_2 is photocatalytically active for at least six days of irradiation (unlike under oxygen atmosphere). Even after this time, suspension still keeps its purple colour. It was also confirmed that the heterogeneous catalytic system (both Au–TiO_2 and Pd/C) can be reused without a loss of activity. Entries 13 and 14 show a conversion after 24 hours with material that was recovered from runs in Entries 3 and 4 (72 hours of irradiation) via centrifugation, washed, and introduced to a fresh mixture of solvent and styrene.

Using more Pd/C catalyst did not lead to a higher conversion (Entries 15 and 16). Also, increasing the amount of Au–TiO_2 in suspension did not have a significantly positive effect (Entries 17 and 18), which is in accordance with light saturation observed in Section 2.2.2.3 (Figure 2.2.13). However, when the overall amount of catalyst suspension was doubled, but the styrene loading stayed the same, conversion in acetone increased almost exactly 2-fold (compare Entries 4 and 20). These observations suggest that at least in acetone, bottleneck of this reaction is the rate of hydrogen production generated by the system.

Coupling of photogenerated THF radical with TEMPO

A third possible synthetic application of Au–TiO_2 is a radical C–H activation for cross-coupling chemistry. The group of Kisch observed that when hydrogen is produced in suspensions of ZnS in aqueous THF upon irradiation ($\lambda > 248$ nm),

dimers of THF are selectively formed as a by-product (Scheme 2.2.6) and proposed a recombination of THF radicals as a plausible mechanism.[25]

When repeating this experiment by irradiating a suspension of Au–TiO_2 at 375 nm in pure (but not dry) THF, a formation of wide variety of different products was observed, among which the THF dimer—identified by GC-MS—was only a minor one (see Figure 2.2.23). This can be explained by an easy further oxidation of the THF radical.[26] However, when TEMPO was present in the reaction mixture, its adduct with the THF radical (Scheme 2.2.7) was identified by LC-MS as the major product and TEMPO was trapped almost quantitatively (see Figure 2.2.24). These results suggest that when a suitable trapping partner is present, the generated THF radical prefers coupling over further oxidation, which has a potential synthetic value. Radical cross-coupling chemistry was widely developed for both homogeneous[33] and heterogeneous[34] systems and this experiment shows that Au–TiO_2 has a potential to be used as a photocatalyst in this area.

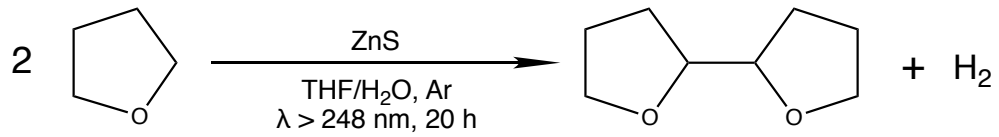

Scheme 2.2.6. Photocatalytic formation of THF dimers observed by the group of Kisch.[25]

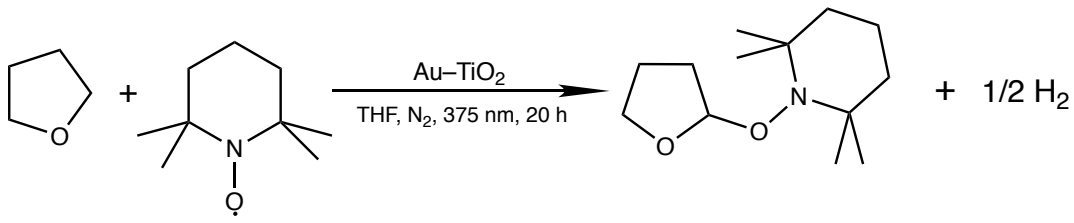

Scheme 2.2.7. Photocatalytic formation of THF–TEMPO adduct.

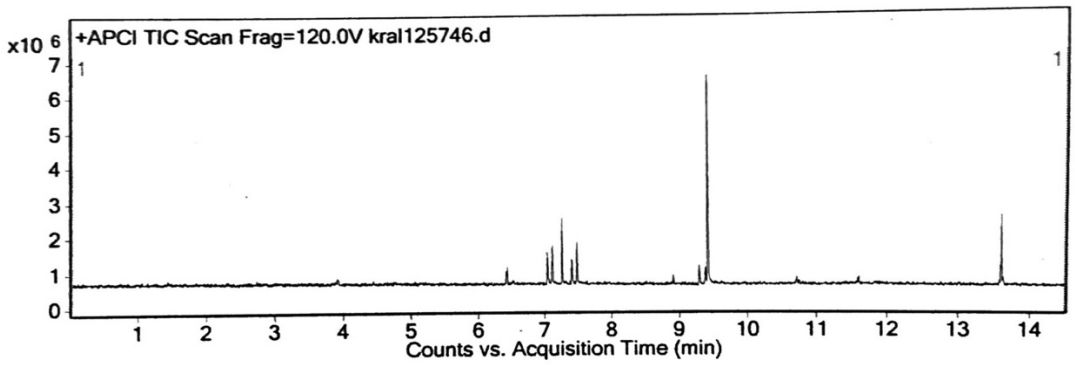

Figure 2.2.23. GC-MS chromatogram of a crude reaction mixture of THF and Au–TiO_2 after 20 hours of 375 nm irradiation. Desired THF dimer is represented by the peak with retention time of 7.1 min.

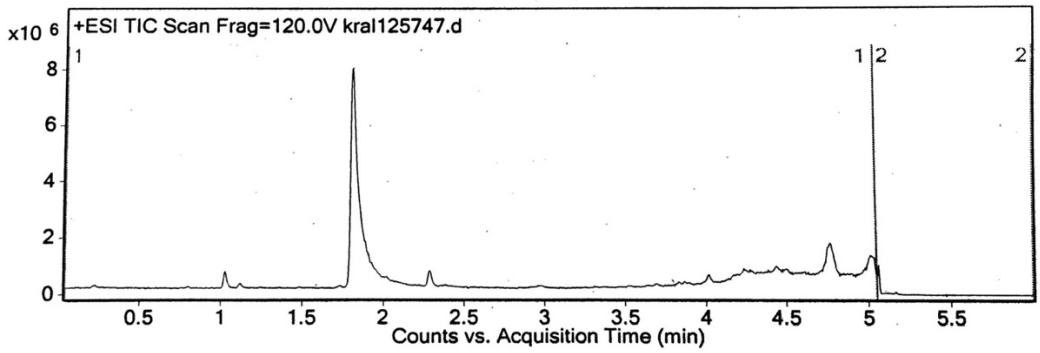

Figure 2.2.24. LC-MS chromatogram of a crude reaction mixture of THF and Au–TiO_2 with an addition of TEMPO after 20 hours of 375 nm irradiation. Desired THF–TEMPO adduct is represented by the peak with retention time of 1.8 min.

2.2.3 Conclusions

In this study, photocatalytic properties of titanium dioxide doped with gold nanoparticles and its potential application in organic synthesis were examined. Upon irradiation at 375 nm, the material is able to oxidise water, but its overall behaviour strongly depends on the reaction conditions. When irradiated under oxygen atmosphere, hydrogen peroxide is produced via reduction of molecular oxygen, but the catalyst itself shows a relatively low photostability when it's fully bleached and inactive after 24 hours of UV-A irradiation. On the other hand, when irradiated under inert atmosphere, hydrogen is generated through proton reduction and the material shows no signs of inactivation in the course of at least one week.

Behaviour of Au–TiO_2 in different solvents was studied. The material remains photocatalytically active even in one- and two-phase mixtures of water with organic solvents, while some of them—specifically acetone—significantly increase the rate (or efficiency) of water splitting. This observation is important for the use of Au–TiO_2 in organic synthesis, since it doesn't have to rely only on polar, water-miscible systems.

Three different potential synthetic applications were found for this catalytic system, while water was successfully used as a source of redox equivalents for both oxidation and reduction of organic compounds. Benzyl alcohol was oxidised to benzaldehyde by photocatalytically generated hydrogen peroxide in a presence of catalytic amounts of bromine. However, main problems of this system under oxidative conditions are relatively low steady-state concentration of H_2O_2 and low photostability of Au–TiO_2, which cause a relatively low-yield product formation. Also, photocatalytically generated hydrogen was used to reduce α-methylstyrene to cumene in relatively high yield. Additionally, the formation of THF radicals upon irradiation in tetrahydrofuran was observed and these radicals were successfully trapped with TEMPO.

2.2.4 Experimental section

2.2.4.1 General methods and materials

Head-space CG measurements were performed on INFICON 3000 Micro GC equipped with MS-5A column and thermal conductivity detector using argon as a carrier gas.

CG measurements were carried out on Agilent Technologies 7890A and 7890B Series instruments equipped with FID detectors and HP–5ms Ultra Inert columns using helium as a carrier gas.

UV-Vis spectra were recorded on Agilent Technologies Cary 100 spectrophotometer.

Solid-state UV-Vis spectra were recorded on Bruins Instruments Omega 20 spectrometer.

Light-source emission spectra were obtained with Avantes AvaSpec-3648 spectrometer.

Light intensity was measured with InternationalLight ILT1400 Portable Digital Radiometer.

XRD data were obtained by a general-purpose X-ray diffractometer (Rigaku, MiniFlex 600, Tokyo, Japan) equipped with a high-speed one-dimensional detector (Rigaku, D/teX Ultra, Tokyo, Japan) and a K_β foil filter. XRD patterns were recorded over the 2θ range of 3°–100°, with a step width of 0.02°, a scanning speed of 5° min^{-1}, and a Cu K_α radiation generated at 40 kV and 15 mA. The measurements were analysed by the Rigaku PDXL software.

UV irradiation was performed using Avonec 370–380 nm UV-A LEDs (λ_{max} = 375 nm, 3.5–4.5 V, 750 mA).

AEROXIDE® TiO_2 P25 from Evonik were used for a preparation of P25-based Au–TiO_2 and TiO_2 (rutile, 99.98 % metal basis) from Aldrich was used for a preparation of rutile-based Au–TiO_2. Gold(III) chloride trihydrate from Sigma-Aldrich (≥49 % Au basis) was used as a source of gold.

2.2.4.2 Preparation of Au–TiO_2

The catalyst was prepared following a literature procedure.[15]

Aqueous solution of $AuCl_3 \cdot 3H_2O$ (5 mL, 5 mM) was heated up to 70 °C and neutralized to pH between 6 and 7 with 0.1 M solution of NaOH. The resulting solution (5.4 mL) was added to 50 mL of Milli-Q water in 100 mL

round-bottom flask preheated to 70 °C (85 °C in oil bath). After stirring for 15 minutes, TiO_2 (0.5 g) was added, the suspension was stirred at 500 RPM for an hour at 70 °C (85 °C in oil bath) and then for another two hours at RT. The solid phase was separated via centrifugation, washed three times with Milli-Q water and dried overnight at 70 °C in a drying cabinet. Then, the material was finely ground and dried again overnight.

Neutralisation of gold solution must be done slowly and dropwise, and the pH should never exceed 7, not even temporarily.

2.2.4.3 General procedure for H_2O_2 generation with one liquid phase

Small crimp-top vial equipped with a magnetic stirring bar containing a suspension of Au–TiO_2 (5 mg) in a solvent of choice (1 mL) was sealed with a septum, the mixture was sonicated for 5 minutes, and the head-space atmosphere was exchanged for oxygen using a balloon. The vial was placed in an aluminium block tempered to 25 °C and irradiated from the bottom with a selected LED for a selected time under slow stirring. Afterwards, the heterogeneous catalyst was removed via centrifugation, the supernatant liquid was diluted 5-times with distilled water, and a concentration of hydrogen peroxide was determined using HRP assay.

2.2.4.4 General procedure for H_2O_2 generation with two liquid phases

Au–TiO_2 (5 mg) was weighed into a small crimp-top vial. Then, the selected amount of water was added and the content was sonicated for 5 minutes. Then, the hydrophobic organic solvent was added so that the overall volume was 1 mL. The vial was sealed with a septum, sonicated for another 5 minutes, and the head-space atmosphere was exchanged for oxygen using a balloon. The vial was placed in an aluminium block tempered to 25 °C and irradiated from the bottom with a selected LED for a selected time under slow stirring. Afterwards, water was added so the volume of aqueous phase was 1 mL, the mixture was

thoroughly shaken and separated via centrifugation. The aqueous phase was then diluted 5-times with distilled water and the concentration of hydrogen peroxide was determined using HRP assay.

2.2.4.5 Horseradish-peroxidase (HRP) assay

A freshly pre-mixed working solution (250 µL) containing DA-64 dye (129 µL, 1 mM), HRP (0.52 µL, 0.4 U/mL), and MES buffer (1160 µL, pH 6.0, 20 mM) was added to the measured sample containing hydrogen peroxide (250 µL). The resulting assay solution was then incubated at RT for 25 min, diluted 12-times, and absorbance of the solution at 725 nm was recorded and compared with a calibration curve to determine H_2O_2 concentration.

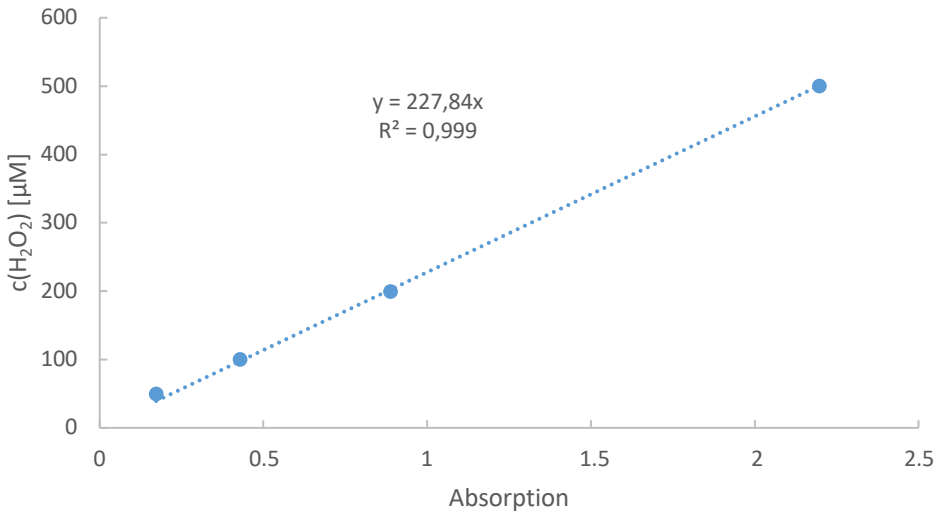

Figure 2.2.25. Calibration curve for HRP assay.

2.2.4.6 General procedure for H_2 generation

Small crimp-top vial equipped with a magnetic stirring bar containing a suspension of Au–TiO_2 (5 mg) in a solvent of choice (1 mL) was sealed with a septum, the mixture was sonicated for 5 minutes, and the head-space atmosphere was evacuated and flushed with nitrogen 5 times. The vial was placed in an aluminium block tempered to 25 °C and irradiated from the bottom

with a selected LED for a selected time under slow stirring. Afterwards, reaction vial was directly connected to head-space GC through septum and the gas phase was analysed.

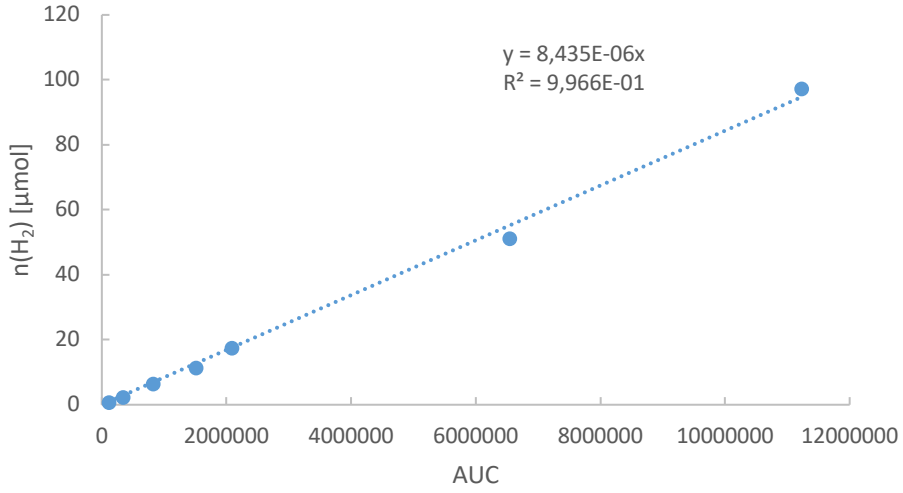

Figure 2.2.26. Calibration curve for head-space GC for aqueous samples.

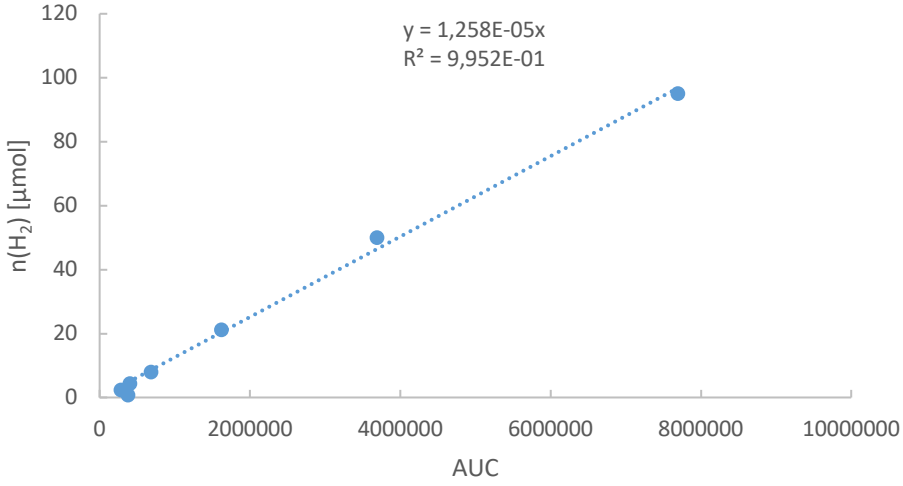

Figure 2.2.27. Calibration curve for head-space GC for organic samples.

2.2.4.7 Oxidation of benzyl alcohol in a presence of Br_2

Au–TiO_2 (5 mg) was weighed into a small crimp-top vial. Then, water (1 mL) and DCM (1 mL) were added together with benzyl alcohol (138 µL, 1.34 mmol). The vial was sealed with a septum, sonicated for 5 minutes, and the head-space

atmosphere was exchanged for oxygen using a balloon. Finally, bromine (5 μL, 98 μmol) was added through septum using a syringe. The vial was placed in an aluminium block tempered to 25 °C, connected to an oxygen balloon through a needle and irradiated from the bottom with 375 nm LED for 24 hours. Afterwards, the heterogeneous catalyst was removed via centrifugation and the supernatant liquid was extracted 2 times with 1 mL of ethyl acetate. Organic phases were collected, toluene (145 μL, 1.36 mmol) was added as an internal standard, and the mixture was analysed by GC.

2.2.4.8 Reduction of α-methylstyrene to cumene

Au–TiO_2 (5 mg) and Pd/C (10 w%, 4 mg, 3.8 μmol of Pd) were weighed into a small crimp-top vial. Then, water or 75 % aqueous acetone (1 mL) were added together with α-methylstyrene (110 μL, 0.85 mmol). The vial was sealed with a septum, sonicated for 5 minutes, and the head-space atmosphere was evacuated and flushed with nitrogen 5 times. The vial was placed in an aluminium block tempered to 25 °C and irradiated from the bottom with 375 nm LED for a selected time under slow stirring. Afterwards, the solid phase was removed via centrifugation and the supernatant liquid was extracted 2 times with 1 mL of ethyl acetate. Organic phases were collected, toluene (45 μL, 0.42 mmol) was added as an internal standard, and the mixture was analysed by GC.

2.2.4.9 Coupling of photogenerated THF radical with TEMPO

Au–TiO_2 (5 mg) and TEMPO (60 mg, 0.38 mmol) were weighed into a small crimp-top vial. Then, THF (1 mL) was added, vial was sealed with a septum, sonicated for 5 minutes, and the head-space atmosphere was evacuated and flushed with nitrogen 5 times. The vial was placed in an aluminium block tempered to 25 °C and irradiated from the bottom with 375 nm LED for 20 hours under slow stirring. Afterwards, the heterogeneous catalyst was removed

via centrifugation. The supernatant liquid was transferred into an Eppendorf tube and evaporated in a slow stream of nitrogen. The oily residue was then submitted for LC-MS analysis.

2.2.5 Contributions

XRD measurements were performed by Melanie Iwanow (Fraunhofer IGB, Straubing, Germany). Solid-state UV-Vis spectra were measure by Thomas Buchecker (Institute of Inorganic Chemistry, University of Regensburg, Regensburg, Germany). GC-MS and LC-MS measurements were performed by the Central Analytical Department of the University of Regensburg. Reference sample of Au–TiO_2 was provided by Dr. Wuyuan Zhang (Department of Biotechnology, Delft University of Technology, Delft, Netherlands).

2.2.6 References

1. Gamba Sanchez, D. A., Hydrogen Peroxide: A Versatile Reagent in Organic Synthesis. *Synlett* **2008**, *2008* (07), 1101-1102.
2. M., C.-M. J.; Gema, B.-B.; G., F. J. L., Hydrogen Peroxide Synthesis: An Outlook beyond the Anthraquinone Process. *Angew. Chem. Int. Ed.* **2006**, *45* (42), 6962-6984.
3. Diesen, V.; Jonsson, M., Formation of H2O2 in TiO2 Photocatalysis of Oxygenated and Deoxygenated Aqueous Systems: A Probe for Photocatalytically Produced Hydroxyl Radicals. *J. Phys. Chem. C* **2014**, *118* (19), 10083-10087.
4. Ni, M.; Leung, M. K. H.; Leung, D. Y. C.; Sumathy, K., A review and recent developments in photocatalytic water-splitting using TiO2 for hydrogen production. *Renew. Sust. Energ. Rev.* **2007**, *11* (3), 401-425.
5. Ozawa, K.; Emori, M.; Yamamoto, S.; Yukawa, R.; Yamamoto, S.; Hobara, R.; Fujikawa, K.; Sakama, H.; Matsuda, I., Electron–Hole Recombination

Time at TiO2 Single-Crystal Surfaces: Influence of Surface Band Bending. *J. Phys. Chem. Lett.* **2014**, *5* (11), 1953-1957.

6. Li, X.; Chen, C.; Zhao, J., Mechanism of Photodecomposition of H2O2 on TiO2 Surfaces under Visible Light Irradiation. *Langmuir* **2001**, *17* (13), 4118-4122.
7. Maurino, V.; Minero, C.; Mariella, G.; Pelizzetti, E., Sustained production of H2O2 on irradiated TiO2 – fluoride systems. *Chem. Comm.* **2005**, (20), 2627-2629.
8. Teranishi, M.; Naya, S.-i.; Tada, H., In Situ Liquid Phase Synthesis of Hydrogen Peroxide from Molecular Oxygen Using Gold Nanoparticle-Loaded Titanium(IV) Dioxide Photocatalyst. *J. Am. Chem. Soc.* **2010**, *132* (23), 7850-7851.
9. Teranishi, M.; Hoshino, R.; Naya, S.-i.; Tada, H., Gold-Nanoparticle-Loaded Carbonate-Modified Titanium(IV) Oxide Surface: Visible-Light-Driven Formation of Hydrogen Peroxide from Oxygen. *Angew. Chem. Int. Ed.* **2016**, *55* (41), 12773-12777.
10. Wang, C.; Astruc, D., Nanogold plasmonic photocatalysis for organic synthesis and clean energy conversion. *Chem. Soc. Rev.* **2014**, *43* (20), 7188-7216.
11. Zhu, S.; Liang, S.; Gu, Q.; Xie, L.; Wang, J.; Ding, Z.; Liu, P., Effect of Au supported TiO2 with dominant exposed {001} facets on the visible-light photocatalytic activity. *Appl. Catal. B-Environ.* **2012**, *119-120*, 146-155.
12. Linsebigler, A. L.; Lu, G.; Yates, J. T., Photocatalysis on TiO2 Surfaces: Principles, Mechanisms, and Selected Results. *Chem. Rev.* **1995**, *95* (3), 735-758.
13. Tsukamoto, D.; Shiro, A.; Shiraishi, Y.; Sugano, Y.; Ichikawa, S.; Tanaka, S.; Hirai, T., Photocatalytic H2O2 Production from Ethanol/O2 System Using TiO2 Loaded with Au–Ag Bimetallic Alloy Nanoparticles. *ACS Catal.* **2012**, *2* (4), 599-603.

14. Priebe, J. B.; Karnahl, M.; Junge, H.; Beller, M.; Hollmann, D.; Brückner, A., Water Reduction with Visible Light: Synergy between Optical Transitions and Electron Transfer in Au-TiO2 Catalysts Visualized by In situ EPR Spectroscopy. *Angew. Chem. Int. Ed.* **2013**, *52* (43), 11420-11424.
15. Priebe, J. B.; Radnik, J.; Lennox, A. J. J.; Pohl, M.-M.; Karnahl, M.; Hollmann, D.; Grabow, K.; Bentrup, U.; Junge, H.; Beller, M.; Brückner, A., Solar Hydrogen Production by Plasmonic Au–TiO2 Catalysts: Impact of Synthesis Protocol and TiO2 Phase on Charge Transfer Efficiency and H2 Evolution Rates. *ACS Catal.* **2015**, *5* (4), 2137-2148.
16. Armaroli, N.; Balzani, V., The Future of Energy Supply: Challenges and Opportunities. *Angew. Chem. Int. Ed.* **2007**, *46* (1-2), 52-66.
17. Rylander, P., *Catalytic Hydrogenation over Platinum Metals*. Academic Press: 1967.
18. Zhang, W.; Fernández-Fueyo, E.; Ni, Y.; van Schie, M.; Gacs, J.; Renirie, R.; Wever, R.; Mutti, F. G.; Rother, D.; Alcalde, M.; Hollmann, F., Selective aerobic oxidation reactions using a combination of photocatalytic water oxidation and enzymatic oxyfunctionalizations. *Nat. Catal.* **2018**, *1* (1), 55-62.
19. Liu, Z.; Hou, W.; Pavaskar, P.; Aykol, M.; Cronin, S. B., Plasmon Resonant Enhancement of Photocatalytic Water Splitting Under Visible Illumination. *Nano Lett.* **2011**, *11* (3), 1111-1116.
20. Miyata, K.-i.; Miyashita, M.; Nose, R.; Otake, Y.; Miyagawa, H., Development of a Colorimetric Assay for Determining the Amount of H2O2 Generated in Tobacco Cells in Response to Elicitors and Its Application to Study of the Structure-Activity Relationship of Flagellin-Derived Peptides. *Biosci. Biotech. Bioch.* **2006**, *70* (9), 2138-2144.
21. Kimura, K.; Naya, S.-i.; Jin-nouchi, Y.; Tada, H., TiO2 Crystal Form-Dependence of the Au/TiO2 Plasmon Photocatalyst's Activity. *J. Phys. Chem. C* **2012**, *116* (12), 7111-7117.

22. Ahmed, A. Y.; Kandiel, T. A.; Oekermann, T.; Bahnemann, D., Photocatalytic Activities of Different Well-defined Single Crystal TiO2 Surfaces: Anatase versus Rutile. *J. Phys. Chem. Lett.* **2011**, *2* (19), 2461-2465.
23. Ohtani, B.; Prieto-Mahaney, O. O.; Li, D.; Abe, R., What is Degussa (Evonik) P25? Crystalline composition analysis, reconstruction from isolated pure particles and photocatalytic activity test. *J. Photoch. Photobio. A* **2010**, *216* (2), 179-182.
24. Cherevatskaya, M.; Neumann, M.; Füldner, S.; Harlander, C.; Kümmel, S.; Dankesreiter, S.; Pfitzner, A.; Zeitler, K.; König, B., Visible-Light-Promoted Stereoselective Alkylation by Combining Heterogeneous Photocatalysis with Organocatalysis. *Angew. Chem. Int. Ed.* **2012**, *51* (17), 4062-4066.
25. Zeug, N.; Buecheler, J.; Kisch, H., Catalytic formation of hydrogen and carbon-carbon bonds on illuminated zinc sulfide generated from zinc dithiolenes. *J. Am. Chem. Soc.* **1985**, *107* (6), 1459-1465.
26. Woźnica, M.; Chaoui, N.; Taabache, S.; Blechert, S., THF: An Efficient Electron Donor in Continuous Flow Radical Cyclization Photocatalyzed by Graphitic Carbon Nitride. *Chem.-Eur. J* **2014**, *20* (45), 14624-14628.
27. Greenwood, N. N.; Earnshaw, A., *Chemistry of the Elements*. Pergamon Press Plc: Oxford, 1984.
28. Harbour, J. R.; Tromp, J.; Hair, M. L., Photogeneration of hydrogen peroxide in aqueous TiO2 dispersions. *Can. J. Chem.* **1985**, *63* (1), 204-208.
29. Boonstra, A. H.; Mutsaers, C. A. H. A., Relation between the photoadsorption of oxygen and the number of hydroxyl groups on a titanium dioxide surface. *J. Phys. Chem.-US* **1975**, *79* (16), 1694-1698.
30. Boonstra, A. H.; Mutsaers, C. A. H. A., Adsorption of hydrogen peroxide on the surface of titanium dioxide. *J. Phys. Chem.-US* **1975**, *79* (18), 1940-1943.
31. Amati, A.; Dosualdo, G.; Zhao, L.; Bravo, A.; Fontana, F.; Minisci, F.; Bjørsvik, H.-R., Catalytic Processes of Oxidation by Hydrogen Peroxide in

the Presence of Br2 or HBr. Mechanism and Synthetic Applications. *Org. Process Res. Dev.* **1998**, *2* (4), 261-269.

32. Shiraishi, Y.; Kanazawa, S.; Tsukamoto, D.; Shiro, A.; Sugano, Y.; Hirai, T., Selective Hydrogen Peroxide Formation by Titanium Dioxide Photocatalysis with Benzylic Alcohols and Molecular Oxygen in Water. *ACS Catal.* **2013**, *3* (10), 2222-2227.
33. Yi, H.; Zhang, G.; Wang, H.; Huang, Z.; Wang, J.; Singh, A. K.; Lei, A., Recent Advances in Radical C–H Activation/Radical Cross-Coupling. *Chem. Rev.* **2017**, *117* (13), 9016-9085.
34. Kisch, H., Semiconductor Photocatalysis for Chemoselective Radical Coupling Reactions. *Accounts Chem. Res.* **2017**, *50* (4), 1002-1010.

2.3 Atom-Economic Electron Donors for Photobiocatalytic Halogenations

Section 2.3 was published as:

Seel, C. J.; Králík, A.; Hacker, M.; Frank, A.; König, B.; Gulder, T., Atom-Economic Electron Donors for Photobiocatalytic Halogenations. *ChemCatChem* ***2018***.
DOI: 10.1002/cctc.201800886
– Published by Wiley-VCH and ChemPubSoc Europe

CJS performed expression of enzymes, studied different homogeneous methods for H_2O_2 dosing, performed homogeneous photobiocatalytic brominations and chlorinations and their kinetic studies, prepared and characterised standards of non-commercial compounds, provided HPLC measurements, and wrote corresponding parts of the manuscript as well as the Introduction. AK evaluated properties of Au–TiO_2, studied comparison between FMN-mediated homogeneous and Au–TiO_2-mediated heterogeneous photocatalytic generation of H_2O_2, performed heterogeneous photobiocatalytic brominations, provided GC, head-space GC, and oxygen-probe measurements, and wrote corresponding parts of the manuscript. MH performed a minor part of homogeneous photobiocatalytic halogenations. AF provided know-how for expression of enzymes. BK and TG supervised the project and are corresponding authors.

2.3.1 Introduction

Biocatalysts are playing a key role in establishing environmentally friendly processes, as they offer high and often unique reactivities and selectivities under mild reaction conditions. Peroxidases (EC1.11.1x) are a class of antioxidant enzymes ubiquitous in Nature. They catalyze a plethora of interesting transformations, like *e.g. C,H*-oxidations and halogenations, by making use of cellular hydrogen peroxide rather than utilizing complicated electron delivery

chains via nicotinamide cofactors.[1] Their sensitivity towards the inevitable oxidant is a key limitation for their broad application. Heme-dependent peroxidases, in particular, suffer from irreversible oxidative inactivation of the prosthetic group by H_2O_2. Keeping the H_2O_2 level low during the whole reaction is thus crucial for *in vitro* biocatalytic processes.[2] Various methods providing continuous oxidant supply have been developed to overcome this drawback, such as slow dosage of hydrogen peroxide via a syringe pump[3] or a H_2O_2-stat.[4] Additionally, *in situ* H_2O_2-delivery systems were studied: electrochemical generation of H_2O_2,[5] Pd/H_2 in supercritical CO_2,[6] or biocatalytic formation by glucose oxidase (GOx).[7] The drawbacks of these procedures reach from low atom economy to simply being not practical, in particular on preparative scale.

One innovative approach to acquire the electrons needed by the redox enzymes is photocatalysis.[8] The photocatalyst, like, *e.g.*, flavin mononucleotide (FMN),[9] is excited to FMN^* by blue light followed by its reduction to $FMNH_2$ at the expense of an electron donor. $FMNH_2$ is then re-oxidized by atmospheric O_2 to form H_2O_2 (Scheme 2.3.1). This continuous, light-driven process guarantees a constant, but low hydrogen peroxide concentration in solution and thus renders its combination with biocatalytic processes ideal, especially if oxidation sensitive enzymes are involved. The sacrificial electron donor, however, can constitute an obstacle in this photobiocatalytic setup, as commonly employed reductants, such as EDTA, formates, or 4-methoxybenzyl alcohol, may suffer *e.g.* from incompatibility with the enzyme and cumbersome separation from the products.[10]

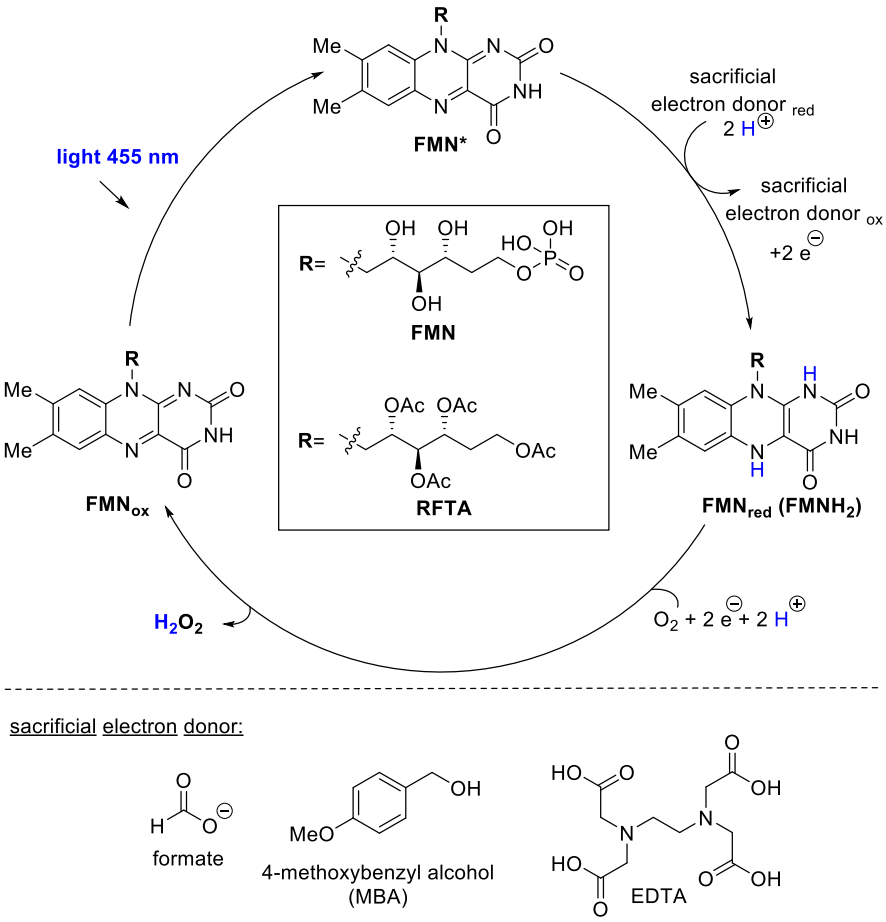

Scheme 2.3.1. General mechanism of visible-light promoted electron transfer employing flavin-derived redox mediators.

2.3.2 Results and discussion

However, intrigued by the advantages offered by this photobiocatalytic concept,[11] we started to evaluate alternative and more environmentally benign electron sources. We first turned our attention on employing buffers as possible reductants. As enzymatic transformations intrinsically require buffered solutions, to adjust and maintain a distinct pH value at which the enzyme is operating, these buffer components are always present in any biocatalytic reaction mixtures. Employing any other, external electron donors besides the buffer salt or the solvent, however, constitutes always an 'extra', (over)stoichiometric additive to the reaction mixture. While screening different redox-active buffers, we observed that those containing tertiary amines,[12]

such as MOPS, MES, HEPES and Tris, gave the best results as electron donors for the photocatalytic production of H_2O_2 in our system (see SI). Both FMN and RFTA worked with equal success, but the hydrophilic nature of FMN makes its application more convenient. Kinetic experiments (see Figure 2.3.2) revealed that the H_2O_2 production catalyzed by FMN using MES buffer as an electron source is very fast and reaches a plateau at 2 mM H_2O_2 after 10 min, possibly due to an equilibrium between newly generated and decaying hydrogen peroxide. For irradiation at the absorption maximum of FMN (455 nm, blue LEDs), we did not observe any impact of the FMN loading on the O_2-consumption rate (see SI), indicating that the energy output of the light source rather than the catalyst loading determines the H_2O_2 generation rate, at least at the FMN concentrations tested here (37 μM–2 mM, see SI). Consequently, the light intensity can be used to control the H_2O_2 release and thus to fine tune the oxidative conditions depending on the H_2O_2 sensitivity of the enzyme.

We next turned our focus on combining this H_2O_2-generating system with enzymatic halogenations. For these photobiocatalytic studies we picked the vanadium-dependent haloperoxidase (VHPO) *Am*VHPO from the cyanobacterium *Acaryochloris marina* MBIC 11017.[13] *Am*VHPO shows a remarkable robustness towards organic solvents and heat together with a broad substrate scope for aromatic bromination. Nevertheless, sensitivity to high H_2O_2 concentrations, as already reported for many VHPOs,[14] was also observed for *Am*VHPO and thus makes it the perfect model enzyme to evaluate photobiocatalytic halogenations.

Very low catalyst loadings of 0.5 mol% and buffer concentrations as low as 25 mM turned out to be sufficient for achieving halogenations of a manifold of different electron-rich (hetero)aromatic compounds **1** in MES buffer (Scheme 2.3.2 and for details SI) without any change in the pH during the course of the reaction. No conversion of **1** was observed if the reaction was conducted in the dark or in the absence of enzyme and of FMN.[15] Lyophilized cell lysate

of *Am*VHPO, constituting a more time-efficient alternative to the purified enzyme, and the more reactive isoenzyme *Am*VHPO II (cf. SI) were likewise applicable under these conditions without any loss in reactivity. The enzyme's activity was not affected by 0.5 mol% FMN or irradiation itself,[16] but inactivation became a critical factor at higher FMN concentrations (cf. SI). Interaction of excited FMN* with highly electron-rich substrates **1**, however, was detectable even at such low catalyst concentrations (see SI), resulting in oxidative degradation of highly activated compounds such as **1c**, **1i** and **1j**. To overcome this limitation, we slightly varied our protocol and pre-generated H_2O_2 prior to the addition of the substrate. This procedure resulted in good conversions of oxidation-sensitive molecules and avoided substrate or product decomposition.

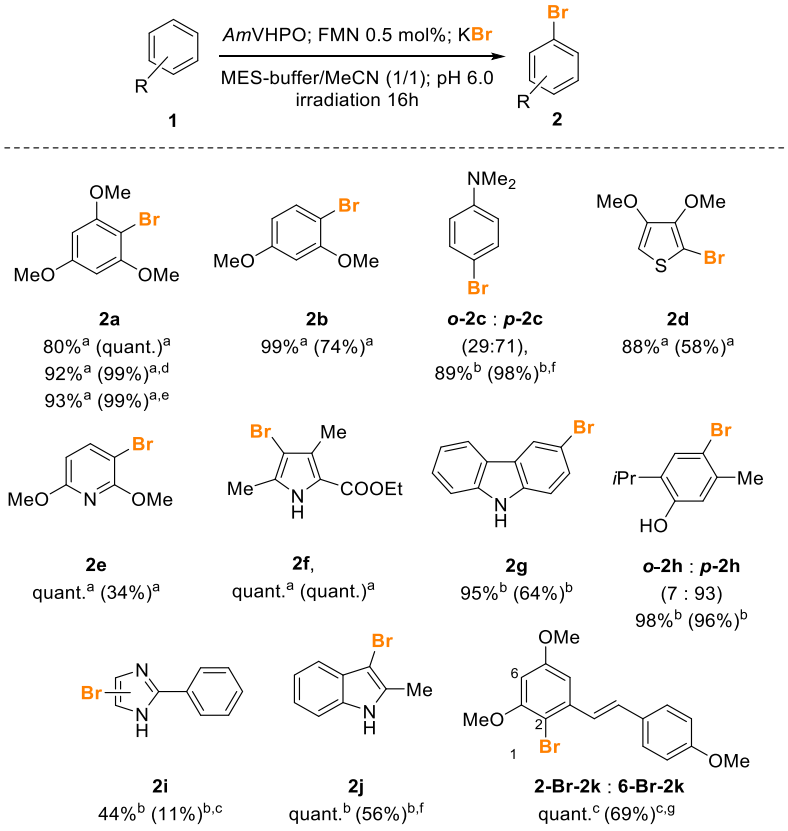

Scheme 2.3.2. Photobiocatalytic aromatic bromination using *Am*VHPO. Reactions were carried out using 7.43 mM substrate, 0.5 mol% FMN, 3.77 µM *Am*VHPO, 188 µM Na_3VO_4, 100 mM MES (pH 6.0), and 8.13 mM KBr at rt under irradiation (455 nm). Yields are based on recovered starting material and have been determined by [a]HPLC, [b]GC, or [c]NMR using

dodecane, toluene or phenol as internal standard. Conversions (shown in brackets) and ratios of isomers were determined by [a]HPLC, [b]GC, or [c]NMR using dodecane, toluene or phenol as internal standard. [d]50 mM MES buffer was used. [e]25 mM MES buffer was used. [f]15 mol% FMN (15 min irradiation), additional 15 mol% FMN (15 min irradiation) followed by addition of **1** and enzyme. [g]Partial isomerization of the double bond was observed upon irradiation.

The method was further advanced by evaluating its application in aromatic chlorinations, which are generally more difficult to achieve than the corresponding brominations.[17] Here, the fungal VHPO from *Curvularia inaequalis* (*Ci*VHPO)[18] was employed as it offers a higher oxidation potential compared to *Am*VHPO. By simply changing the added halide salt from KBr to KCl the desired chlorination of activated arenes was likewise possible, albeit, as expected, in lower chemical yields (Scheme 2.3.3). It is noteworthy that the regioselectivity for **3c** with predominant *ortho*-substitution differs from that observed during the enzymatic bromination (see Scheme 2.3.2), hinting at a mechanism involving an *N*-chlorination followed by intramolecular transfer of the chloro atom to the *ortho* position.

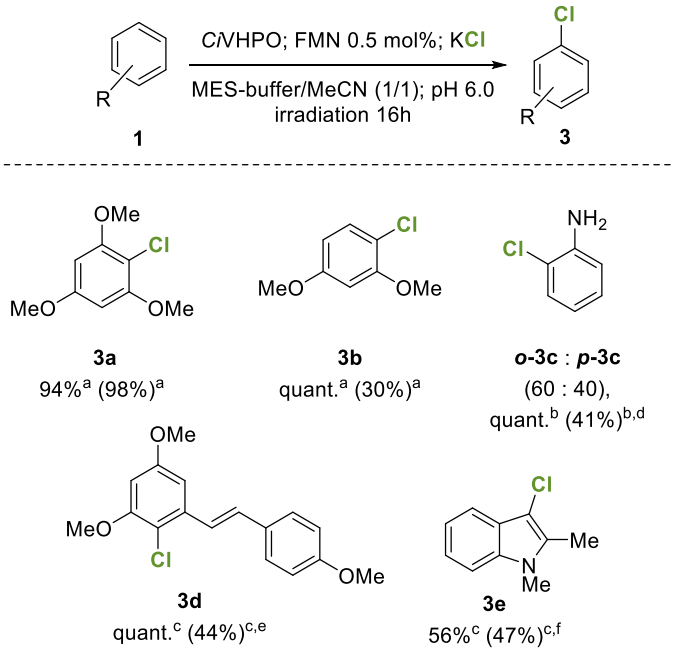

Scheme 2.3.3. Photobiocatalytic aromatic chlorinations using *Ci*VHPO. Reactions were carried out using 7.43 mM substrate, 0.5 mol% FMN, 1.60 μM CiVHPO, 188 μM Na_3VO_4, 100 mM MES (pH 5.0) and 8.13 mM KCl at rt under irradiation (455 nm). Yields are based

on recovered starting material and have been determined by [a]HPLC, [b]GC, or [c]NMR using dodecane, toluene or phenol as internal standard. Conversions (shown in brackets) and ratios of isomers were determined by [a]HPLC, [b]GC, or [c]NMR using dodecane, toluene or phenol as internal standard. [d]15 mol% FMN (15 min irradiation), additional 15 mol% FMN (15 min irradiation) followed by addition of **1** and enzyme. [e]Isomerization of the product was observed upon irradiation. [f]Decomposition of the product occurred during NMR measurement.

Although the use of buffer components as an electron source is convenient, since the presence of buffer is necessary due to the requirements of the enzymatic reaction, the ultimate goal of sustainable chemistry is utilizing water to provide redox equivalents.[19,20] During our studies, a method for heterogeneous photocatalytic H_2O_2 evolution from methanol[19] and water[22] oxidation in the presence of air using TiO_2 doped with gold nanoparticles[23] was reported. We thus set out to evaluate the activity of this catalyst more closely (for details see SI). For these studies, TiO_2 was used in its rutile form, which makes the photocatalyst more enzyme-compatible due to its hydrophobic properties preventing hydrophilic enzymes from adsorption to the TiO_2 surface. This spatial separation might protect the enzyme from highly reactive – but short-lived – hydroxyl radicals formed by titanium dioxide in aerated aqueous solution upon irradiation.[22] We first investigated the ability of Au-TiO_2 to generate H_2O_2 via water oxidation under irradiation with different narrow-emission-band light sources, in particular, UV-A (375 nm), blue (455 nm), green (535 nm), and white (as a visible-light-only, broad-emission source) LEDs. Although Au-TiO_2 was previously described as a visible-light photocatalyst,[22] hydrogen peroxide evolution exclusively occurred at 375 nm UV irradiation in our hands (Figure 2.3.1).

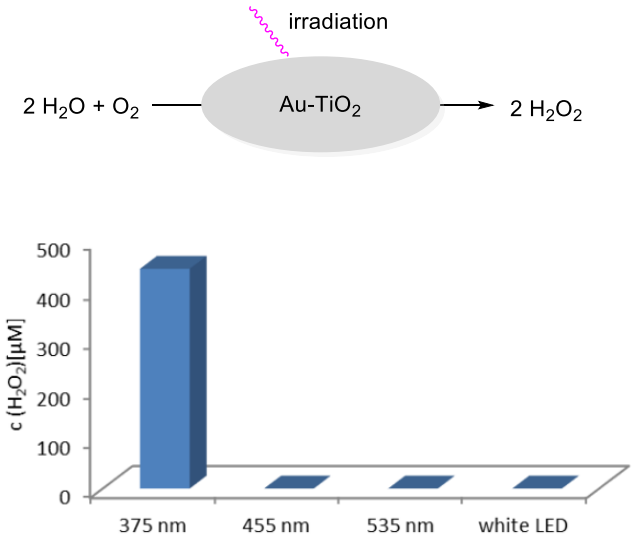

Figure 2.3.1. Schematic depiction of the photocatalytic generation of H_2O_2 using gold-nanoparticle-doped TiO_2 as a photocatalyst and concentration of hydrogen peroxide after irradiation (1 h) of an Au-TiO_2 suspension in pure water using different light sources.

When a degassed suspension of Au-TiO_2 in water was irradiated under N_2 atmosphere, only traces of H_2O_2 and no oxygen were detected in the solution and the gas phase, respectively. *Am*VHPO-mediated bromination of **1e** showed only low conversion (4 %), when performed under an inert atmosphere (cf. SI). These observations correspond to a two-electron water oxidation and a two-electron oxygen reduction taking place under the given conditions.

Kinetic measurements of the catalyst's activity showed a similar profile of H_2O_2 generation as the FMN-containing system within the first 240 s (Figure 2.3.2, black). Upon further irradiation the Au-TiO2-based system reached a plateau[24] with an equilibrium concentration of H_2O_2 3–4 times lower than that observed for FMN (ca. 600 mM). This heterogeneous water-splitting system is thus a milder source of in situ-generated hydrogen peroxide, which can be favorable for more sensitive biocatalysts than *Am*VHPO and *Ci*VHPO.

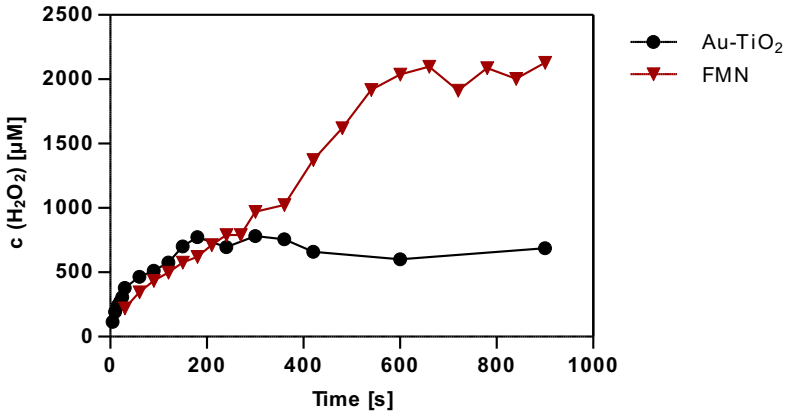

Figure 2.3.2. Kinetic of the H_2O_2 evolution by FMN in a MES-buffered solution and Au-TiO_2 in pure distilled water under standard conditions. H_2O_2 concentration was determined by horseradish peroxidase assay.

In situ hydrogen-peroxide evolution using Au-TiO_2 under irradiation at 375 nm was then successfully applied to a bromination of 2,6-dimethoxypyridine (**1e**) catalyzed by *Am*VHPO reaching results superior to the above mentioned flavin systems (Scheme 2.3.4). This shows a clear advantage of a milder source of H_2O_2 in an enzymatic reaction. For this reaction, non-oxidizable phosphate buffer was used to ensure that water is the sole source of electrons. The results of the control reactions (see SI) show a vital role of all reaction elements – light, photocatalyst, oxygen, and enzyme. It is also worth mentioning that the enzyme keeps its activity even in the presence of phosphate (10 mM), which is an inhibitor[25] of VHPOs due to its isosteric nature to the crucial vanadate present in the active center of these enzymes. Moreover, the tolerance of UV light underlines the high robustness of this class of enzymes and makes it thus ideally suited for the use in photobiocatalysis.

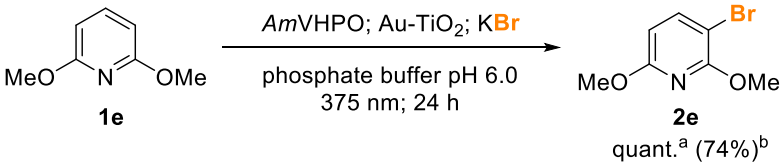

Scheme 2.3.4. Application of the photocatalytic Au-TiO2-mediated generation of H_2O_2 with an *Am*VHPO-catalyzed bromination. [a]Yield is based on recovered starting material and has been determined by HPLC chromatography using an internal standard. [b]Conversion and ratio of isomers were determined by HPLC chromatography using an internal standard.

2.3.3 Conclusions

In summary, we have shown that combining photocatalysis with biocatalysis represents a mild and environmentally benign approach to overcome the pending problem of supplying oxidative enzymes with their redox equivalents. The previously used, wasteful and thus far from ideal sacrificial electron donors, have been replaced by either redox-active buffers or even water itself, both ubiquitously present in enzymatic reactions. These *in-situ* H_2O_2-delivering setups stand out due to their practicability by simply utilizing light with the help of low-concentrated organic or heterogenous metal photocatalysts. Proof of concept towards the applicability of the buffer/FMN/visible light as well as the water/Au-TiO_2/UVA approach was given by establishing efficient photobiocatalytic halogenations using *Am*VHPO and *Ci*VHPO as convenient model enzymes. Both photochemical methods proved to be beneficial for sustaining halogenation activity over several hours. The described methods for oxidative H_2O_2 generation, however, are neither limited to (aromatic) halogenations nor to the VHPO class of enzymes. Having now a robust and biocompatible method in hands, expansion of this versatile principle to different transformations by utilizing even more delicate oxidation enzymes is currently conducted in our laboratories.

2.3.4 Experimental section

Description of experimental procedures and other supporting information relevant to this part of Chapter 2 can be found in an electronic appendix on the attached CD.

2.3.5 References

1. Leak, D. J.; Sheldon, R. A.; Woodley, J. M.; Adlercreutz, P., Biocatalysts for selective introduction of oxygen. *Biocatal. Biotransform.* **2009**, *27* (1), 1-26.
2. Valderrama, B.; Ayala, M.; Vazquez-Duhalt, R., Suicide Inactivation of Peroxidases and the Challenge of Engineering More Robust Enzymes. *Chem. Biol.* **2002**, *9* (5), 555-565.
3. Tuynman, A.; Vink, M. K. S.; Dekker, H. L.; Schoemaker, H. E.; Wever, R., The sulphoxidation of thioanisole catalysed by lactoperoxidase and Coprinus cinereus peroxidase: Evidence for an oxygen-rebound mechanism. *Eur. J. Biochem.* **1998**, *258* (2), 906-913.
4. Van Deurzen, M. P. J.; Seelbach, K.; van Rantwijk, F.; Kragl, U.; Sheldon, R. A., Chloroperoxidase: Use of a Hydrogen Peroxide-Stat for Controlling Reactions and Improving Enzyme Performance. *Biocatal. Biotransform.* **1997**, *15* (1), 1-16.
5. Lee, K.; Moon, S.-H., Electroenzymatic oxidation of veratryl alcohol by lignin peroxidase. *J. Biotechnol.* **2003**, *102* (3), 261-268.
6. Karmee, S. K.; Roosen, C.; Kohlmann, C.; Lütz, S.; Greiner, L.; Leitner, W., Chemo-enzymatic cascade oxidation in supercritical carbon dioxide/water biphasic media. *Green Chem.* **2009**, *11* (7), 1052-1055.
7. Okrasa, K.; Guibé-Jampel, E.; Therisod, M., Tandem peroxidase–glucose oxidase catalysed enantioselective sulfoxidation of thioanisoles. *J. Chem. Soc., Perkin Trans. 1* **2000**, (7), 1077-1079.

8a. Lee, S. H.; Choi, D. S.; Kuk, S. K.; Park, C. B., Photobiocatalysis: Activating Redox Enzymes by Direct or Indirect Transfer of Photoinduced Electrons. *Angew. Chem. Int. Ed.* **2018**, *57* (27), 7958-7985.

8b. Maciá-Agulló, J. A.; Corma, A.; Garcia, H., Photobiocatalysis: The Power of Combining Photocatalysis and Enzymes. *Chem.-Eur. J.* **2015**, *21* (31), 10940-10959.

9. Perez, D. I.; Grau, M. M.; Arends, I. W. C. E.; Hollmann, F., Visible light-driven and chloroperoxidase-catalyzed oxygenation reactions. *Chem. Commun.* **2009**, (44), 6848-6850.

10. For a more detailed discussion on the advantages and disadvantages of additive sacrificial electron donors please see ref. 8a.

11. Rudroff, F.; Mihovilovic, M. D.; Gröger, H.; Snajdrova, R.; Iding, H.; Bornscheuer, U. T., Opportunities and challenges for combining chemo- and biocatalysis. *Nat. Catal.* **2018**, *1* (1), 12-22.

12. Tertiary amines, such as EDTA and TEOA, have already been proven to be efficient sacrificial electron donors in photobiocatalysis. For an overview on most divers examples see ref. 8a.

13. Frank, A.; Seel, C. J.; Groll, M.; Gulder, T., Characterization of a Cyanobacterial Haloperoxidase and Evaluation of its Biocatalytic Halogenation Potential. *ChemBioChem* **2016**, *17* (21), 2028-2032.

14a. Meister Winter, G. E.; Butler, A., Inactivation of Vanadium Bromoperoxidase: Formation of 2-Oxohistidine. *Biochemistry* **1996**, *35* (36), 11805-11811.

14b. Soedjak, H. S.; Walker, J. V.; Butler, A., Inhibition and inactivation of vanadium bromoperoxidase by the substrate hydrogen peroxide and further mechanistic studies. *Biochemistry* **1995**, *34* (39), 12689-12696.

15. For **1a** halogenation was observed to some extend even in the absence of FMN suggesting a photocatalytic background reaction. Control

experiments revealed that H_2O_2 is generated by a direct auto-oxidation of the electron-rich substrate **1a** (see SI for details).

16a. Photochemically excited FMN can promote crosslinking of photosensitive side chains, such as Cys, His, Trp, or Tyr, in proteins. For examples see SI and Bhattacharya, D.; Basu, S.; Mandal, P. C., Visible radiation effects on flavocytochrome b2 in dilute aqueous solution: a steady-state and laser flash photolysis study. *J. Photochem. Photobiol. B* **1998**, *47* (2), 173-180.

16b. Spikes, J. D.; Shen, H.-R.; Kopečková, P.; Kopeček, J., Photodynamic Crosslinking of Proteins. III. Kinetics of the FMN- and Rose Bengal-sensitized Photooxidation and Intermolecular Crosslinking of Model Tyrosine-containing N-(2-Hydroxypropyl)methacrylamide Copolymers. *Photochem. Photobiol.* **1999**, *70* (2), 130-137.

17. Hering, T.; Mühldorf, B.; Wolf, R.; König, B., Halogenase-Inspired Oxidative Chlorination Using Flavin Photocatalysis. *Angew. Chem. Int. Ed.* **2016**, *55* (17), 5342-5345.

18a. For previous examples on CiVHPO being used in organic synthesis see: Fernández-Fueyo, E.; van Wingerden, M.; Renirie, R.; Wever, R.; Ni, Y.; Holtmann, D.; Hollmann, F., Chemoenzymatic Halogenation of Phenols by using the Haloperoxidase from Curvularia inaequalis. *ChemCatChem* **2015**, *7* (24), 4035-4038.

18b. Dong, J. J.; Fernández-Fueyo, E.; Li, J.; Guo, Z.; Renirie, R.; Wever, R.; Hollmann, F., Halofunctionalization of alkenes by vanadium chloroperoxidase from Curvularia inaequalis. *Chem. Commun.* **2017**, *53* (46), 6207-6210.

18c. Fernández-Fueyo, E.; Younes, S. H. H.; Rootselaar, S. v.; Aben, R. W. M.; Renirie, R.; Wever, R.; Holtmann, D.; Rutjes, F. P. J. T.; Hollmann, F., A Biocatalytic Aza-Achmatowicz Reaction. *ACS Catal.* **2016**, *6* (9), 5904-5907.

18d. ten Brink, H. B.; Dekker, H. L.; Schoemaker, H. E.; Wever, R., Oxidation reactions catalyzed by vanadium chloroperoxidase from Curvularia inaequalis. *J. Inorg. Biochem.* **2000**, *80* (1), 91-98.

18e. ten Brink, H. B.; Tuynman, A.; Dekker, H. L.; Hemrika, W.; Izumi, Y.; Oshiro, T.; Schoemaker, H. E.; Wever, R., Enantioselective Sulfoxidation Catalyzed by Vanadium Haloperoxidases. *Inorg. Chem.* **1998**, *37* (26), 6780-6784.

19. Mifsud, M.; Gargiulo, S.; Iborra, S.; Arends, I. W. C. E.; Hollmann, F.; Corma, A., Photobiocatalytic chemistry of oxidoreductases using water as the electron donor. *Nat. Commun.* **2014**, *5*, 3145.

20. Teranishi, M.; Hoshino, R.; Naya, S.-i.; Tada, H., Gold-Nanoparticle-Loaded Carbonate-Modified Titanium(IV) Oxide Surface: Visible-Light-Driven Formation of Hydrogen Peroxide from Oxygen. *Angew. Chem. Int. Ed.* **2016**, *55* (41), 12773-12777.

21a. Ni, Y.; Fernández-Fueyo, E.; Baraibar, A. G.; Ullrich, R.; Hofrichter, M.; Yanase, H.; Alcalde, M.; van Berkel, W. J. H.; Hollmann, F., Peroxygenase-Catalyzed Oxyfunctionalization Reactions Promoted by the Complete Oxidation of Methanol. *Angew. Chem. Int. Ed.* **2016**, *55* (2), 798-801.

21b. Zhang, W.; Burek, B. O.; Fernández-Fueyo, E.; Alcalde, M.; Bloh, J. Z.; Hollmann, F., Selective Activation of C−H Bonds in a Cascade Process Combining Photochemistry and Biocatalysis. *Angew. Chem. Int. Ed.* **2017**, *56* (48), 15451-15455.

22. Zhang, W.; Fernández-Fueyo, E.; Ni, Y.; van Schie, M.; Gacs, J.; Renirie, R.; Wever, R.; Mutti, F. G.; Rother, D.; Alcalde, M.; Hollmann, F., Selective aerobic oxidation reactions using a combination of photocatalytic water oxidation and enzymatic oxyfunctionalizations. *Nat. Catal.* **2018**, *1* (1), 55-62.

23. Priebe, J. B.; Radnik, J.; Lennox, A. J. J.; Pohl, M.-M.; Karnahl, M.; Hollmann, D.; Grabow, K.; Bentrup, U.; Junge, H.; Beller, M.; Brückner, A., Solar

Hydrogen Production by Plasmonic Au–TiO2 Catalysts: Impact of Synthesis Protocol and TiO2 Phase on Charge Transfer Efficiency and H2 Evolution Rates. *ACS Catal.* **2015**, *5* (4), 2137-2148.

24. Li, X.; Chen, C.; Zhao, J., Mechanism of Photodecomposition of H2O2 on TiO2 Surfaces under Visible Light Irradiation. *Langmuir* **2001**, *17* (13), 4118-4122.
25. Tanaka, N.; Wever, R., Inhibition of vanadium chloroperoxidase from the fungus Curvularia inaequalis by hydroxylamine, hydrazine and azide and inactivation by phosphate. *J. Inorg. Biochem.* **2004**, *98* (4), 625-631.

Chapter 3

Photocatalytic Reoxidation of Thallium(III)

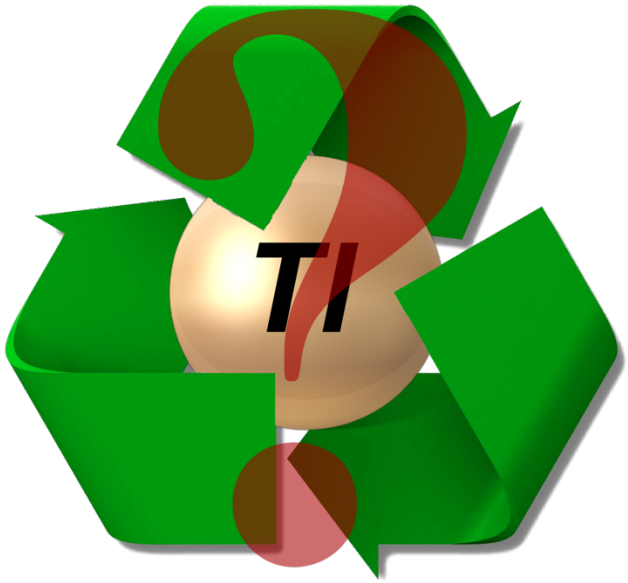

3.1 Introduction

In organic synthesis, thallium trinitrate (TTN) is a reactant capable of a broad variety of unique transformations—mainly oxidative rearrangements with high yields and regioselectivity.[1,2] However, high toxicity[3,4] of both Tl^{III} and Tl^{I}, which is formed as a by-product, and the fact that TTN has to be used in stoichiometric amounts is making a wider use of this compound problematic. A possible solution could be using only a catalytic amount of TTN and reoxidise it *in situ* from Tl^{I}. Known techniques for an oxidation of thallium(I) include chemical methods using strong oxidising agents, such as cerium(IV),[5] permanganate,[6] or chromium(VI),[7] electrochemical methods,[8,9] or oxidation of excited Tl^{I*} with oxygen under 254 nm irradiation.[10] Electrochemical methods found use in decontamination of ground waters,[8,9] but none of these techniques were employed in synthetic applications.

Literature-found redox potential $E(Tl^{III}/Tl^{I})$ is 1.0 V vs. SCE,[11] which was confirmed by our own CV measurements. Although this value is within the reach of oxidative powers of several common photocatalysts (see Figure 3.1), no visible-light photocatalytic method for oxidation of thallium(I) has been reported yet. Therefore, the project described in this chapter examined the possibility of *in situ* oxidation of Tl^{I} to Tl^{III} by means of visible-light photoredox catalysis.

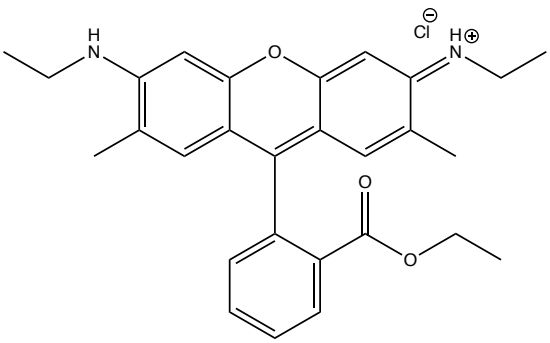

Rhodamine-6G
$E(Rh\text{-}6G^{*}/Rh\text{-}6G^{\bullet-}) = 1.2\ V$[12]

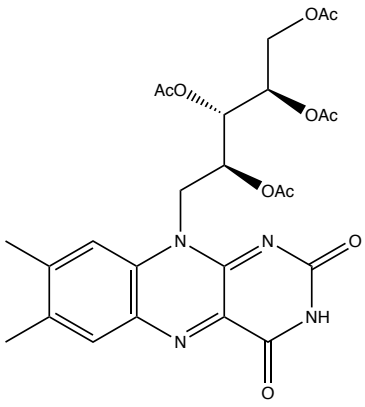

Riboflavin tetraacetate
$E(RFTA^{*}/RFTA^{\bullet-}) = 1.67\ V$[13]

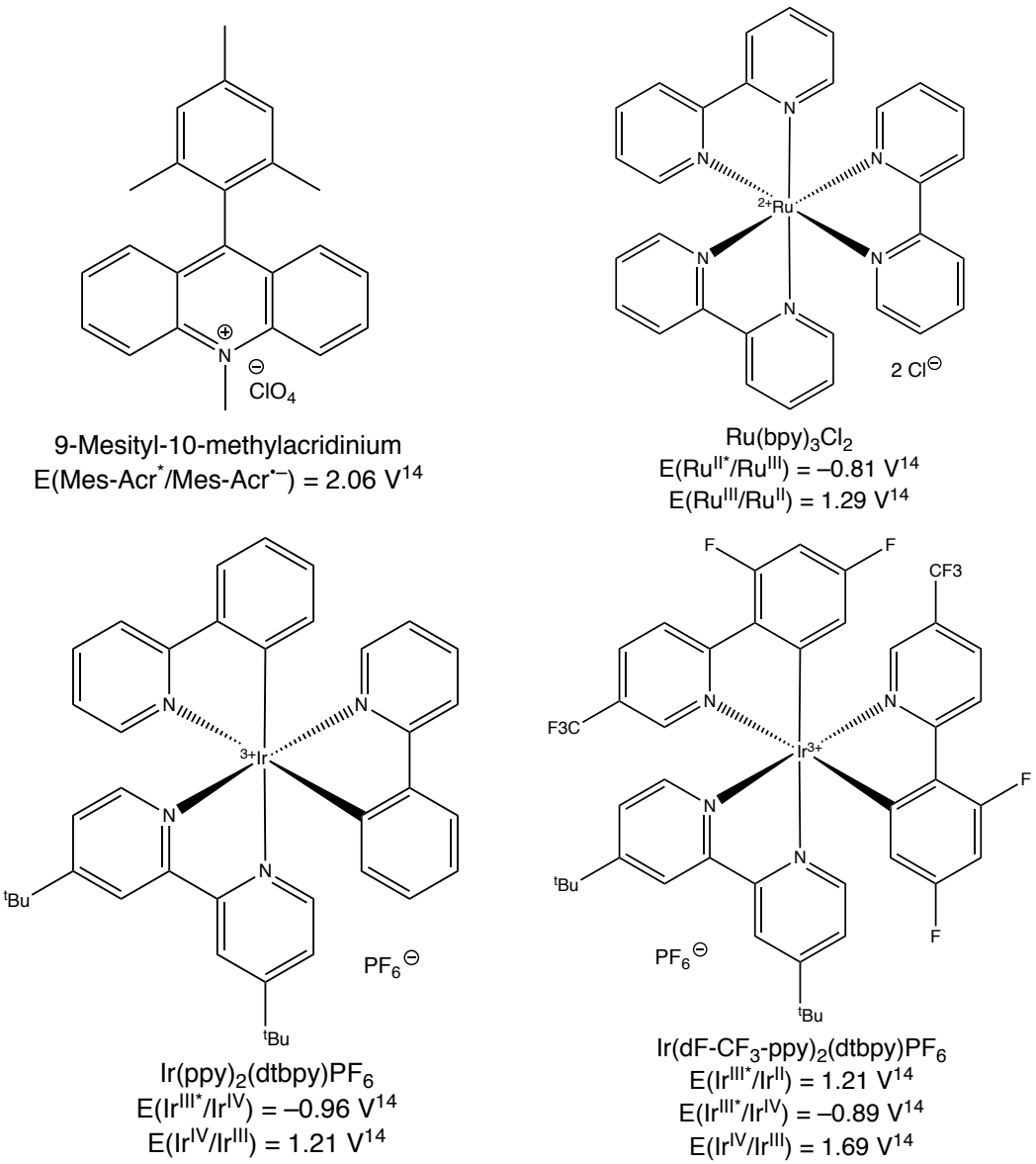

Figure 3.1. Photocatalysts used in this study and their oxidation potentials (given vs. SCE).[12-14]

3.2 Results and discussion

Oxidative rearrangement of acetophenone to methyl phenylacetate (Scheme 3.1) was chosen as a model reaction. Non-catalytic setup using 1 eq. of TTN provided conversion of 65 % after 5 hours of reaction time, which was taken as a benchmark.

Scheme 3.1. Oxidative rearrangement with thallium trinitrate used as a model reaction.

Rhodamine 6G, Fukuzumi dye (9-mesityl-10-methylacridinium), and $Ru(bpy)_3Cl_2$ were used as photocatalysts during an initial screening. Reaction mixture containing 10 mol% of TTN, 5 mol% of catalyst, and a terminal oxidant—2 eq. of sodium persulfate or oxygen—was irradiated at 455 nm overnight at 25 °C and analysed by GC. Results can be seen in Table 3.1.

Table 3.1. Results of initial screening for *in situ* photocatalytic reoxidation of Tl^{III}.

Entry	Photocatalyst	Oxidant	Conversion
1	Rhodamine 6G	O_2	–
2	Rhodamine 6G	$Na_2S_2O_8$	–
3	Fukuzumi dye	O_2	traces
4	Fukuzumi dye	$Na_2S_2O_8$	traces
5	$Ru(bpy)_3Cl_2$	O_2	–
6	$Ru(bpy)_3Cl_2$	$Na_2S_2O_8$	–

With the negative initial set of experiments, fluorescence-quenching study for a set of dyes depicted in Figure 3.1 using thallium(I) nitrate as a quencher was conducted. As can be seen in Table 3.2, only fluorescence of Rhodamine 6G was quenched by Tl^I (Figure 3.2). Control experiment with a solution of perchloric acid without $TlNO_3$ confirmed that fluorescence quenching was not caused by a decrease of pH. In the case of RFTA, acidic conditions lead to a decomposition of the sample.

Table 3.2. Fluorescence quenching of chosen photocatalysts with thallium(I) nitrate.

Entry	Photocatalyst	Fluorescence quenched
1	Rhodamine 6G	+
2	Fukuzumi dye	–
3	RFTA	–[a]
4	$Ru(bpy)_3Cl_2$	–
5	$Ir(ppy)_2(dtbpy)PF_6$	–
6	$Ir(dF\text{-}CF_3\text{-}ppy)_2(dtbpy)PF_6$	–

[a]decomposition of the dye

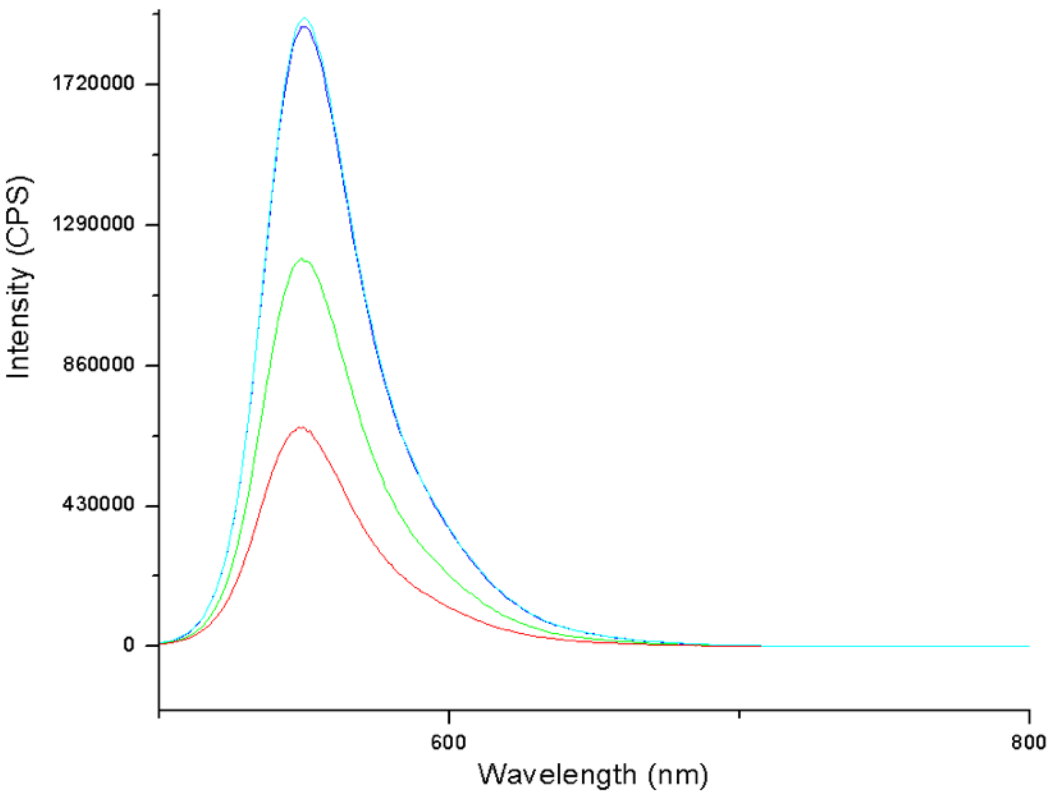

Figure 3.2. Fluorescence quenching of aqueous solution of Rhodamine 6G (5 μM) with thallium(I) nitrate (*cyan* – no quencher; *blue* – 0.5 mM; *green* – 2.5 mM; *red* – 5 mM).

Further experiments using Rhodamine 6G as a photocatalyst under different conditions were conducted. In some cases, 18-crown-6-ether was employed

to promote solubility of Tl^{I}. However, as can be seen in Table 3.3, nothing led to a product formation.

Table 3.3. Attempts for reoxidation of Tl^{III} with Rhodamine 6G under different conditions.

Entry	Rh-6G [mol%]	$HClO_4$ [M]	Oxidant	18-Crown-6 [eq.]	Solvent	Conversion
1	5	1.8	$Na_2S_2O_8$	–	MeOH	–
2	10	1.8	$Na_2S_2O_8$	–	MeOH	–
3	5	–	$Na_2S_2O_8$	–	MeOH	–
4	5	0.9	$Na_2S_2O_8$	–	MeOH	–
5	5	1.8	$Na_2S_2O_8$	0.1	MeOH	–
6	5	1.8	$Na_2S_2O_8$	1	MeOH	–
7	5	1.8	$Na_2S_2O_8$	–	MeOH/H_2O	–
8	5	1.8	$Na_2S_2O_8$	0.1	MeOH/H_2O	–
9	5	1.8	$Na_2S_2O_8$	1	MeOH/H_2O	–
10	5	1.8	$Na_2S_2O_8$	–	MeCN	–
11	5	1.8	$Na_2S_2O_8$	0.1	MeCN	–
12	5	1.8	$Na_2S_2O_8$	1	MeCN	–
13	5	1.8	$Na_2S_2O_8$	–	MeCN/H_2O	–
14	5	1.8	$Na_2S_2O_8$	0.1	MeCN/H_2O	–
15	5	1.8	$Na_2S_2O_8$	1	MeCN/H_2O	–
16	5	1.8	$Na_2S_2O_8$	–	DMSO	–
17	5	1.8	$Na_2S_2O_8$	0.1	DMSO	–
18	5	1.8	$Na_2S_2O_8$	1	DMSO	–
19	5	1.8	O_2	1	MeOH	–
20	5	1.8	O_2	1	MeOH/H_2O	–
21	5	1.8	O_2	1	MeCN	–
22	5	1.8	O_2	1	MeCN/H_2O	–
23	5	1.8	O_2	1	DMSO	–

acetophenone – 80 μmol; TTN – 10 mol%; overall volume – 4 mL

To rule out the possibility that the photocatalyst is affecting the rearrangement reaction itself, a mixture containing stoichiometric amount of TTN and 5 mol%

of Rhodamine 6G was irradiated with 455 nm LED for five hours reaching 58 % conversion to methyl phenylacetate—a value similar to the benchmark. In another approach, concentrated solution of thallium(I) nitrate, sodium persulfate, perchloric acid, and crown-ether in a mixture of water and acetonitrile containing 5 mol% of Rhodamine 6G was irradiated for three days to possibly pre-generate thallium(III). This mixture was then added to a solution of acetophenone and stirred overnight. Also in this case, no formation of desired product was observed.

To examine if the Rhodamine 6G radical anion is generated upon irradiation in a presence of Tl^{I}—*i.e.* if excited state of Rh-6G is able to oxidise thallium(I)—transient UV-Vis spectroscopic measurement was performed. Degassed DMSO solution containing Rhodamine 6G and $TlNO_3$ was irradiated with 455 nm LED under inert atmosphere and UV-Vis spectra were collected every 5 minutes for 5 hours. However, no increase of absorption around 420 nm—which would indicate a presence of the radical anion[12]—was detected. Therefore, previously observed fluorescence quenching was most probably not related to an electron transfer. Possibly, a complex formation between Tl^{+} and Rhodamine 6G and a fluorescence quenching via heavy-atom effect could have taken place.[15]

3.3 Conclusions

Based on results presented above, we can conclude that thallium(I) cannot be photocatalytically oxidised to thallium(III) using redox photocatalysts. Plausible explanation is that all of the examined dyes—with the exception of RFTA—are only capable of one-electron oxidation, which means that Tl^{II} species would have to be generated throughout the process. However, elements from Group 13 are stable in this oxidation state only in a presence of specialised ligands.[16] Also, redox potential of the first oxidation step $E(Tl^{II}/Tl^{I})$ is 1.97 V,[17] which is too high for any of the examined photocatalyst (or borderline, as in case

of Fukuzumi dye). RFTA, which is flavin-based dye, and therefore could be capable of a direct two-electron oxidation, is unfortunately unstable in highly acidic conditions that are required for the stability of Tl^{3+} ions in a solution.

3.4 Experimental section

3.4.1 General methods and materials

CG measurements were carried out on Agilent Technologies 7890A Series instrument equipped with FID detector and HP–5ms Ultra Inert column using helium as a carrier gas.

Fluorescence spectra were recorded on HORIBA Scientific FluoroMax-4 Spectrofluorometer.

CV measurements were performed with Autolab PGSTAT302N potentiostat/galvanostat using glassy carbon working electrode, platinum counter electrode, and silver reference electrode. Ferrocene was used as an internal standard.

3.4.2 Benchmark reaction

Solution of acetophenone (234 μL, 2 mmol), thallium(III) nitrate (780 mg, 2 mmol), and perchloric acid (70 w%, 1 mL) in 5 mL of MeOH in a 25 mL round-bottom flask was stirred at room temperature for 5 hours. Afterwards, the precipitate of thallium(I) nitrate was filtered off, the filtrate was diluted with 10 mL of water and extracted 2 times with 10 mL of chloroform. Collected organic phases were dried with sodium sulphate and analysed by GC.

3.4.3 General procedure for photocatalytic reaction

Acetophenone (175 μL, 1.5 mmol), TTN (58 mg, 0.15 mmol), photocatalyst, perchloric acid, crown ether, and terminal oxidant were added to a small crimp-top vial equipped with a stirring bar followed by 4 mL of solvent. After sealing with a septum, the head space was flushed with nitrogen, the vial was placed over an LED into an aluminium block tempered to 25 °C and irradiated at 455 nm overnight. When using O_2 as the terminal oxidant, the head space was flushed with oxygen and an oxygen balloon was connected to the vial through septum during the irradiation. The reaction mixture was then filtered, diluted with 8 mL of water, and extracted 2 times with 8 mL of chloroform. Collected organic phases were dried with sodium sulphate and analysed by GC.

3.4.4 Generation of Tl^{III} from Tl^{I} in a separate reaction

Saturated solution of thallium(I) nitrate in aqueous MeCN (50 vol% H_2O, 4 mL) containing perchloric acid (70 w%, 0.8 mL), sodium persulfate (476 mg, 2 mmol), 18-crown-6-ether (0.53 g, 2 mmol), and Rhodamine 6G (35 mg, 0.075 mmol) was irradiated for 72 hours at 455 nm in a sealed crimp-top vial under nitrogen at 25 °C. Aliquot of the resulting solution (1 mL) was then added to 3 mL of MeOH containing acetophenone (175 μL, 1.5 mmol) and perchloric acid (70 w%, 0.6 mL). After stirring overnight, the reaction mixture was filtered, diluted with 8 mL of water, and extracted 2 times with 8 mL of chloroform. Collected organic phases were dried with sodium sulphate and analysed by GC.

3.4.5 Fluorescence quenching

Degassed 10 μM stock solution of photocatalyst in aqueous methanol (5 mL) was mixed with degassed 50 mM aqueous stock solution of $TiNO_3$ acidified with perchloric acid to pH below 1 (100 μL for 0.5 mM final solution; 500 μL

for 2.5 mM final solution; 1 mL for 5 mM final solution) in 10 mL volumetric flask and the overall volume was adjusted with aqueous methanol to 10 mL. Fluorescence emission of prepared solutions was recorded at excitation wavelengths appropriate for each dye.

3.4.6 Transient UV-Vis spectroscopy

Degassed saturated solution of $TlNO_3$ in DMSO containing 5 μM of Rhodamine 6G was irradiated with 455 nm LED in a gas-tight cuvette under nitrogen atmosphere in an online UV-Vis spectrometer. Absorption spectrum of the solution was recorded every 5 minutes for 5 hours.

3.5 Contributions

CV measurements were done by Regina Hoheisel (Institute of Organic Chemistry, University of Regensburg, Regensburg, Germany).

3.6 References

1. Ferraz, H. M. C.; Silva Jr, L. F.; Vieira, T. d. O., Thallium(III) in Organic Synthesis. *Synthesis* **1999**, *1999* (12), 2001-2023.
2. Silva, J. L. F.; Carneiro, V. M. T., Thallium(III) in Organic Synthesis. *Synthesis* **2010**, *2010* (07), 1059-1074.
3. Galván-Arzate, S.; Santamaría, A., Thallium toxicity. *Toxicol. Lett.* **1998**, *99* (1), 1-13.
4. Rickwood, C. J.; King, M.; Huntsman-Mapila, P., Assessing the fate and toxicity of Thallium I and Thallium III to three aquatic organisms. *Ecotox. Environ. Safe.* **2015**, *115*, 300-308.

5. Gryder, J. W.; Dorfman, M. C., One Step Oxidation of Thallium(I) to Thallium(III). *J. Am. Chem. Soc.* **1961**, *83* (5), 1254-1255.
6. Hiremath, G. A.; Timmanagoudar, P. L.; Nandibewoor, S. T., Kinetics of oxidation of thallium(I) by permanganate in aqueous hydrochloric acid medium using the stopped-flow technique. *Transit. Metal. Chem.* **1996**, *21* (6), 560-564.
7. Gokavi, G. S.; Raju, J. R., Chromium(VI) oxidation of thallium(I). *Polyhedron* **1987**, *6* (9), 1721-1725.
8. Li, Y.; Zhang, B.; Borthwick, A. G. L.; Long, Y., Efficient electrochemical oxidation of thallium (I) in groundwater using boron-doped diamond anode. *Electrochim. Acta* **2016**, *222*, 1137-1143.
9. Tian, C.; Zhang, B.; Borthwick, A. G. L.; Li, Y.; Liu, W., Electrochemical oxidation of thallium (I) in groundwater by employing single-chamber microbial fuel cells as renewable power sources. *Int. J. Hydrogen. Energ.* **2017**, *42* (49), 29454-29462.
10. Kirkbright, G. F.; Mayne, P. J.; West, T. S., Photo-oxidation of thallium(I) with the production of hydrogen peroxide. *J. Chem. Soc. Dalton* **1972**, (17), 1918-1920.
11. Greenwood, N. N.; Earnshaw, A., *Chemistry of the Elements*. Pergamon Press Plc: Oxford, 1984.
12. Ghosh, I.; König, B., Chromoselective Photocatalysis: Controlled Bond Activation through Light-Color Regulation of Redox Potentials. *Angew. Chem. Int. Ed.* **2016**, *55* (27), 7676-7679.
13. Mühldorf, B.; Wolf, R., Photocatalytic benzylic C–H bond oxidation with a flavin scandium complex. *Chem. Comm.* **2015**, *51* (40), 8425-8428.
14. DiRocco, D. Electrochemical Series of Photocatalysts and Common Organic Compounds. https://yoon.chem.wisc.edu/sites/yoon.chem.wisc.edu/files/Merck-Photocatalysis-Chart.pdf.

15. Ando, T.; Asai, H., Charge Effects on the Dynamic Quenching of Fluorescence of 1, N6-Ethenoadenosine Oligophosphates by Iodide, Thallium (I) and Acrylamide. *J. Biochem.* **1980**, *88* (1), 255-264.
16. Protchenko, A. V.; Dange, D.; Harmer, J. R.; Tang, C. Y.; Schwarz, A. D.; Kelly, M. J.; Phillips, N.; Tirfoin, R.; Birjkumar, K. H.; Jones, C.; Kaltsoyannis, N.; Mountford, P.; Aldridge, S., Stable GaX2, InX2 and TlX2 radicals. *Nat. Chem.* **2014**, *6*, 315.
17. Falcinella, B.; Felgate, P. D.; Laurence, G. S., Aqueous chemistry of thallium(II). Part I. Kinetics of reaction of thallium(II) with cobalt(II) and iron(III) ions and oxidation–reduction potentials of thallium(II). *J. Chem. Soc. Dalton* **1974**, (13), 1367-1373.

4. Summary

This Thesis describes a path towards development of a heterogeneous photocatalytic system capable of utilising water as a source of redox equivalents in organic synthesis. Specific focus was given to *in situ* generation of hydrogen and hydrogen peroxide using water oxidation as an electron source. Such approach is not only "green", since water is non-toxic and abundant, but also synthetically elegant, as—in ideal case—purification of reaction mixture requires only a removal of the solid-state catalyst via filtration or centrifugation.

Chapter 1 focuses on non-covalent immobilisation of amphiphilic metal complexes for photocatalytic water oxidation on a solid support. Ruthenium-complex photosensitiser and ruthenium-complex catalyst bearing long, hydrophobic alkyl chains are selectively adsorbed onto a surface of untreated, commercial silica gel. This structure shows a high stability against leakage in aqueous suspension. Also, the complexes keep their photocatalytic activity where oxygen is produced under blue-light irradiation in a presence of sodium persulfate as a sacrificial oxidant. However, fast degradation of the photosensitiser under given condition—limiting the reaction to ca. 50 TON—observed during previous applications of this system remained unchanged.

Chapter 2 deals with evaluation of photocatalytic properties in terms of additive-free photocatalytic water splitting of two semiconducting materials. Titanium disilicide ($TiSi_2$), described in the first part of this chapter, is mentioned in literature as a cheap, commercially available material capable of absorbing light within the whole visible spectrum and producing hydrogen and oxygen under visible-light irradiation in pure water. According to our observations, hydrogen is generated chemically via hydrolysis of the material and claims

of the original authors about photocatalytic properties are based on an incomplete data set.

Second part of the chapter focuses on TiO_2 doped with gold nanoparticles (Au–TiO_2), which is described in literature as a material capable of hydrogen-peroxide generation via water oxidation and subsequent reduction of oxygen under irradiation with visible light. Analysis of activity as a function of wavelength shows that Au–TiO_2 is capable of water splitting, but only under UV-A light (375 nm). Interestingly, the system behaves differently under different atmospheres. When oxygen is present, hydrogen peroxide is generated, whereas under inert atmosphere, hydrogen is produced via proton reduction. Au–TiO_2 also keeps its activity in mixtures of organic solvents with water, which potentially allows its use in syntheses requiring a non-polar environment. In aqueous acetone, both H_2O_2 and H_2 production is even significantly increased compared with pure water. Possibility to use Au–TiO_2 in organic synthesis is demonstrated on oxidation of benzyl alcohol to benzaldehyde with photocatalytically generated hydrogen peroxide, on reduction of α-methylstyrene to cumene with photocatalytically generated hydrogen, and on trapping of photocatalytically generated THF radicals with TEMPO. These observations prove that water can be used as a source of redox equivalents for both oxidative and reductive transformations.

Third part of this chapter describes a successful utilisation of hydrogen peroxide generated photocatalytically via water splitting using Au–TiO_2 under UV-A irradiation in a biocatalytic reaction employing VHPO class of enzymes, which is capable of electrophilic halogenation of electron-rich arenes in aqueous solutions in a presence of halide and hydrogen peroxide. Two methods of *in situ* evolution of H_2O_2 are compared—flavin-mediated homogeneous system using amine-based buffers as a source of electrons and Au–TiO_2-mediated heterogeneous system using water oxidation as a source of electrons. Heterogeneous method turns out to be a milder source of H_2O_2, which

is beneficial due to inhibition activity of hydrogen peroxide in higher concentrations, achieving a significantly higher conversion in bromination of 2,6-dimethoxypyridine than flavin-based setup.

Attempts for photocatalytic reoxidation of thallium(I) to thallium(III) are described in **Chapter 3**. Thallium trinitrate is capable of wide variety of unique organic transformations, especially oxidative rearrangements with high yields and regioselectivity. However, it has to be used in stoichiometric amounts and high toxicity of both Tl(III) and Tl(I), which is formed during those reactions, is making a wider use of this reactant problematic. Therefore, its use in a catalytic amount and *in situ* reoxidation would be beneficial. Screening covering several redox photocatalysts (both organic and metal-complex-based) is reported. However, none of them shows the ability to oxidise thallium(I).

5. Zusammenfassung

Die vorliegende Arbeit beschäftigt sich mit der Entwicklung eines heterogenen photokatalytischen Systems, das Wasser als Quelle für Redoxäquivalente in der organischen Synthese nutzen kann. Ein besonderer Fokus liegt dabei auf der *in situ* Herstellung von Wasserstoff und Wasserstoffperoxid als Elektronenquelle. Ein solcher Ansatz ist nicht nur „grün", da Wasser allgegenwärtig und ungiftig ist, sondern auch synthetisch elegant, da die Aufarbeitung der Reaktionsmischung im Idealfall lediglich das Abtrennen des im festen Zustand vorliegenden Katalysators durch Filtration oder Zentrifugation erfordert.

Zentraler Gegenstand des **ersten Kapitels** liegt auf der nichtkovalenten Immobilisierung amphiphiler Metallkomplexe für photokatalytische Wasseroxidation auf einem festen Trägermaterial. Dabei konnten Rutheniumkomplex-Photosensibilisatoren und Katalysatoren über langkettige, hydrophobe Alkylketten selektiv auf der Oberfläche von unbehandeltem, handelsüblichen Silicagel adsorbiert werden. Diese Struktur zeigt eine hohe Stabilität gegenüber Ausbluten in wässrigen Suspensionen. Darüber hinaus behalten die Komplexe ihre photokatalytische Aktivität bei, wenn Sauerstoff unter Bestrahlung mit blauem Licht erzeugt wird, wobei Natriumpersulfat als Oxidationsmittel verwendet wird. Jedoch unterliegt der Photosensibilisator einer Zersetzung unter den gegebenen Reaktionsbedingungen, die bereits während früherer Anwendungen dieses Systems beobachtet wurde und die Reaktion auf ca. 50 TON limitiert.

Kapitel 2 befasst sich mit der Evaluierung photokatalytischer Eigenschaften bezogen auf die additivfreie photokatalytische Wasserspaltung von zwei halbleitenden Materialien. Titandisilizid ($TiSi_2$), Gegenstand des ersten Teils des Kapitels, ist in der Literatur als günstiges, kommerziell verfügbares Material

bekannt, das Wasserstoff und Sauerstoff aus reinem Wasser generieren kann, unter Absorption von Licht aus dem gesamten sichtbaren Spektrum. Unsere Untersuchungen zeigten allerdings, dass Wasserstoff chemisch durch Hydrolyse des Materials erzeugt wird und die Behauptungen der ursprünglichen Autoren über die photokatalytische Aktivität des Materials auf einem unvollständigen Datensatz basieren.

Der zweite Teil des Kapitels konzentriert sich auf Goldnanoartikel dotiertes TiO_2 (Au–TiO_2), das in der Literatur als ein Material beschrieben wird, das die Erzeugung von Wasserstoffperoxid durch Wasseroxidation und anschließende Sauerstoffreduktion unter Bestrahlung mit sichtbarem Licht ermöglicht. Die Analyse der Aktivität als Funktion der Wellenlänge zeigt, dass Au–TiO_2 tatsächlich in der Lage ist, Wasser zu spalten, allerdings nur unter Verwendung von UV-A-Licht (375 nm). Interessanterweise verhält sich das System unter verschiedenen Atmosphären unterschiedlich. Wenn Sauerstoff vorhanden ist, wird Wasserstoffperoxid erzeugt, wohingegen unter inerten Bedingungen Wasserstoff durch die Reduktion von Protonen generiert wird. Au–TiO_2 behält darüber hinaus seine Aktivität in Gemischen aus organischen Lösungsmitteln mit Wasser bei, was potenziell Synthesen zugänglich macht, die bevorzugt in unpolaren Medien ablaufen. In wässrigem Aceton ist die Erzeugung von sowohl Wasserstoffperoxid als auch von Wasserstoff im Vergleich zu reinem Wasser sogar deutlich erhört. Die Möglichkeit, Au–TiO_2 in der organischen Synthesechemie einzusetzen, wird an der Oxidation von Benzalkohol zu Benzaldehyd mittels photokatalytisch generiertem Wasserstoffperoxid, an der Reduktion von α-Methylstyrol zu Cumol durch *in situ* generierten Wasserstoff oder das Abfangen von photokatalytisch erzeugten THF-Radikalen mit TEMPO demonstriert. Die Beobachtungen belegen, dass Wasser als Quelle für Redoxäquivalente sowohl für oxidative als auch für reduktive Transformationen verwendet werden kann.

Der dritte Abschnitt dieses Kapitels beschreibt eine erfolgreiche Anwendung des von Au–TiO_2 unter UV-A-Bestrahlung photokatalytisch aus Wasser erzeugten Wasserstoffperoxids in einer biokatalytischen Reaktion der VHPO-Enzymklasse. Diese Enzymklasse ist in der Lage elektrophile Halogenierungen von elektronenreichen Aromaten in wässrigen Lösungen in Gegenwart von Halogeniden und Wasserstoffperoxid zu katalysieren. Dabei wurden zwei Methoden der *in situ*- Erzeugung von H_2O_2 verglichen — ein Flavin-mediiertes homogenes System mit aminbasierten Puffern als Elektronenquelle und ein Au–TiO_2-mediiertes heterogenes System, das Elektronen aus der Oxidation von Wasser bezieht. Die heterogene Methode stellt sich dabei als mildere Quelle für Wasserstoffperoxid heraus, was zu höheren Umsätzen in der Bromierung von 2,6-Dimethoxypyridin führt als das Flavin-basierte System, da H_2O_2 in höheren Konzentrationen inhibitorische Aktivität gegenüber dem Enzym zeigt.

Untersuchungen zur photokatalytischen Reoxidation von Thallium(I) zu Thallium(III) werden in **Kapitel 3** beschrieben. Thalliumtrinitrat ist in der Lage, eine große Bandbreite einzigartiger organischer Transformationen zu ermöglichen, wie zum Beispiel Umlagerungsreaktionen in hohen Ausbeuten und Regioselektivitäten. Allerdings ist die breite Anwendung der Reaktanden problematisch, da hochtoxisches Tl(III) und während der Reaktion gebildetes, ebenfalls hochtoxisches Tl(I) in stöchiometrischen Mengen vorliegen müssen. Daher wäre eine Verwendung katalytischer Mengen in Kombination mit einer *in situ*- Reoxidation vorteilhaft. Zur Realisierung dieses Vorhabens werden verschiedenste Photoredoxkatalysatoren (sowohl organische Farbstoffe als auch Oragnometalkomplexe) getestet. Trotzdem konnte bislang kein System gefunden werden, dass in der Lage ist Thallium(I) zu oxidieren.

6. Abbreviations

A	acceptor
Au-TiO2	gold-nanoparticle-doped titanium dioxide
AuNP	gold nanoparticle
Cat	catalyst
CB	conduction band
CV	cyclic voltammetry
D	donor
DCM	dichloromethane
DMSO	dimethyl sulfoxide
EC	enzyme-classification number
EDTA	ethylenediaminetetraacetic acid
EDX	energy-dispersive X-ray spectroscopy
eV	electronvolt
FID	flame ionisation detector
FMN	flavin mononucleotide
GC	gas chromatography
GOx	glucose oxidase
HEPES	4-(2-hydroxyethyl)-1-piperazineethanesulfonic acid
HPLC	high-performance liquid chromatography
HRP	horseradish peroxidase
IET	interfacial electron transfer
L-AuNP	large gold nanoparticle
LC-MS	liquid chromatography–mass spectrometry
LED	light-emitting diode
LSPR	localised surface plasmon resonance
MeCN	acetonitrile
MeOH	methanol

MES	2-(*N*-morpholino)ethanesulfonic acid
MOPS	3-(*N*-morpholino)propanesulfonic acid
NADH	nicotinamide adenine dinucleotide (reduced form)
NHE	normal hydrogen electrode
NMR	nuclear magnetic resonance
NP	nanoparticle
P25	standardised formulation of titanium dioxide
PS	photosensitiser
RFTA	riboflavin tetraacetate
Rh-6G	Rhodamine 6G
RPM	revolutions per minute
RT	room temperature
S-AuNP	small gold nanoparticle
SCE	standard calomel electrode
SILP	supported ionic-liquid phase
TEMPO	(2,2,6,6-tetramethylpiperidin-1-yl)oxyl
THF	tetrahydrofuran
TON	turn-over number
Tris	tris(hydroxymethyl)aminomethane
TTN	thallium trinitrate
UV	ultraviolet light
UV-A	long-wave ultraviolet light
VB	valence band
VHPO	vanadium haloperoxidase
Vis	visible light
XRD	X-ray diffraction

7. Acknowledgements

First, I would like to express my gratitude to Prof. Dr. Burkhard König. Burkhard, you gave me the opportunity to be a part of your amazing group, guided me through all the often complicated projects, and you did not give up on me, even though things did not always go smoothly. For that I will be entirely grateful.

I also want to thank Prof. Dr. Arno Pfitzner, Prof. Dr. Robert Wolf, and Prof. Dr. Julia Rehbein for taking part in my final examination and for the time it cost.

I would like to thank Prof. Dr. Hubert Motschmann and Prof. Dr. Radek Cibulka for being my mentors within the *ChemPharm* graduate school.

My huge appreciation belongs to Catharina Seel and Prof. Dr. Tanja Gulder as my cooperation partners. Catharina, Tanja, I had a great time working with you. It was a tough project to push through, but we made it!

I would also like to thank Thomas Buchecker for always being ready to help me with anything even remotely inorganic, Uli Lennert for GC-MS measurements, and Melanie Iwanow for material analyses.

And here we go...

AK König, thank you for being the best group of the finest people I've had the honour to meet. I will remember the time here till the end of my days. Coffee breaks at 9AM sharp (and 11.45AM and 3PM...no wonder my hands are always shaking), daily trips to Mensa, cake breaks, BBQs, Weißwurstfrühstücke, beer tastings, skiing, trips, sports,... It was legendary here.

Thank you, Andi, for being ready to appreciate my childish jokes—no matter how stupid—and always playing along. Thank you, Melli, for brightening even

the gloomiest day in the lab. Thank you, Simone, for being so kind-hearted and sophisticated, yet still free–cool–in little lady; you're one of a kind. Thank you, Karin, for being always ready to talk about nothing and everything and to drop a kind word whenever I needed it. Thank you, Anna, for your unique sense of humour and our shared interest in movies (even though you're a cat person). Thank you, Ranit, for constantly motivating me. Thank you, Alex, Daniel, and Matthias, for sharing my biggest hobby.

Our group would never be the same without the permanent staff. Kathi, Julia, Britta, Simone, Regina, Viola, Rudi, Ernst, thank you for the work you do for us. Thank you for always being ready to help with any problem I came up with, but also always being ready to chit-chat or to send a smile my way to light up the day.

Nadja, if I had to list everything we've ever been through, this section would be as long as the rest of the Thesis. And I'm pretty sure I would still forget something. Therefore, I will focus on something different, something for which I'll be always grateful—you've made me a part of the community here. Helping me with stuff that was beyond my language level or my knowledge of how things are going in Germany. Including me in coffee breaks since day one, taking me to KHG, teaching me German. Without you, I would have never enjoyed the four years here as much as I did.

Elisa and Andreas, the way we immediately clicked was unbelievable. And the fact that you've moved in just across the street from me simply could not have been a coincidence. I love you, guys. Thanks for everything.

Malte and Mischko, who would have thought that common interest in weird stuff can form such a bond? Our correspondence is always a highlight of my day. Mischko, stay the way you are. It's unique to find a Renaissance personality such as yourself nowadays and I'm proud I can call myself your friend. Malte, I would

like to express my gratitude to whomever invented the handegg in the USA. Your friendship is very dear to me and Super Bowl XLIX was the ice-breaker that started it. Also, it gives me the chance to see you at least once a year and I'm always looking forward to it. Guys, thanks for all the laughter that helped me through tough times here!

Daní, tvoje podpora bylo to hlavní, co mě tu—hlavně v posledních měsících—drželo nad vodou. Miluju tě a už se těším, až spolu strávíme zbytek života.

Maminko, taťko, děkuju za vaši podporu. Vím, že to asi nebylo snadné přijmout, když jsem vám oznámil, že mizím na několik let do zahraničí. A vy jste mě nejen podpořili, ale kdykoli jsem potřeboval s něčím pomoct—hlavně v těch nelehkých začátcích a teď na konci—byli jste tu pro mě. A já si toho moc cením. Mám vás rád.